INFORMATION TO USERS

This manuscript has been reproduced from the microfilm master. UMI films the text directly from the original or copy submitted. Thus, some thesis and dissertation copies are in typewriter face, while others may be from any type of computer printer.

The quality of this reproduction is dependent upon the quality of the copy submitted. Broken or indistinct print, colored or poor quality illustrations and photographs, print bleedthrough, substandard margins, and improper alignment can adversely affect reproduction.

In the unlikely event that the author did not send UMI a complete manuscript and there are missing pages, these will be noted. Also, if unauthorized copyright material had to be removed, a note will indicate the deletion.

Oversize materials (e.g., maps, drawings, charts) are reproduced by sectioning the original, beginning at the upper left-hand corner and continuing from left to right in equal sections with small overlaps.

Photographs included in the original manuscript have been reproduced xerographically in this copy. Higher quality 6" x 9" black and white photographic prints are available for any photographs or illustrations appearing in this copy for an additional charge. Contact UMI directly to order.

ProQuest Information and Learning
300 North Zeeb Road, Ann Arbor, MI 48106-1346 USA
800-521-0600

Université d'Ottawa · University of Ottawa

CHAR COMBUSTION IN A PACKED BED REACTOR

Jennifer Ryan

A thesis submitted to the School of Graduate Studies and Research
in partial fulfilment of the requirements for the
degree of

MASTER OF APPLIED SCIENCE

in the Department of Chemical Engineering
University of Ottawa

April 2000

ABSTRACT

This study reports on overfeed packed bed char combustion experiments and modelling. Experimental results are used to verify the assumptions of an existing char combustion simulation. The computer model uses finite volume discretization methods to predict temperature and concentration profiles for packed bed char combustion. Also, the behaviour of ash in a packed bed is explored and incorporated into the model by accounting for the effect of ash on such properties as bed void fraction and heat and mass transfer processes. The effects of air flow rate and bed depth on the burning rate, the bed temperature and gas concentrations are also examined. Experiments were performed in a reactor 23 cm in diameter and 20 cm high. Thermocouples measured bed temperatures and a water-cooled probe sampled bed gases. Gas samples were analysed for CO_2, CO and O_2 using a gas chromatograph. The fuel was foundry coke with a particle diameter in the 1 cm size range.

Experiments were run for bed heights ranging from 5 to 15 cm and air flow rates of 191 to 520 kg/m^2hr. Comparison of the experimental bed profiles and burning rates with model predictions shows good agreement, indicating that the model can reliably predict packed bed char combustion. Species concentrations are shown to be only dependent on bed depth; whereas the burning rate is a function of both the bed depth and air flow rate. The data also show that the ash properties are highly dependent on the operating conditions; since the model predictions are very sensitive to the ash properties, a relationship between ash properties and temperature needs to be developed and included in the model. More research is also needed on the CO_2 reduction reaction parameters and pore diffusion model and the oxidation kinetics in the ash layer.

RÉSUMÉ

Cette étude présente des expériences et une simulation de combustion de charbon en lit fixe. Les résultats expérimentaux sont employés pour vérifier les suppositions d'une simulation de combustion de charbon. Utilisant des méthodes discrètes de volume, le modèle d'ordinateur produit des courbes correspondant à la température et la concentration associée à la combustion de charbon en lit fixe. Le comportement de la cendre dans un lit fixe également est exploré et incorporé dans le modèle. L'effet de la cendre sur la fraction vide du lit et les procédés de transfert de la chaleur et de la masse sont inclus. Les effets du débit d'air et de la profondeur de lit sur le taux de combustion, la température de lit et des concentrations de gaz ont également été examinés. Les expériences ont été exécutées dans un réacteur de 23 cm de diamètre par 20 cm de haut. Les thermocouples ont mesuré la température et une sonde, refroidie à l'eau, a échantillonné les gaz dans le lit. Les échantillons de gaz ont été analysés pour la présence du CO_2, de la CO et d'O_2 par la chromatographie des phases gazeuses. Le combustible était le coke de fonderie avec un diamètre d'environ 1 cm.

Des expériences ont été exécutées pour des hauteurs de lit variant entre 5 et 15 cm et le débit d'air variant entre 191 et 520 kg/m^{2}hr. La comparaison des profils expérimentaux et des taux de combustion avec les prédictions du modèle montre une bonne concordance. Ainsi, l'efficacité du modèle pour simuler la combustion du charbon en lit fixe est vérifiée. Les résultats montrent que les concentrations d'espèce, sont seulement dépendantes de la profondeur de lit, tandis que le taux de combustion est une fonction de la profondeur du lit et du débit de l'air. Les données prouvent également que les propriétés des cendres dépendent presqu'entièrement des conditions d'opération. Puisque les prévisions du modèle sont très

sensibles aux propriétés des cendres, un rapport entre les propriétés des cendres et la température doit être développé et inclus dans le modèle. Plus de recherches seront nécessaires pour determiner les paramètres de réaction de réduction du CO_2, le modèle de diffusion de pore et la cinétique d'oxydation dans la couche de cendres.

ACKNOWLEDGMENTS

I would like to thank Dr. William Hallett for all of his assistance and guidance throughout this project. Additional thanks are given to the departmental technicians, Madan Makasare, Derek Leang, Greg Duschene, Mike Burns, Lou Tremblay, Gérard Nina and Frank Ziroldo, for all their technical support. I would also like to thank NSERC for funding this research and Dr. John Gransden of CANMET, Natural Resources Canada for supplying the coke.

A special thanks to my husband, Andrew, for all of his help and encouragement over the course of this project.

TABLE OF CONTENTS

LIST OF FIGURES

LIST OF TABLES

NOMENCLATURE

A	area, m^2
A	pre-exponential, kg/m^2skPa
a_B	specific surface area, 1/m
a_I	specific internal surface area, 1/m
b_H	grate bar height, m
b_S	grate bar spacing, m
b_W	grate bar width, m
c_P	specific heat, J/kgK
d	diameter, m
D	diffusivity, m^2/s
E	activation energy, kJ/kmol
f	response factor
$F_{B\infty}$	shape factor for radiation between two infinitely long parallel plates
$\overline{F_{B\infty}}$	effective view factor for radiation between the bottom of the bed and the ashpan
f_ε	fraction of the void volume "associated with" the fuel
$F_{T\infty}$	shape factor for radiation between two parallel disks
$\overline{F_{T\infty}}$	effective view factor for radiation between the top of the bed and the surroundings
G	carbon consumption rate per unit area of particle surface, kg/m^2s
G_ε	Westman equation fit parameter
h_{RS}	solid to solid radiation heat transfer coefficient, W/m^2K

h_{RV} void to void radiation heat transfer coefficient, W/m^2K

k thermal conductivity, W/mK

K reaction rate, kg/m^2skPa

K_I effective reaction rate, kg/m^2skPa

k_y fluid-to-particle mass transfer coefficient, kg/m^2s

L bed height, m

m mass, kg

M Ergun equation correction factor

M molecular weight, kg/kmol

n number of particles

N number of particles per unit bed volume, $1/m^3$

$\dot{N}$ particle number flux per unit area of bed, $1/m^2s$

Nu Nusselt number

Pr Prandlt number

$\dot{q}_R$ net radiant heat transfer, W/m^2

r radius, m

r_{str} structural ratio

R universal gas constant = 8.314 kJ/kmolK

Re Reynolds number

s_G grate solidity

Sh Sherwood number in the bed

Sh_0 Sherwood number in the gas phase

T temperature, K

ν superficial velocity, m/s

V solid volume per unit bed volume

V_ε void volume per unit bed volume

w actual velocity, m/s

W weight, kg

x height of the refractory above the bed surface

X volume fraction

Y mass fraction

Greek letters

α ash mass fraction in the fuel

β dimensionless effective length between particle centres

χ fraction of the fuel void volume filled with the ash phase

ΔP pressure drop, Pa

Δx cell height, m

ε void fraction

ε_R emissivity

ϕ Thiele modulus

γ dimensionless effective length of the solid relating to conduction

η_P effectiveness

φ dimensionless effective gas film thickness near the particle contact points

μ viscosity, kg/ms

Θ specific volume

ρ density, kg/m^3

σ Stefan-Boltzmann constant = $5.669 \cdot 10^{-8}$ W/m^2K^4

τ tortuosity

ψ sphericity

Subscripts and Superscripts

0 feed particle

A ash

B bulk, bed

C fuel ("char")

CO carbon monoxide

CO_2 carbon dioxide

eff effective

G gas

i species i

O_2 oxygen

P particle

S solid (fuel+ash), standard

Z Westman equation empirical parameter

∞ surroundings

1.0 INTRODUCTION

Packed bed combustion, also called fixed bed combustion, is the oldest method of burning solid fuels. Centimeter-sized fuel particles are burned as a bed and are supported by a grate. The combustion air is supplied from below the grate at velocities less than the fluidization velocity.

Packed bed combustion used to be the most common method for burning coal. Presently, it is used for the burning of municipal waste in incinerators and by pulp and paper mills to burn wood wastes for producing steam for other parts of the plant. One of the newer applications is the burning of wood for steam and hot water production in district heating systems.

There are three general types of packed bed reactors, which are distinguished by the way in which the air and fuel are combined. In each case, the combustion air is supplied from below the grate. In overfeed reactors, the air and fuel are in counterflow. Fuel is distributed on the top of the bed and moves down through the bed as it is consumed. The fuel in crossflow reactors moves at right angles to the direction of the air flow. Travelling grate and inclined grate reactors use this process. The fuel is deposited at one end of the grate and moves across the airflow as it burns. Underfeed reactors are combined cocurrent and crossflow. As the fuel is pushed up from underneath the grate, cocurrent flow occurs; once the fuel has been pushed up, it travels along the grate in crossflow. Overfeed and crossflow are the most common type of packed bed reactors and have similar combustion zones.

Figure 1.1 shows the cross-section of a typical overfeed packed bed. Fresh fuel is continuously added to the top of the bed to maintain a constant bed height. As the fuel

particles burn, they become progressively smaller and move down toward the grate. Once the fuel is completely consumed, the remaining ash either falls through the grate bars or builds up in the bed. The combustion products leave through the top of the bed. Combustion in an overfeed bed occurs in a number of steps. The fresh fuel is first heated and dried by the burning in the lower portions of the bed. Once the fuel is hot, chemical decomposition will occur and volatiles (light hydrocarbons, "tars," CO and CO_2) will evolve and then burn in the gas phase. After devolatilization, a residual solid composed of carbon and ash, called char, remains and is consumed by solid phase reactions. In the oxidation zone, the incoming O_2 passes through the grate and ash layer and reacts with the char to produce CO. The CO is then oxidized in the gas phase to CO_2; this reaction is highly exothermic. If the bed is thick enough, all the O_2 will be consumed and the CO_2 concentration and temperatures will reach a maximum. The CO_2 is then reduced to CO by the endothermic reduction reaction. Overfire

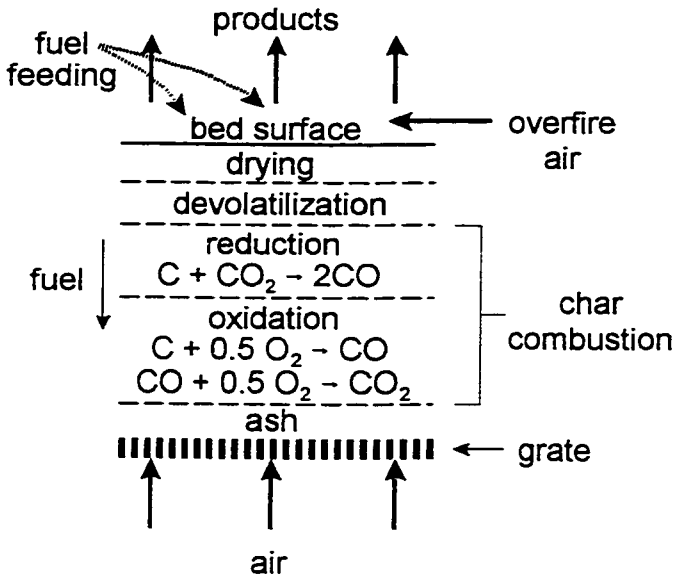

Figure 1.1 Combustion zones in an overfed packed bed reactor.

air is usually introduced above the bed to burn off the CO and volatiles produced. This study focuses on char combustion, creating a foundation for later work on volatile evolution and combustion.

Packed bed reactors can be classified as combustors or gasifiers, the difference being the thickness of the fuel bed. Gasifiers have thick beds (up to several meters) with the focus on the production of CO. Combustors are run with thin beds and produce heat for steam generation. The CO_2 produced by combustors has no industrial importance and is exhausted with the other combustion products. The focus of this research is the use of packed bed as a combustor where the main concern is predicting the concentrations of various pollutants in the combustion gases.

The temperature and chemistry in a packed bed are highly non-uniform and strongly dependent on the bed geometry and operating conditions. Thus, to be able to predict the formation and destruction of pollutants it is necessary to have a complete description of the bed processes. The first step in this research was the development of a numerical model by Cooper (1996) which describes char combustion in an overfeed reactor. Owing to a lack of suitable modern data, model validation has only been done using old data (Nichols, 1935).

In the packed bed combustion of solid fuels, the formation and accumulation of ash particles can have a significant influence on the bed processes, including combustion, heat and mass transfer, and solid and gas flows. Ash can affect the efficiency and operation of combustion systems by fouling reactor walls and heat transfer surfaces. Ash also plays a role in the amount of unburnt carbon losses. Another concern is the pollutant properties of ash (particulate emissions, sulfur formation and transport of heavy metals). Even though ash can

have a significant effect of fuel bed processes, it is an aspect of bed combustion which has been largely neglected. As ash is always present in solid fuel combustion there is a need for understanding the nature and behaviour of ash during the combustion of solid fuels.

1.1 Objectives

During this study, an overfeed packed bed reactor was designed and constructed. Controlled combustion experiments were performed to obtain more detailed knowledge and information on char combustion in a packed bed. The main purposes of these experiments were first to model the behaviour of ash in a fuel bed and incorporate it into the existing numerical model (Cooper, 1996); secondly, to validate the modified char combustion model by comparing experimental species concentrations, temperatures and burning rates with model predictions; and finally, to study the effect of operating conditions, including air flow and bed depth, on the burning rate and on temperature and gas concentration profiles.

A review of previous experimental studies on packed bed combustion, methods for obtaining accurate experimental data in combustion systems and previous attempts at modelling ash formation in a packed bed is contained in the following pages. The char combustion model is also described, including the equations required to model ash formation, migration and accumulation and the effect of ash on heat and mass transfer processes. This is followed by a section describing the experimental apparatus, instrumentation, fuel and experimental procedures. Finally, the experimental results are presented and used to validate the char combustion model (including the ash sub-model) and examine the effect of operating conditions on packed bed combustion.

2.0 LITERATURE SURVEY

A summary of previous experimental studies having a similar scope to this study is presented. The experimental apparatus, instrumentation and procedure of these previous studies were used as a starting point for the design of this work. A review of measurement devices and techniques for accurate measurement in reactive flows is also presented. In packed beds, fluid-particle interactions are dependent on the size, shape and density of the particles (Geldart, 1990). For accurate modelling of experiments, characterization of the particles and the bed is therefore necessary. An overview of previously used methods is presented and their suitability for this study is examined. The final section focuses on the formation of ash in fixed beds and previous attempts at modelling ash.

2.1 Past Experimental Studies on Packed Bed Combustion

This section details previous work done on the packed bed combustion of coke and coal. Coal combustion studies were included as coke (char) combustion occurs when coal is burned. In the majority of the studies the reactors were run as gasifiers rather than combustors. While gasifiers are not totally relevant to the present study, because thick beds make the oxidation zone much less important, they were included owing to the lack of information on combustors. Outlined are the objectives of each of the studies, a brief description of the apparatus and a summary of the conclusions. Table 2.1 contains the operating conditions used in each of the studies. In all cases, the combustion air was kept constant for a given experiment and was supplied from below the grate (except for Arai et al.

Table 2.1 Summary of the operating conditions used by the experimental studies reviewed in the literature survey.

Source	Fuel	Particle Diameter (cm)	Bed Depth (cm)	Bed Diameter (cm)	Burning Rate (kg/m^2hr)
Kreisinger et al. (1916)	Coal & Coke	3.2	15 & 30	34	97 - 902
Nichols (1935)	Coke	2.5 - 3.8	61	51	122
Marskell and Miller (1946a,b)	Coal	0.6 - 1.3	15	30	84 - 454
Dunningham (1950)	Coke & Coke	0.3 - 3.8	15 & 30	30	49 & 84
Moles and Thring (1958)	Coke	0.6 - 2.5	15	24	0.88 - 5.3
Rogers et al. (1972)	Wood Paper Glass Metal	~4.4x4.1x1.9 ~14.6x6.4 ~7.6x5.7 ~10.2x8.6	76	79	107
Eapen et al. (1977)	Coke	1.0 - 2.5	45	16 x 39	25 - 122
Goldman et al. (1984)	Coal	1.5	40 - 120	16 x 39	4 - 18
Bhattacharya et al. (1986)	Char	0.2	86	8.9	22
Arai et al. (1989)	Sludge-char	0.3-0.6	61	8.3	11 - 23
Ford et al. (1992)	Coal	not reported	140	30	39 - 152

(1989) who used a parallel flow reactor). With the exception of Moles and Thring (1958), who used a water-cooled reactor, a refractory-lined reactor was used in all of the studies.

In most of the previous experimental studies no fuel feeding was performed, so that the bed level dropped as combustion progressed. These transient tests used a fixed bed reactor to simulate a travelling grate. This is possible if the top of the bed is ignited and the ignition plane travels down through the bed burning the fuel until all that remains is ash. To compare the data with a real travelling grate, the time taken for an experiment has to be correlated with the distance the fuel would have moved along a travelling grate.

In the earliest of these transient studies, Marskell and Miller (1946a) investigated the effect of combustion rate on the composition of the fuel bed by analysing the fuel bed at intervals. The reactor consisted of a series of 2.5 cm separable rings with a grate made of stoker links (small sections of a travelling grate). The experiment was started and after a set time, the primary air was shut off and the bed was sampled as quickly as possible. A metal tray was inserted below each ring (giving a 2.5 cm sample) and the sample was placed in a container immersed in cooling water. The samples were then analysed for ash and volatiles using standard methods. The analysis indicated that at low combustion rates coal combustion occurs in two distinct stages: volatile combustion and char combustion, with char combustion not occurring until the volatiles have been completely evolved and burned. At higher reaction rates, however, the volatiles and carbon consumption occur simultaneously as the fuel travels down towards the grate.

A second study by Marskell and Miller (1946b), using the same apparatus, investigated the effect of primary air temperature and flow rate on the combustion rate and

bed temperatures. Bed temperature measurements were obtained with six platinum/platinum rhodium thermocouples spaced vertically, 2.5 cm apart. These were contained in a single refractory sheath which was inserted vertically into the bed. Increasing the primary air temperature was found to decrease the ignition time but not affect the maximum bed temperature or the combustion rate. However, increasing the air flow rate was shown to increase the ignition and combustion rates. Also, at higher rates the maximum temperature decreased slightly.

Dunningham (1950) looked at the factors affecting temperatures in fuel beds. Experiments were performed in a reactor with a layer of crushed silica at the bottom, which acted as a grate. A thermocouple, sheathed in a refractory tube, was inserted vertically into the bed to obtain temperature profiles. Experiments studied the effect of burning rate, fuel size and fuel reactivity on the fuel bed temperature. It was found that the bed temperatures were hottest nearest the grate (oxidation zone) and deceased higher in the bed (due to the endothermic reduction reaction), and that higher burning rates increased the bed temperatures. The size of the fuel had little effect on the temperatures in the oxidation zone, but in the reduction zone smaller sizes resulted in lower temperatures. Fuel rank also had little effect in the oxidation zone, but in the reduction zone a lower rank would give lower temperatures. As lower ranked coals are more reactive to CO_2, this is a result of the extent of the endothermic reduction reaction.

The largest-scale reactor found in the literature was used by Rogers et al. (1972) to study the combustion of refuse under conditions found in a typical travelling grate incinerator. An examination of the effect of the primary airflow on burning and ignition rates and the

combustible content of the gases exiting the bed was performed. A radiant heat flux was used to ignite the bed. Chromel-alumel thermocouples measured temperatures and water-cooled probes obtained gas samples through 27 sample ports located 2.5 cm apart. The gas samples were analysed continuously for O_2, CO and CO_2. Heat leakage from the fuel bed was measured using thermocouples inserted in the reactor's refractory lining. A load cell measured the weight of the fuel bed. The feedstock was a combination of the materials listed in Table 2.1 and had an average composition of 30% water, 16% inert and 54% combustible. Results from preliminary experiments showed that different burning rates were obtained before and after the fuel was completely dried. Also, near the end of a run the burning rate and over-bed CO_2 concentrations drop dramatically. It was found that with some operating conditions the overfire air requirements were greater than the primary air requirements.

Eapen et al. (1977) looked at the kinetics of the reduction reaction. Experiments were carried out on coke in a reactor with a grate of perforated steel. Gas samples at various heights in the bed were obtained using vertical water-cooled probes. The concentrations of O_2, CO_2 and CO were measured using on-line analysers. A thermocouple, inserted vertically in the bed, obtained temperature profiles. Their conclusion was that the reaction rate in the oxidation zone is controlled by diffusion and in the reduction zone by chemical kinetics. The density of the bed contents was found to be constant, indicating that although the reduction zone was kinetically controlled, internal burning inside the fuel particles was not significant.

Experiments were performed by Goldman et al. (1984) to validate a computer model. This work is believed to be the first model to be fully validated using both temperature and concentration measurements. The reactor was run as a coal gasifier rather than a combustor,

with a very deep bed. Gasification was done with air and air/steam mixtures (steam is added to the primary air to produce hydrogen by the water gas reaction). The reactor had 20 ports spaced 6.4 cm apart for insertion of temperature measurement and gas sampling devices. A gas chromatograph analysed the gas samples for O_2, N_2, CO and H_2; CO_2 was measured using an absorption method. In general, the agreement between predicted and experimental profiles was acceptable. The best agreement occurred when the primary air contained steam.

A model proposed by Bhattacharya et al. (1986) for fixed bed char gasification was validated using temperature profiles from an experimental reactor. Two fixed vertical thermowells, located in the centre and at the wall, contained a total of twelve thermocouples for measuring the bed temperatures. Comparison of experimental and model predictions of the axial temperature profiles showed good agreement initially. However, a comparison of temperature histories showed less agreement, with the disagreement increasing with time.

The most recent investigation found was done by Ford et al. (1992). A laboratory scale fixed-bed reactor was used to simulate industrial scale gasifiers. Four ports at intervals of 4 cm above the grate allowed for the insertion of thermocouples into the bed, and product gases were analysed for CO, NO_x and SO_2. Data collected from industrial plants was compared with the data obtained from the laboratory reactor. A comparison of bed temperatures, gasification rates and efficiencies showed good agreement. Product gas compositions were also similar, except for the CO concentrations.

Four studies were found which were performed at steady state, with fuel being fed into the top of the bed at intervals to maintain the bed height and the ash produced being allowed to fall through the grate. Kreisinger et al. (1916) performed a series of experiments

to study the combustion processes in an overfeed reactor. The reactor contained holes through which gas sampling and temperature probes could be inserted radially into the bed at intervals of 3.8 cm above the grate. Gas samples were obtained using water-cooled probes and were analysed for CO_2, O_2, H_2, CH_4 and unsaturated hydrocarbons using a modified Hempel apparatus. Bed temperatures were measured using an optical pyrometer focused on holes poked in the bed. For a constant bed height, the gas compositions were found to be independent of air supply, indicating that fuel beds are self-regulating. Also, fuel beds need to be no thicker than 10 to 15 cm to obtain high CO_2 and low O_2 concentrations in the products leaving the bed. Thick beds were found to increase the chance of "clinker" formation (i.e. fusion of ash). Also, overfire air needs to be supplied to obtain complete combustion of the product gases.

Nichols (1935) studied the effect of air preheat on combustion processes in an overfeed reactor, with a steel bar grate. Sampling ports were located at 3.8 cm intervals above the grate. Water-cooled probes used for sampling gases and optical pyrometers used for measuring bed temperatures could be inserted into these ports. The gas samples were analysed for O_2, CO_2 and CO using the Orsat analysis technique. It was found that increasing the air temperature increased the burning rate, the rate of CO production and the bed temperatures.

The concentration and temperature data presented by Kreisinger et al. (1916) and Nichols (1935) are actually averages of all the measurements (at a given bed height) taken over the course of a test. While every attempt was made to remove all of the ash and clinkers formed, some still remained in the bed, causing non-uniform conditions. Some of the

individual values for a given height differed substantially, influencing the average value (Nichols, 1935).

Moles and Thring (1958) studied the minimum burning rates in fuel beds, obtaining data on combustion rates near the lower extinction limit. The apparatus had a cast-iron grate and temperature measurements were taken by refractory-sheathed thermocouples (type-K) at 3.8, 7.6 and 11.4 cm above the grate. The thermocouples were inserted vertically into the bed. Once the bed was ignited, the primary air was reduced to a preset value, with the minimum air rate determined by trial and error. The lower extinction limit was found to be characterized by stable temperatures. Also, the minimum burning rate was found to be highly dependent on the type of fuel.

Arai et al. (1989) burnt sludge-char in a parallel-flow reactor to examine the effect of NH_3 injection on the reduction of NO_x. Axial temperature and concentration (CO_2, CO, O_2, N_2, NO and NH_3) measurements were obtained through five fixed sampling ports. NH_3 was found to dramatically reduce NO_x, but only at air-to-fuel ratios of 1.05-1.3. The experimental measurements were also used to validate a char combustion simulation; good agreement between experimental values and model predictions was obtained.

2.1.1 Conclusions

A significant amount of previous research has been done to further the understanding of packed bed combustion. However, these studies do not provide sufficiently detailed data regarding the processes occurring inside the fuel bed. Most of the studies focused on the effect of operating conditions on the burning rate and temperature profiles, while only four

studies measured gas concentrations in the bed. Concentration profiles are important as they show the formation and destruction of species in the bed and give direct information on the progress of reaction. Also, as most of the studies used fixed ports for insertion of the measurement devices into the bed, it was impossible to obtain the necessary resolution to map the steep gradients in the oxidation zone.

Detailed data on temperature, gas concentration and composition profiles are needed for validating fixed-bed models; however, as noted by Hobbs (1993), there is a serious lack of this type of data in the literature. Only four of the studies reviewed have both temperature and concentration profiles. Even these are lacking information (i.e., fuel density and bed void fraction) which is required to fully validate a model. Unfortunately, the two studies which are the most comprehensive (Kreisinger et al., 1916 and Nichols, 1935), are dated. Questions could be raised about the accuracy of the sampling methods and of the equipment used. Also, the inability of these experimenters to completely remove the ash and clinkers formed affect the accuracy of the data.

Due to this lack of detailed experimental data, it was decided to undertake controlled experiments which would study both the effect of operating conditions on packed bed combustion processes and provide data which could be used to validate the char combustion model of Cooper (1996).

2.2 Instrumentation

The evaluation and verification of combustion models require accurate combustion measurements. One purpose of the experiments was to provide detailed profiles of

temperature and gas concentrations in a fuel bed. A review of the instruments and methods used to obtain representative data is included in the following sections. The main considerations in the choice and design of these measurement devices were the high temperatures and the presence of O_2 and CO.

2.2.1 Concentration Measurements

Combustion gases are typically obtained using gas sampling probes which draw gas from a fixed point in a bed. To obtain accurate gas samples in reactive flows, two requirements have to be met. First, in order not to disturb the flow in the bed the probe has to sample isokinetically. Secondly, effective quenching of the sample is required.

The criterion for isokinetic sampling in a flame is that the velocity of the gas entering the probe be equal to the velocity of the gas in the undisturbed (no probe) flow stream. In an unbounded gas flow, this is usually accomplished by matching probe wall static pressure to the free stream static pressure (Becker, 1993). No criterion for isokinetic gas sampling in a bed of stationary particles has been found in the literature.

The high temperatures and the presence of CO and O_2 mean that it is necessary to immediately quench the sample drawn into the probe, "freezing" the species concentrations. Quenching is usually accomplished by rapid temperature or pressure reduction. Common quenching mechanisms used in gas sample probes are convection, expansion and mixing. With convective quench probes, the sample is cooled by convective heat transfer to a coolant stream across the sample tube wall. The probe mouth and sample tube are of a constant diameter over the distance required for quenching. Further down the sample tube may

enlarge to reduce pressure drop (Becker, 1993). The coolant is typically water, though sometimes heat transfer liquids are used. Fast expansion of the sample stream through a small sonic nozzle is the technique used in expansion quench probes. Typically, the inner diameter of the probe diverges before coming to a constant diameter. Expansion probes are usually not employed when particulates are present, as the small sample tube can become easily clogged. Mixing quench probes cool and dilute the sample by mixing it with a cool stream of inert gas. Bilger (1976) reviewed quenching rates of a number of probes in the literature and found that expansion probes have cooling rates from 10^8 to $2 \cdot 10^6$ K/s and convective-type probes have rates of the order of $2 \cdot 10^6$ K/s.

2.2.2 Temperature Measurement

It is well recognized that platinum-rhodium alloys are reliable sensing elements for the high temperatures expected in combustion applications. However, the bare metal surfaces act as a catalyst for radical recombination reactions. These exothermic reactions cause additional energy to be transferred to the junction, resulting in the thermocouple reading a higher temperature than the surrounding environment. Leah and Carpenter (1952) have shown that bare platinum thermocouple wires will catalyze the combustion of CO and O_2. This source of error can be eliminated by coating the thermocouple with a non-catalytic coating. In the literature, a number of different coatings have been employed for this purpose. Kaskan (1956), Cookson et al. (1964), Fristrom and Westenburg (1965) and Madson and Theby (1984) have used a "flame-plating" technique to coat thermocouples with silica, thereby eliminating the catalytic effects. This technique involves aspirating

hexamethyldisiloxane into propane. The mixture is burned in a Meker burner and the coating is formed by passing the thermocouple through the flame which contains silica particles. Friedman (1952) and Burton and Ladouceur (1992) attempted the silica coating, but found it too fragile to be useful. Another, more durable coating was proposed by Kent (1970), who painted a mixture of yttrium and beryllium oxide onto the thermocouples in several thin coats, firing between each coat. Becker (1993) notes that extreme caution should be taken by persons handling beryllium due to its high toxicity. A study by Heitor and Moreira (1993) has shown that alumina-based coatings are also commonly used. After the silica coating failed, Burton and Ladouceur (1992), tried a commercially available high temperature alumina-based adhesive, consisting of alumina in a silicate base (Aremco's Ceramabond 569). The coating was found to eliminate catalytic effects, to be very durable and to adhere well to the thermocouples. This technique involves dipping the thermocouple leads into the liquid adhesive and then firing according to the manufacturer's instructions.

2.3 Particle Characterization

The size and shape of the fuel and ash particles affect the processes in the bed, and therefor the particles have to be characterized as to their size, shape and density. Size and shape are easily specified for regular particles, such as spheres or cubes, but for irregular particles these are not as well defined. The following sections review characterization methods for porous irregular particles and methods for determining the characteristics of a bed of particles (void fraction and density).

2.3.1 Diameter

Normally, the screen size is used to define the particle diameter for irregularly shaped particles (McCabe et al., 1990). The arithmetic average of the smallest and largest particle diameters in the increment is used. However, for particles which can be identified individually, a more accurate method is to weigh a known number of particles (Geldart, 1990 and Lin et al., 1990).

For a mixture of particles having a wide range of sizes, an average value for the diameter is used. McCabe et al. (1993) list a number of standard definitions for the average particle size of a mixture: volume-surface mean diameter, arithmetic mean diameter, mass mean diameter and volume mean diameter. According to Geldart (1990) the relevant particle size for packed beds is the volume-surface mean diameter. Calculation of the volume-surface mean diameter requires the sample to be sorted into fractions of approximately constant size. For the size range expected in fuel beds, Geldart (1990) states that screening is the most practical method.

2.3.2 Density

A bed of particles is defined by two densities: the bulk density, ρ_B, and the particle or apparent density, ρ_S. The bulk density is the density of all of the bed as a whole (including voids) and the apparent density is the density of an individual particle ("apparent" because it includes the pore volume).

For porous irregular particles, the particle density is not easily obtained. The difficulty in determining the particle density lies in the determination of the volume of the particle, as

the weight determination of a solid is not a problem. The literature has a number of methods for determining the particle density. According to Geldart (1990), there are seven techniques for indirectly measuring the particle density of a porous solid: mercury porosimeter, caking end-point, comparative, gas flow (permeametry), photographic, powder displacement and minimum fluidization velocity. Geldart (1990) concludes from a comparison of these methods that the gas flow technique is the best. This method, proposed by Ergun (1951), requires that the bed be packed to different bulk densities. However, this is usually difficult to achieve. Ergun (1951) also reviewed density calculation techniques, one of which was liquid immersion, in which solid particles are immersed in a liquid and the volume displaced is measured. The problem with porous solids is that the liquid will penetrate some distance into the pores, resulting in a density value which is in between the particle and true solid density. To eliminate this problem, a variety of liquids have been tried to reduce the degree of penetration. Another modification is to first soak the solids in the liquid to impregnate the pores; the liquid is then drained, after which the solid is re-immersed to determine the displacement volume. According to Lowry (1963), the liquid immersion methods are commonly used in the determination of the apparent density of coals. The ASTM Standard D 167-93 "Standard Test Method for Apparent and True Specific Gravity and Porosity of Lump Coke" is also based on this technique.

The only method found in the literature for determining the bulk density of a bed of particles was by measuring the volume occupied by a bed of known weight. This method has been used by a number of different researchers, including Margiatto and Siegell (1983), Ichida

et al. (1991), Lin et al. (1990) and Hinkey and Waters (1990) and was thus deemed acceptable.

2.3.3 Bed Void Fraction

The bed void fraction, ε, is the voidage due to the interstitial voids between the particles. From the experimentally measured bulk and particle densities, the void fraction of the bed can be determined through the following relationship

$$\varepsilon = 1 - \frac{\rho_B}{\rho_S} \tag{2-1}$$

2.3.3.1 Binary Mixtures

When two particle sizes are mixed the packed bed void fraction will change, as the smaller particles will fill the voids between the larger particles. Three equations were found in the literature which predict the void fraction of binary particle mixtures as a function of the proportions of large and small particles. Yerazunis et al. (1962) proposed an empirical relation for determining the void fraction of randomly packed binary mixtures of spheres. A geometrical model was developed by Aim and le Goff (1967/1968). A comparison of experimental and calculated void fractions for spherical particles showed good agreement for both of these relations. However, there was no indication in the literature as to whether these relations could be extended to non-spherical particles. Westman (1936) developed an empirical relation which contains a single fit parameter. Only two relations for the fit parameter for non-spherical particles were found in the literature. Yu et al. (1993) proposed

an empirical relation which is based on the equivalent packing diameter of non-spherical particles. The equivalent packing diameter is related to the particle's equivalent volume diameter through the sphericity and three empirical constants. Comparisons of predictions with experimental results indicate that the void fraction of non-spherical binary mixtures can be adequately predicted using the Westman equation and the proposed parameter of Yu et al. (1993). Another relation has been proposed by Finkers and Hoffmann (1998). A structural ratio, defined as the ratio of the volume of a small particle and its associated interstitial region to the volume of the interstitial region associated with a large particle (Finkers and Hoffmann, 1998), is used. The method proposed relates the ratio to the fit parameter through one empirical constant. Finkers and Hoffman (1998) evaluated the proposed relation using a considerable number of experimental measurements from the literature and found it predicted the void fraction of both spherical and non-spherical binary mixtures very well.

2.3.4 Sphericity

The shape of a particle is described by its sphericity. Sphericity is defined by Wadell (1932) as the ratio of the surface area of a sphere having the same volume as the particle to the actual surface area of the particle. With irregularly shaped particles, a direct calculation of the surface area from particle measurements cannot be made. Ergun (1952) reviewed various methods which have been developed to measure surface area. The methods include dissolution, adsorption, size analysis, photometric analysis and permeametry. Permeametry uses a packed bed flow equation to calculate the surface area from pressure drop and flowrate

measurements. Ergun (1952) developed a permeametry method to determine the specific surface area of coke particles using the Ergun pressure loss equation. Wagstaff and Nirmaier (1955) compared the work done in five investigations of different methods of determining surface areas. Wood and plastic particles with a known surface area were used. They concluded that the best estimate of surface area is obtained from the method proposed by Ergun (1952). The permeametry method proposed by Ergun (1952) has been used by a number of investigators to determine the surface area of porous materials: Rankin et al. (1985), Hinkley and Waters (1990), Lin et al. (1990), Ichida et al. (1991).

When particles are packed into a cylindrical container, the radial distribution of the void fraction is not uniform due to the wall. The void fraction close to the wall is larger than the rest of the bed; this is called the "wall effect." An increase in the void fraction reduces the resistance to flow, resulting in an increase in the velocity. "Wall effect" is measured by the aspect ratio, bed diameter to particle diameter (d_B/d_P). Schwartz and Smith (1953) have shown experimentally that as the aspect ratio decreases, significant velocity variations exist in the bed. For ratios less than 30, the "wall effects" become significant. Mehta and Hawley (1969) concluded that "wall effects" are not significant if the ratio is greater than 50. Mehta and Hawley (1969) have modified the Ergun equation to include the effects of the wall. A parameter is defined to take into account the effect the aspect ratio has on the hydraulic radius. Experiments performed by Mehta and Hawley (1969) show that for aspect ratios, ranging from 91:1 to 7:1, including the "wall effects" in the Ergun equation greatly improved the predictions of the sphericity.

2.4 Ash

The mineral matter (inorganics) in coal is transformed to ash during combustion. Mineral matter in coal is primarily composed of discrete mineral particles, the major groups being silicates, oxides, carbonates, sulfides, sulfates, phosphates (Benson et al., 1993). However, the specific types vary with the rank of the coal. Coal ash contents range from 5%-40%.

The physical and chemical transformation of the mineral matter into ash is dependent on the chemical composition of the mineral matter and the operating conditions of the reactor. Decomposition, melting, volatilization and increased chemical activity can all occur during the transformation (Ely and Barnhart, 1963). This results in the ash produced having a different chemical composition than the original mineral matter.

Depending on the type of reactor and the operating conditions, ash can be formed as fly ash, sintered ash or molten slag. In fixed beds, the ash is formed primarily as sintered particles which move downwards with the fuel and either collect on the grate or fall through the grate spaces. The ash particles formed may soften and coalesce with other particles. As they move to cooler regions in the bed they resolidify and sinter together, forming agglomerates. Small agglomerates do not affect a fuel bed's operation; however, large agglomerates or clinkers are unwanted as they cause uneven flow distributions in the bed. The formation of clinkers can be eliminated by operating at low temperatures or using high ash fusion temperature coals. For the continuous operation of packed beds, the ash has to be removed, by either shaking or dumping the grate.

Most of the information regarding mineral matter transformation is from studies on pulverized coal (Solomon and Beér, 1987). Fouling of heat transfer surfaces by ash is a major problem in pulverized coal boilers. Therefore, most of the studies done (experimental and modelling) looked at fly ash formation and deposition on heat transfer surfaces. Also, work has been done on determining the distribution, composition and size of the mineral matter in an attempt to predict ash behaviour as a function of coal composition and operating conditions; however, this has not had much success (Solomon and Beér, 1987).

There is very little information in the literature on ash in fixed beds. Smoot and Smith (1985) summarized the effects that the presence of ash can have on combustion processes in a packed bed. The difference in the properties of the ash and the fuel can affect the thermal properties in the bed. Ash will also affect radiation in the bed by providing another medium for radiative heat transfer. Some of the minerals present in the ash, in particular calcium (Essenhigh, 1981) and iron (Gransden, 1997), have been shown to increase char reactivity. Also, the presence of ash hinders the mass transfer of the reactants to the surface of the particles.

Solomon and Beér (1987) state that modelling of ash requires the prediction of the conversion of mineral matter into ash, the properties of the ash produced (size, composition, optical properties and fluidity) and the ash concentrations in the reactor. The following section outlines the modelling of ash in packed beds which has been done previously.

2.4.1 Modelling of Ash in Packed Bed Reactors

In the literature there exist two different models describing ash formation in char combustion: shell progressive and ash segregation. The shell progressive mechanism assumes that the ash produced during combustion remains attached to the fuel particle, forming a layer of ash around an unreacted core. Reactants and products of char combustion must diffuse through this ash shell. The ash segregation model assumes that the ash produced crumbles completely away from the fuel particle and is formed as particles of a fixed diameter. Figure 2.1 illustrates the two ash production mechanisms.

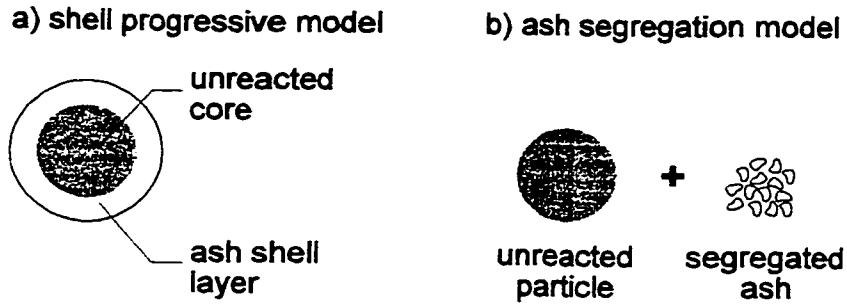

Figure 2.1 Schematics of the two models describing ash formation in a fixed bed.

Cooper (1996) reviewed the more successful of the existing coal conversion simulations. This section summarizes the modelling of ash in these simulations. Goldman et al. (1984) do not seem to take account of the production of ash in their model, even though the model predictions are being compared to experimental results obtained from a reactor in which the ash builds up. They state that at the time sampling was started, the top of the ash layer was taken as the origin and that measurements were completed as quickly as possible

to eliminate concentration shifts caused by ash build-up. Barriga and Essenhigh (1980) used a layer of ash at the bottom of the bed to preheat the air, as the model required an initial high temperature for reaction to take place. Amundson and Arri (1978) assumed that no ash was produced in the reduction zone. However, once the particles enter the oxidation zone, an ash layer forms around each particle, creating a shell (shell progressive model), through which the reactants and products diffused. It was assumed that only O_2 diffused in and CO_2 diffused out. The temperature in the ash layer was defined as an average between the core temperature and the particle surface temperature, assuming a pseudo steady state profile. The models of Yoon et al. (1978), Yu et al. (1983), Bhattacharya et al. (1986) and Hobbs et al. (1992) had provisions to use either of the two ash production models. The reaction of a single carbon particle was calculated as a function of three resistances: resistance to bulk gas phase diffusion, diffusional resistance through the ash layer and the intrinsic reaction rate resistance. If the ash segregation model was used, the resistance through the ash layer was excluded. Also, with the ash segregation model, the carbon reaction rate was multiplied by the fraction of space occupied by the fuel particles. These models accounted for the amount of ash produced, but not for its effects on heat and mass transfer and on bed properties.

2.4.2 Ash Properties

Ash properties found in the literature were either for deposits on heat transfer surfaces (Benson et al., 1993) or for molten slags (Mills and Rhine, 1989). If the density of the ash is unknown, Elliott (1981) states an average value of 2700 kg/m^3 can be used. However, it is recommended that experimental values or mineral grain densities be used. The ash from

different coals can vary, which results in physical properties variations. Most of the above mentioned models assume that the ash and fuel properties are the same. Hobbs et al. (1992) used the model of Merrick (1983a) to calculate the specific heat of the ash.

2.4.3 Conclusions

While the presence of ash in a fuel bed can have a significant effect on the bed processes, it has been neglected in most of the existing packed bed models. Some models include the formation of ash; however the effect that it has on combustion, heat and mass transfer and solid and gas flows have been overlooked. Thus, it was decided to extend the model of Cooper (1996) to include the formation, migration and accumulation of ash in a packed bed.

3.0 NUMERICAL MODELLING

A computer program developed by Cooper (1996) simulates the combustion of char particles in an overfeed packed bed. The following sections outline the main features of the model and modifications made to simulate the present experiments. Also, changes made to the modelling of the reaction kinetics and the development and implementation of the ash model are described. The final section outlines the numerical method and solution technique.

3.1 Packed Bed Combustion Model

The packed bed combustion simulation developed by Cooper (1996) includes most of the relevant packed bed processes and does not contain the simplifying assumptions found in other models in the literature. Temperature and gas concentration changes are described by differential mass, species and energy balances. Separate solid and gas phase energy and mass balances are employed. Consumption of the particles is modelled using the shrinking particle model. The shrinking of fuel particles as they move down through the bed and are consumed is accounted for through a particle number balance. Finite rate kinetics models describe oxidation and reduction at the solid surface and CO oxidation in the gas phase. The reverse reaction for CO oxidation is included to account for dissociation at high temperatures. Also included are heat transfer in the gas and solid phases and heat and mass transfer between the two phases. The model is one-dimensional, so radial variations in temperature, concentration, velocity and particle size are neglected. Since combustor beds are generally thin, pressure gradients have also been neglected. All of the transient terms have been

included in the numerical model to study unsteady phenomena, e.g., ignition and extinction. The mass, species and energy balances are solved using the finite volume discretization techniques of Patankar (1980). At present, the model considers char combustion only; volatiles evolution and combustion are not yet included. The model predicts the changes in the gas and solid temperatures, gas (O_2, CO_2 and CO) concentrations and fuel particle size as a function of bed height. The numerical model is coded in Fortran and is included in Appendix B. Figure 3.1 shows the geometry of the fuel bed and the grate and Figure 3.2 shows the division of the bed and the grate into the control volumes.

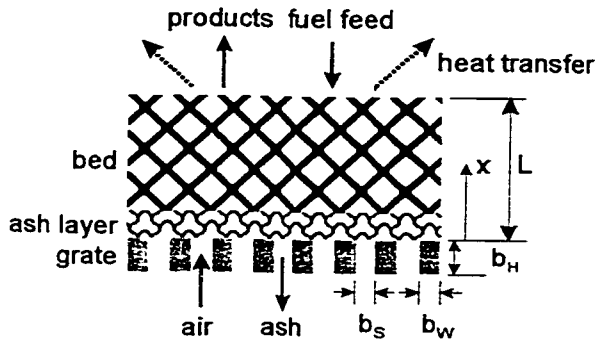

Figure 3.1 Schematic of the fuel bed and grate structure.

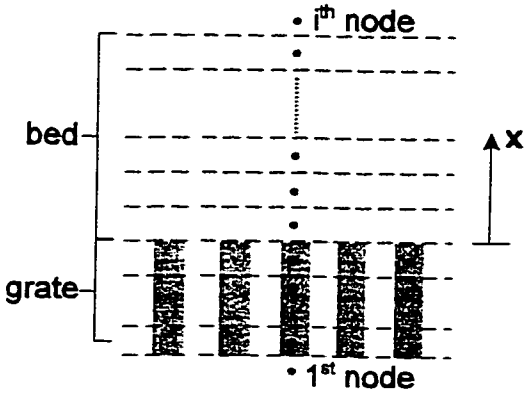

Figure 3.2 Schematic of the fuel bed and grate showing the control volumes.

3.1.1 Modelling of Experimental Apparatus

To ensure an accurate verification of the model, the model had to simulate the experimental apparatus. Modifications were made to include a grate and radiation boundaries which were representative of the experimental apparatus.

3.1.1.1 Grate

The model developed by Cooper (1996) modelled the grate as a packed bed of steel or refractory balls. As a steel bar grate was used in the experimental apparatus, a new grate model was required. The steel bar grate is treated as a series of straight bars defined by width, b_W, height, b_H, and spacing, b_S, see Figure 3.1. The spacing of the bars is defined by the solidity, which is given as

$$s_G = \frac{b_W}{b_W + b_S} \tag{3-1}$$

The void fraction of the grate is then given by

$$\varepsilon = 1 - s_G \tag{3-2}$$

The transport equations require values for the effective thermal conductivity of the solid and gas phases, the effective diffusivity and the heat transfer coefficient. In the grate, the only heat transfer mechanism is conduction, therefore the effective solid conductivity is given by

$$k_{Seff} = k_S s_G \tag{3-3}$$

where k_S is the thermal conductivity of steel. As the steel bar grate is not a packed bed there is no flow term in the expression for the effective gas thermal conductivity and diffusivity, which are given as

$$k_{Geff} = \varepsilon k_G \tag{3-4}$$

and

$$D_{ieff} = \varepsilon D_i \tag{3-5}$$

respectively. The heat transfer coefficient is obtained from a correlation for heat transfer to a cylinder in cross-flow (Holman, 1990)

$$Nu = \left(0.43 + 0.5\, Re^{0.5}\right) Pr^{0.38} \tag{3-6}$$

The specific surface of the grate in m^2 per m^3 of total bed volume was derived to be

$$a_B = \frac{2s_G}{b_W} \tag{3-7}$$

The specific surface of the first grate cell is larger than the rest of the grate because the frontal surface area of the bar has to be included (see Figure 3.2). This gives a specific surface of

$$a_B = \frac{2s_G}{b_W} + \frac{s_G}{\Delta x} \tag{3-8}$$

where Δx is the cell height.

Equations for calculating the thermal properties of the stainless steel, as a function of temperature, were derived from the data given in Smithells (1992). The thermal conductivity in W/mK is given by

$$k_S = 0.014T_S + 15.1 \tag{3-9}$$

and the specific heat in J/kgK is given by

$$c_P = 0.21T_S + 492.7 \tag{3-10}$$

The solid temperature, T_S, is in °C. The density of the grate bars was assumed to be 7920 kg/m^3 (Smithells, 1992).

3.1.1.2 Radiation Boundary Conditions

The radiation boundary condition at the top of the bed was modified to include the presence of refractory walls above the bed. This is illustrated in Figure 3.3 where the walls of the cooling jacket and the outside surroundings are considered to be at the same temperature (T_{BOILER}). The refractory surface above the bed is assumed to have zero heat flux. The net radiant heat transfer from the top of the bed to the cooling jacket ("boiler") is given by

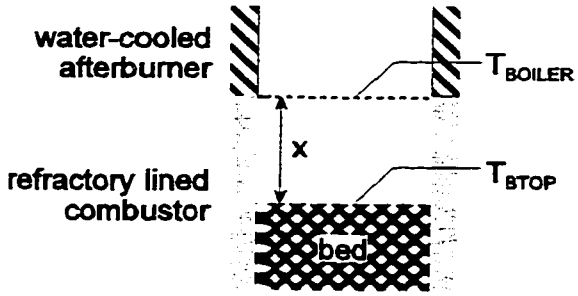

Figure 3.3 Schematic of the radiant boundary condition at the top of the bed.

$$\dot{q}_R = \sigma \overline{F_{T\infty}} \left(T_{BTOP}^4 - T_{BOILER}^4 \right) \tag{3-11}$$

where σ is the Stefan-Boltzmann constant, T_{BTOP} is the temperature at the top surface of the bed and T_{BOILER} is the temperature of the cooling jacket. $\overline{F_{T\infty}}$ is an effective view factor for two surfaces enclosed by a third which is non-conducting but re-radiating. Simplified by the fact that the area of the bed is equal to the area of the surroundings, it is given by (Holman, 1990)

$$\overline{F_{T\infty}} = \left[\frac{2}{\left(1 + F_{T\infty}\right)} + \frac{1}{\varepsilon_{RP}} + \frac{1}{\varepsilon_{R\infty}} - 2 \right]^{-1} \tag{3-12}$$

where ε_{RP} and $\varepsilon_{R\infty}$ are the emissivities of the particles and surroundings, respectively. $F_{T\infty}$ is the radiation shape factor for radiation between parallel disks given by (Siegel and Howell, 1972)

$$F_{T\infty} = \frac{1}{2}\left[1 + \frac{1 + \left(\frac{r_B}{x}\right)^2}{\left(\frac{r_B}{x}\right)^2} - \sqrt{\left(1 + \frac{1 + \left(\frac{r_B}{x}\right)^2}{\left(\frac{r_B}{x}\right)^2} \right)^2 - 4} \right] \tag{3-13}$$

where r_B is the radius of the bed and x is the height of the refractory surface above the bed.

The original model included radiation from the bottom of the grate to the ashpan; however, it neglected radiation from the bottom of the bed through the spaces between the grate bars. Net radiant heat transfer from the bottom of the bed to the ashpan is given by

$$\dot{q}_R = \sigma \overline{F}_{B\infty}\left(T^4_{BBOTTOM} - T^4_{ASHPAN}\right) \tag{3-14}$$

where $T_{BBOTTOM}$ is the temperature of the bottom surface of the bed and T_{ASHPAN} is the temperature of the ashpan. Assuming that the sides of the grate bars act like refractory surfaces, the effective view factor, $\overline{F_{B\infty}}$ can be given by the same expression as equation (3-12):

$$\overline{F_{B\infty}} = \left[\frac{2}{\left(1 + F_{B\infty}\right)} + \frac{1}{\varepsilon_{RP}} + \frac{1}{\varepsilon_{R\infty}} - 2 \right]^{-1} \tag{3-15}$$

$F_{B\infty}$ is approximated as the view factor between two infinitely long parallel plates and is given by (Siegel and Howell, 1972)

$$F_{B\infty} = \sqrt{1 + \left(\frac{b_H}{b_S}\right)^2} - \frac{b_H}{b_S} \tag{3-16}$$

The fuel particle emissivity was assumed to be 0.8 and the surroundings emissivity was assumed to be 1.0. The modifications made to the radiation boundary conditions had little effect on the temperature predictions (less than 50 K at a given bed location).

3.2 Char Reaction Kinetics

With porous particles, the overall reaction rate may be influenced by diffusion and reaction in the pores. However, the rate expressions for the particle surface reactions used originally in the packed bed combustion model did not account for this effect. The carbon oxidation reaction employed the widely-used rate expression of Field (1969)

$$K_{O_2} = 860 \exp\left(\frac{-18000}{T_S}\right) \tag{3-17}$$

and the rate of CO_2 reduction used the correlation of Goetz et al. (1982)

$$K_{CO_2} = A\,exp\left(\frac{-E}{RT_S}\right) \tag{3-18}$$

where values for the activation energy, E, and pre-exponential factor, A, for four different coal chars were given.

As it is well known that the structure and porosity of the char affects the reactivity, a more realistic model would account for internal char reaction. Also, the char oxidation and reduction reactions occur over a wide temperature range and may be controlled by kinetics or mass transfer. To include these effects an effective reaction rate, K, based on particle external surface is used (Hallett, 1996)

$$K = \frac{d_{PC}}{6}\eta_P a_I K_I \tag{3-19}$$

The intrinsic reaction rate K_I is the reaction rate based on pore surface area and is related to the effective reaction rate through the specific internal (pore) surface area a_I and the effectiveness η_P, which accounts for pore diffusion limitations. The theory for this is the same as for a porous catalyst particle, and gives the effectiveness for a particle as (Bird et al., 1960)

$$\eta_P = \frac{3}{\phi^2}\left(\phi\,coth\,\phi - 1\right) \tag{3-20}$$

where ϕ is the Thiele modulus, defined as the ratio of the reaction rate to the pore diffusion rate (Bird et al., 1960)

$$\phi = r_{PC}\sqrt{\frac{K_I RT_S}{M_C}\frac{1}{D_{eff}}} \tag{3-21}$$

where r_{PC} is the radius of the particle, R is the gas constant and M_C is the molecular weight of carbon. The effective diffusivity of the gas in the pores is given by (Denbigh and Turner, 1984)

$$D_{eff} = \frac{D\varepsilon_P}{\tau} \tag{3-22}$$

where D is the diffusivity of the gas, ε_P is the particle internal void fraction and τ is the tortuosity of the pores.

The pore diffusion model requires knowledge of the structure of the fuel particles including the internal surface area, particle porosity and tortuosity. The internal surface area of cokes and coal chars has been found to vary from 1 to 10^3 m^2/g by Smith (1982). Valix et al. (1992) obtained values in the range of 10^2 m^2/g for the total surface area of chars and states that the tortuosity can vary from 1 to 10. Thibaut (1963) listed 18 cokes with void fractions ranging from 0.46 to 0.56.

3.2.1 Char Oxidation Reaction

The intrinsic rate for the char oxidation reaction has been given by Smith (1978) as

$$K_{IO_2} = 678 exp\left(\frac{-179400}{RT_S}\right) \quad (3\text{-}23)$$

It was not expected that including internal (pore) reaction should greatly affect the char oxidation rate, as in the oxidation zone, the high temperatures produced by the exothermic reaction result in this zone being largely controlled by diffusion rather than by chemical kinetics (Cooper, 1996).

3.2.2 Char Reduction Reaction

The rate of the reduction reaction is known to depend on the structure of the char (Goetz et al., 1982). Thus, inclusion of the pore reaction model should have an effect on the reaction kinetics in the reduction zone. As the literature contains no intrinsic rate data for the reduction reaction, initially the rate coefficients given by Goetz et al. (1982) were used.

3.3 Ash Sub-Model Development

Originally, the numerical model assumed that all of the ash produced fell through the grate with a mass flux equal to the feed fuel ash content. However, in the present experiments ash builds up in the bed. An ash sub-model was therefore developed for inclusion in the packed bed combustion model of Cooper (1996). The model assumptions are based on experimental observations of the behaviour of the ash.

Based on the experimental observations described in section 5.1.2 the following assumptions were made. First, the ash segregates from the fuel particles as monosized particles. Once separated, the ash particles are transported downwards towards the grate at same velocity as the fuel. Finally, the ash layer is retained on the grate and builds up with time. These assumptions were used in developing an ash sub-model which predicts ash formation, transport and accumulation during the packed bed combustion of char particles. The following sections describe the sub-components of the model, including the properties for a bed which is a mixture of two particle sizes, ash layer buildup and the effects of ash on heat and mass transfer in the bed. No attempt was made to model sintering or fusion of the ash.

3.3.1 Properties of a Bed which is a Binary Mixture

The fuel and ash particles are characterized by their diameters, density, sphericity and void fraction. The ash particles are assumed to be formed with a uniform size d_{PA}, with a density of ρ_A, sphericity ψ_A and a void fraction of the ash phase by itself of ε_A. Equivalent properties for the fuel are d_{PC}, ρ_C, ψ_C and ε_C. All of these properties are assumed to be constant, except the fuel particle diameter. The size of the fuel particle decreases as it moves downwards in the bed and is consumed (see section 3.3.2). For non-spherical particles d_{PC} and d_{PA} are defined by the volume-equivalent diameter.

3.3.1.1 Composition

The quantity of ash at any given point in the bed is defined by the local ash volume fraction

$$X_A = 1 - X_C \tag{3-24}$$

where X_C is the local volume fraction of fuel

$$X_C = \frac{fuel\ volume}{fuel\ volume\ +\ ash\ volume} \tag{3-25}$$

Since it is assumed that the ash and fuel move together through the bed, a fuel particle of initial size d_{PC0} which has burned down to a diameter of d_{PC} will produce an ash volume of

$$\frac{\pi}{6}\frac{\rho_C}{\rho_A}\alpha\left(d_{PC0}^3 - d_{PC}^3\right) \tag{3-26}$$

where α is the mass fraction of ash in the fuel, and the volume of fuel remaining is

$$\frac{\pi}{6}d_{PC}^3 \tag{3-27}$$

Substituting (3-26) and (3-27) into (3-25) gives the local volume fraction of fuel as

$$X_C = \frac{1}{1 + \frac{\rho_C}{\rho_A}\alpha\left(\frac{d_{PC0}^3}{d_{PC}^3} - 1\right)} \tag{3-28}$$

3.3.1.2 Void Fraction

The void fraction, ε, of the bed as a whole (fuel and ash) is calculated using the correlation originally proposed by Westman (1936)

$$\left(\frac{\Theta - \Theta_C X_C}{\Theta_A}\right)^2 + 2G_\varepsilon\left(\frac{\Theta - \Theta_C X_C}{\Theta_A}\right)\left(\frac{\Theta - X_C - \Theta_A X_A}{\Theta_C - 1}\right) + \left(\frac{\Theta - X_C - \Theta_A X_A}{\Theta_C - 1}\right)^2 = 1 \qquad (3\text{-}29)$$

where Θ is the specific volume of the bed (bed volume per unit solids volume) and is equal to

$$\Theta = \frac{1}{1-\varepsilon} \qquad (3\text{-}30)$$

Θ_C is the fuel specific volume and Θ_A is the ash specific volume; they are equal to $1/(1-\varepsilon_C)$ and $1/(1-\varepsilon_A)$ respectively. The correlation of Finkers and Hoffman (1998) was used to calculate the fit parameter (G_ε), as it can be used for spherical or non-spherical particles, whereas the correlation of Yu et al. (1993) requires different ratios for spherical and non-spherical particles. Also, the fit parameter of Yu et al. (1993) has three empirical constants, whereas that of Finkers and Hoffmann (1998) has only one. The structural ratio, r_{str}, is defined by Finkers and Hoffmann (1998) as

$$r_{str} = \frac{\left[\left(\frac{1}{\varepsilon_C}\right) - 1\right]\left(\frac{d_{PA}}{d_{PC}}\right)^3}{\left(1-\varepsilon_A\right)} \qquad (3\text{-}31)$$

The empirical relation between G_ε and r_{str} is given as

$$G_\varepsilon = r_{str}^{Z} + \left(1 - \varepsilon_C^{-Z}\right) \tag{3-32}$$

The value of Z is given as -0.63 for monosized particle fractions and -0.345 for fractions with a wide size distribution.

3.3.1.3 Density

An average density describing the solid (ash and fuel) is required for the mass and energy balances. The mean solids density, ρ_S, is defined by

$$\rho_S = X_C \rho_C + \left(1 - X_C\right)\rho_A \tag{3-33}$$

3.3.1.4 Specific Surface

The particle surface area available for reaction and heat and mass transfer in a bed of particles is defined by the specific surface area, a_B, the ratio of total surface area in the bed to total volume of bed. Derived from geometric relations for nonspherical particles in a packed bed, it is shown to be (Geankoplis, 1993)

$$a_B = \frac{6}{d_P \psi}(1 - \varepsilon) \tag{3-34}$$

The above equation is derived for a packed bed of uniform particles. For a bed which is a mixture of particle sizes, component specific surface areas need to be defined. The fuel specific surface per unit total bed volume is

$$a_{BC} = \frac{6 X_C (1-\varepsilon)}{d_{PC} \psi_C} \tag{3-35}$$

As reaction and mass transfer will only occur with the fuel particles, the fuel specific surface area is used for reaction and mass transfer calculations. For heat transfer calculations, the total surface area (fuel and ash) is required

$$a_B = a_{BC} + a_{BA} \tag{3-36}$$

where a_{BA} is the ash specific surface area, given by

$$a_{BA} = \frac{6(1-X_C)(1-\varepsilon)}{d_{PA} \psi_A} \tag{3-37}$$

The specific surface areas used in the gas and solid mass balances, the source terms for the species balances and the solid phase energy balance reaction source term by Cooper (1996) were changed from the bed specific surface area, a_B, to the char specific surface area, a_{BC}.

3.3.1.5 Effective Diameter

The correlations used in the combustion model for the effective gas diffusivity and conductivity and mass transfer coefficient were developed for beds of monosized particles. For a mixture of two particle sizes, a suitable mean value for the particle diameter, d_p, has to be calculated. As packed bed heat and mass transfer and pressure loss correlations are based on the idea that flow through the bed is equivalent to flow through a large number of parallel

channels, the appropriate choice of diameter is one which gives the same hydraulic diameter for the bed of channels (Bird et al., 1960). It can be shown that this is the same as requiring the same surface area in contact with the flow. The total specific surface area, a_B, is the fuel (equation 3-35) and ash (equation 3-37) specific surface areas combined

$$a_B = 6(1-\varepsilon)\left[\frac{X_C}{d_{PC}\psi_C} + \frac{(1-X_C)}{d_{PA}\psi_A}\right] = \frac{6(1-\varepsilon)}{d_P\psi} \tag{3-38}$$

or

$$\frac{1}{d_P\psi} = \frac{X_C}{d_{PC}\psi_C} + \frac{(1-X_C)}{d_{PA}\psi_A} \tag{3-39}$$

From equation (3-39), it can be observed that to define a mean diameter, d_p, a mean sphericity, ψ, must first be defined. Standish and McGregor (1978) note that there are no formulae in the literature for calculating the mean sphericity of a mixture of differently shaped particles. From the definition of sphericity it makes sense to use the equivalent spherical surface areas of the different particles, which gives

$$\psi = \frac{N_C\pi d_{PC}^2 + N_A\pi d_{PA}^2}{a_B} \tag{3-40}$$

where N is the number of particles per unit bed volume (see equation 3-54). A mean sphericity is then given as

$$\psi = \frac{\frac{X_C}{d_{PC}} + \frac{(1 - X_C)}{d_{PA}}}{\frac{X_C}{d_{PC}\psi_C} + \frac{(1 - X_C)}{d_{PA}\psi_A}} \tag{3-41}$$

Another point of view which makes physical sense is to use an area-weighted average, so that the component sphericities are weighted according to their specific surface areas

$$\psi = \frac{\psi_C a_{BC} + \psi_A a_{BA}}{a_B} \tag{3-42}$$

which again gives equation (3-41). Putting equation (3-41) into equation (3-39) gives the following expression for the effective diameter of the mixture

$$d_P = \left[\frac{X_C}{d_{PC}} + \frac{(1 - X_C)}{d_{PA}} \right]^{-1} \tag{3-43}$$

Equation (3-43) is the volume-surface mean diameter, which according to Geldart (1990) is accepted as the relevant mean diameter for packed beds.

3.3.1.6 Specific Heat

Merrick's (1983a) model was used to calculate the overall specific heat of the solid phase. A mixing formula of the form

$$c_{PS} = Y_C c_{PC} + Y_A c_{PA} \tag{3-44}$$

is used, where Y is the mass fraction and c_{PC} and c_{PA} are the individual specific heats of the fuel and the ash, respectively. The overall specific heat of the solid per unit solid mass is given by

$$c_{PS} = \frac{\rho_C X_C c_{PC} + \rho_A (1 - X_C) c_{PA}}{\rho_C X_C + \rho_A (1 - X_C)} \tag{3-45}$$

The individual specific heats of the fuel and ash are also taken from the work of Merrick (1983a).

3.3.2 Transport Equations

The production and transport of ash within the bed, resulting in the accumulation of ash on top of grate, is described by the solid phase mass transport equations and the fuel particle number balance. The solid phase continuity equation is

$$\frac{\partial}{\partial t}\left[(1 - \varepsilon)\rho_S\right] + \frac{\partial}{\partial x}\left(\rho_S v_S\right) = -Ga_{BC} \tag{3-46}$$

where G is the carbon consumption rate per unit surface area of the fuel particles and v_S is the superficial velocity of the bulk solid phase. Note that the specific surface has been changed from the specific surface of the bed (used by Cooper, 1996) to the specific surface of the fuel, because only the fuel reacts. Mass balances can also be written for the fuel and ash phases individually and are given as

$$\frac{\partial}{\partial t}\left[\rho_C X_C(1-\varepsilon)\right]+\frac{\partial}{\partial x}\left(\rho_C v_C\right)=-Ga_{BC}(1+\alpha) \tag{3-47}$$

and

$$\frac{\partial}{\partial t}\left[\rho_A(1-X_C)(1-\varepsilon)\right]+\frac{\partial}{\partial x}\left(\rho_A v_A\right)=Ga_{BC}\alpha \tag{3-48}$$

where α is the mass fraction of ash in the fuel. The last terms of equations (3-47) and (3-48) are the carbon consumption and the ash production rates, respectively. The additional α term in equation (3-47) appears because the fuel particles lose the carbon mass and the ash mass when they are consumed. Note that equations (3-47) and (3-48) add to equation (3-46). The phase mass fluxes can be solved by considering that the total solids mass flux is the sum of the two phase fluxes

$$\rho_S v_S = \rho_C v_C + \rho_A v_A \tag{3-49}$$

Assuming that the char and ash move at the same actual velocity w, the char mass flux is

$$\rho_C v_C = \rho_C w(1-\varepsilon)X_C \tag{3-50}$$

since $(1-\varepsilon)X_C$ of the bed is char. Similarly, the ash mass flux is

$$\rho_A v_A = \rho_A w(1-\varepsilon)\left(1-X_C\right) \tag{3-51}$$

The total solids flux is then

$$\rho_S v_S = w(1-\varepsilon)\left[\rho_C X_C + \rho_A\left(1-X_C\right)\right] \tag{3-52}$$

The solids mass flux, $\rho_S v_S$, is found from the solids continuity equation (3-46). Equation (3-52) can then be used to find the actual velocity w, and the char mass flux, $\rho_C v_C$, is then calculated directly from equation (3-50). To allow for ash to buildup in the bed the solids and char mass fluxes are set to zero in the grate. The ash equation (3-48) does not actually have to be solved, because it is not linearly independent of the other two.

A fuel particle number balance is used to account for the change in the size of the fuel particles as they move downwards in the bed and are consumed. Assuming that no fragmentation or agglomeration of particles occurs, a balance on the fuel particles in a horizontal slice of the bed gives

$$\frac{\partial N_C}{\partial t} = -\frac{\partial \dot{N}_C}{\partial x} \tag{3-53}$$

where N_C is the number of fuel particles per unit bed volume

$$N_C = \frac{(1-\varepsilon)\rho_C X_C}{m_{PC}} \tag{3-54}$$

with m_{PC} as the mass of a single particle, and $\dot{N}_C$ is the fuel particle number flux per unit cross-section

$$\dot{N}_C = \frac{\rho_C v_C}{m_{PC}} \tag{3-55}$$

Combining the above three equations and the fuel continuity equation gives the required transport equation

$$\rho_C X_C (1-\varepsilon)\frac{\partial}{\partial t}\left(\frac{1}{m_{PC}}\right) + \rho_C v_C \frac{\partial}{\partial x}\left(\frac{1}{m_{PC}}\right) = -\frac{Ga_{BC}(1+\alpha)}{m_{PC}} \qquad (3\text{-}56)$$

The variable solved for is $1/m_{PC}$, from which the fuel particle size, d_{PC}, can be calculated. One could re-write equation (3-56) in terms of d_{PC} instead, but attempts to write a d_{PC} equation led to a discretized equation which gave the physically unreasonable result of a fixed ratio between particle sizes near the grate.

3.3.3 Effects on Mass and Heat Transfer Correlations

The correlations used by the bed combustion model to calculate both the fluid-to-solid mass transfer coefficient and the effective thermal solid conductivity were derived for beds of monosized particles. Since the fuel bed is a binary mixture, these correlations were modified to include this effect. The modifications assume that as ash is produced and accumulates in the bed, the smaller ash particles will fill in the voids between the larger fuel particles. It should be noted that the changes to the heat and mass transfer correlations neglect the fact that the fuel and ash particles may actually be at different temperatures.

3.3.3.1 Fluid-to-Solid Mass Transfer Coefficient

Ash in the bed hinders mass transfer in two ways. First, it reduces the surface area available for mass transfer. Secondly, some of the gas will not contact the char as it will flow

in channels bounded by ash. Consequently, the gas which does contact the char becomes more quickly saturated with products. Figure 3.4 illustrates ash buildup in a packed bed.

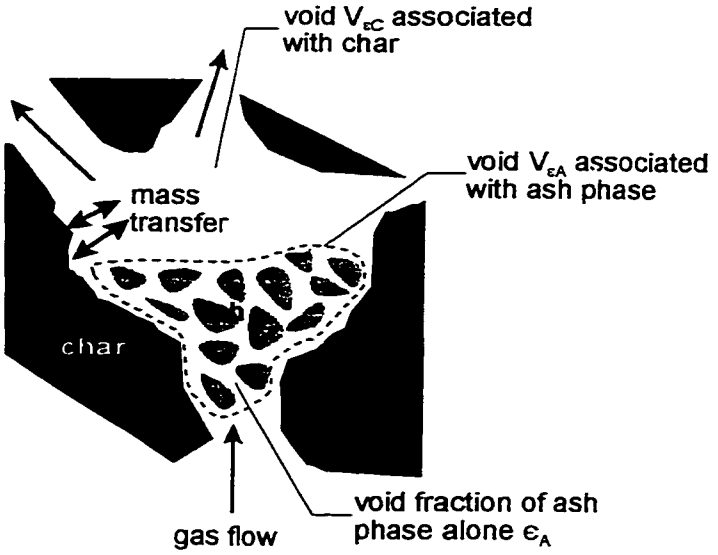

Figure 3.4 Effects of ash buildup on mass transfer.

In fluidized bed combustors, which typically have large numbers of limestone particles surrounding isolated lumps of fuel, the effect of the limestone phase on mass transfer is accounted for by multiplying the Sherwood number in the gas phase, Sh_0, by the void fraction

$$Sh = Sh_0 \varepsilon \tag{3-57}$$

as diffusion can only take place in the portion of the bed not occupied by particles (La Nauze, 1985). For a packed bed, an analogous treatment is to multiply the mass transfer coefficient by the proportion of void volume in contact with or "associated with" the fuel particles. The mass transfer coefficient in an ash-laden bed, k_{yi} is then described by

$$k_{yi} = f_\varepsilon k_{yi0} \tag{3-58}$$

where k_{yi0} is the mass transfer coefficient for a pure fuel bed. The fraction of void volume which is "associated with" the fuel is defined as

$$f_\varepsilon = \frac{void\ volume\ associated\ with\ fuel}{total\ void\ volume} = \frac{V_{\varepsilon C}}{\varepsilon} \tag{3-59}$$

The sum of the void volumes "associated with" the fuel and ash phases gives the total bed void volume

$$\varepsilon = V_{\varepsilon C} + V_{\varepsilon A} \tag{3-60}$$

Assuming that the void volume "associated with" the ash phase is given by the void fraction of the ash phase alone, then

$$\varepsilon_A = \frac{V_{\varepsilon A}}{V_{\varepsilon A} + V_A} \tag{3-61}$$

where V_A is the volume fraction of the bed occupied by ash particles

$$V_A = (1 - \varepsilon)(1 - X_C) \tag{3-62}$$

Substituting equation (3-62) into equation (3-61) and solving for $V_{\varepsilon A}$ gives

$$V_{\varepsilon A} = \varepsilon_A \frac{(1 - \varepsilon)}{(1 - \varepsilon_A)}(1 - X_C) \tag{3-63}$$

The remaining void volume is assumed to be "associated with" the fuel phase, thus

$$V_{\varepsilon C} = \varepsilon - V_{\varepsilon A} \tag{3-64}$$

which gives

$$f_\varepsilon = 1 - \frac{\varepsilon_A}{\varepsilon}\frac{(1-\varepsilon)}{(1-\varepsilon_A)}(1-X_C) \tag{3-65}$$

This modification is used only for mass transfer, not for heat transfer, since both ash and fuel particles are involved in heat transfer.

3.3.3.2 Effective Solid Thermal Conductivity

The packed bed combustion model uses the correlation of Yagi and Kunii (1957) to calculate the effective thermal conductivity. This correlation assumes that there are four methods of heat transfer in a packed bed: solid conduction, gas conduction between particles, particle-to-particle radiation and void-to-void radiation (actually radiation between particles separated by voids). The model gives the effective solid thermal conductivity of a monosized bed of particles as:

$$k_{Seff} = \frac{\beta(1-\varepsilon)}{\frac{\gamma}{k_S} + \frac{1}{\frac{k_G}{\varphi} + d_{PC}h_{RS}}} + \varepsilon\beta d_{PC}h_{RV} \tag{3-66}$$

where the first three heat transfer paths are in parallel with the fourth. Merrick's (1983b) model is used for the thermal conductivity of the fuel, k_C, and the Eucken equation is used to calculate the gas phase conductivity, k_G (Bird et al., 1960) . β, γ and φ are dimensionless parameters defined by Yagi and Kunii (1957): β is the dimensionless effective length between particle centres, γ is a dimensionless effective length of the solid relating to conduction and

φ is dimensionless effective gas film thickness near the particle contact points, with values of 1, 1 and 0.05 respectively. The radiation heat transfer coefficients from solid to solid, h_{RS}, and void to void, h_{RV}, are given by Yagi and Kunii (1957).

To model heat transfer in a bed of two particle sizes, a modified version of equation (3-66) was developed. The new model assumes that as ash is produced, the ash phase fills up a fraction χ of the void space between the fuel particles. The ash phase includes the ash particles plus the void volume "associated with" those particles and has its own void fraction ε_A. The first three heat transfer mechanisms of Yagi and Kunii's (1957) model are unaffected by the buildup of ash in the bed. The fourth mechanism has to be adjusted to account for the reduction of void-to-void radiation as the voids between the fuel particles fill with the ash phase. An additional heat transfer mechanism has to be introduced to account for ash phase conduction. These modifications result in a fraction χ of the void-to-void radiation term being replaced by conduction through the ash phase. The five heat transfer paths in a packed bed of a binary mixture are illustrated in Figure 3.5.

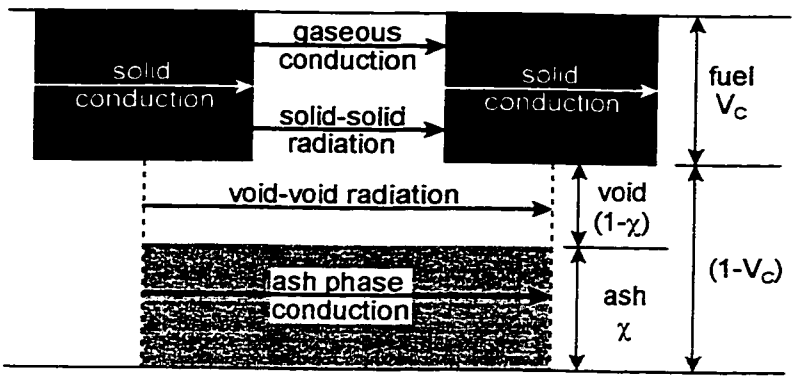

Figure 3.5 Adapted model of heat transfer in a packed bed.

Including these in equation (3-66) gives the following expression

$$k_{Seff} = \frac{V_C \beta}{\frac{\gamma}{k_C} + \frac{1}{\frac{k_G}{\varphi} + d_{PC} h_{RS}}} + (1 - V_C)(1 - \chi) d_{PC} \beta h_{RV} + (1 - V_C) \chi k_{Aeff} \qquad (3\text{-}67)$$

The ash phase has its own effective thermal conductivity, k_{Aeff}, which is calculated by applying the original Yagi and Kunii model (equation 3-66) to the ash fraction alone:

$$k_{Aeff} = \frac{\beta(1 - \varepsilon_A)}{\frac{\gamma}{k_A} + \frac{1}{\frac{k_G}{\varphi} + d_{PA} h_{RSA}}} + \varepsilon_A \beta d_{PA} h_{RVA} \qquad (3\text{-}68)$$

The ash conductivity, k_A, was assumed to be that of firebrick, or 1.09 W/mK (Holman, 1990). The volume of the fuel phase in the bed is given by

$$V_C = X_C(1 - \varepsilon) \qquad (3\text{-}69)$$

and the fraction of the fuel void volume filled with the ash phase is given by

$$\chi = \frac{V_{\varepsilon A} + V_A}{V_{\varepsilon C0}} \qquad (3\text{-}70)$$

where $V_{\varepsilon C0}$ is the volume of the voids between the fuel particles. It remains constant as the voids fill with ash as long as the fuel particles remain in contact and retain the same geometrical relationships to one another. $V_{\varepsilon C0}$ is different from the void volume "associated with" the fuel, $V_{\varepsilon C}$, in equation (3-59), since $V_{\varepsilon C}$ decreases with time as the fuel voids are

filled with the ash phase. Until the ash fraction becomes large enough to entirely fill the voids between the particles, the void volume of the fuel phase is assumed to be given by the void fraction of fuel phase alone:

$$\varepsilon_C = \frac{V_{\varepsilon C0}}{V_{\varepsilon C0} + V_C} \tag{3-71}$$

from which the value of $V_{\varepsilon C0}$ can be determined. Thus,

$$\chi = \frac{(1-\varepsilon_C)}{(1-\varepsilon_A)} \frac{(1-X_C)}{\varepsilon_C X_C} \tag{3-72}$$

If the value of χ equals one, the fuel void volume is completely filled with the ash phase. Thus, χ is constrained to be less than or equal to one. When χ equals one, further ash accumulation will separate the fuel particles. Equation (3-67) continues to be valid, but the second term, void-to-void radiation, is now zero. When the fuel completely disappears, equation (3-67) reduces to the conductivity of the ash phase alone.

In applying these models ε_A and ε_C are assumed to be known from measurements on fuel and ash samples, while X_C is calculated from equation (3-28) with d_{pC} from the solution of equation (3-56).

3.4 Numerical Method

3.4.1 Finite Volume Discretization Techniques

As mentioned previously, the governing equations were solved using the finite volume discretization techniques of Patankar (1980). Discretization of differential equations results in linear algebraic equations which can be easily solved using matrix methods. The work of Cooper (1996) details the discretization of the mass, species and energy balances. The particle number balance presently used in the model is of a different form than that used by Cooper (1996) and the discretized form currently employed can be found in Appendix A. Two options exist for generating the control volumes. An exponentially increasing grid spacing, from the grate to the top of the bed, can be used to ensure good resolution in the oxidation zone near the grate, where the temperature and concentration gradients are the steepest. The control volumes can also be evenly spaced. If the ash is allowed to build up, this is the better option as the oxidation zone will be constantly shifting. In this study 50 evenly spaced control volumes were used (10 in the grate and 40 in the bed).

3.4.2 Solution Technique

Due to the coupling of the velocities, reaction and heat transfer terms, an iterative solution was required. For each time step, convergence was determined by checking the difference between the values of the gas or solid temperature and the CO concentration for two consecutive iterations. As mentioned by Cooper (1996), a tridiagonal matrix algorithm is used to solve the species, energy and particle number balances. The mass balances are

solved for each control volume sequentially. The Westman equation (3-29) is solved using the Newton-Raphson method.

The model input variables and initial estimates are those given by Cooper (1996), with the following changes. An ignition zone was introduced, in which a thin layer of the bed on top of the grate is set at a temperature sufficient for ignition to occur. The remaining solids and the gas are at ambient temperatures. New input parameters include the properties of the ash particles (diameter, density, void fraction and sphericity), the fuel particle pore characteristics (specific internal surface area, void fraction and tortuosity) and the grate bar dimensions. The input parameter data files are in Appendix C.

The simulation can be run using some alternatives. Ash can build up in the bed or fall through the grate. Also, for both the oxidation and reduction reaction, the reaction rates can be calculated with or without the effects of pore diffusion.

4.0 EXPERIMENTAL ASPECTS

An experimental reactor of the overfeed type was designed for studying the combustion processes in a packed bed and generating concentration and temperature profiles. This section comprises a detailed description of the experimental apparatus including the reactor, instrumentation and the data acquisition system. The experimental procedures used to characterize the fuel and ash particles, analyse the bed samples and perform the tests are also described.

4.1 Experimental Reactor

The design of the apparatus used in these experiments is based on the reactors described in section 2.1. As part of the design process, the reactor bed diameter and depth had to be decided. There were two primary considerations in determining the bed diameter. First, a sufficiently large size was required to ensure that the bed conditions were uniform: since the experimental results are to be compared with a one-dimensional model there should not be any significant variation of temperature or concentration in the transverse direction. Secondly, the grate loading should be in the range expected for a commercial unit, 150-200 kg fuel/m^2hr. A bed diameter of 23 cm was chosen. Calculations of fuel, air and product mass flows showed that a 23 cm bed could produce the desired grate loadings without demanding excessive quantities of fuel. The effect of a water-cooled probe on radial bed temperature profiles was also estimated. This calculation indicated that beds smaller than 23 cm would have unacceptable temperature non-uniformities. As wall effects depend on the

ratio of bed diameter to particle diameter (see section 2.3.4), the effect of the fuel particle size on the chosen bed diameter was considered. The fuel size was limited by two factors. First, if the particles are too large, the bed will not settle evenly as it burns. This will lead to "bridging" and the formation of large voids in the bed. Particles which are a significant fraction of the bed size will have this effect, therefore the maximum particle size was limited to 2 cm. Secondly, if the particles are too small, the bed will be fluidized, not packed. Minimum fluidization velocity calculations as a function of particle size indicated that the minimum particle size should be approximately 1 cm. The maximum bed height was determined to be 20 cm, as this bed depth produces a fully developed reduction zone.

As seen in Figures 4.1-4.3, the reactor consists of four sections: a grate, a combustor, an afterburner and an overhead exhaust hood. The walls of the reactor are constructed of 14 gauge steel and the flanges are 0.95 cm steel plate. Incoming combustion air enters the reactor through a metal foam air straightener at the bottom of the grate section and then enters a plenum below the grate. The grate section is 15 cm high and 25 cm in diameter and supports the grate at the top. Stainless steel bars, 3 mm x 19 mm, are used to construct the grate. The spacing of the bars is 3.3 mm, which causes ash to build up in the bed. This section is supported on a traversing slide, allowing it to be lowered in precisely measured steps to obtain sample "slices" of the bed.

The combustor or fuel bed section is 23 cm in diameter and 20 cm high, lined with 5 cm thick refractory (Fiberfrax Duraboard 3000 insulating board). Thermocouples can be radially inserted into the fuel bed through eight ports in this section, located at 2.2 cm, 3.8 cm, 5.1 cm, 6.4 cm, 7.6 cm, 10.2 cm, 12.7 cm and 15.2 cm above the grate. The afterburner

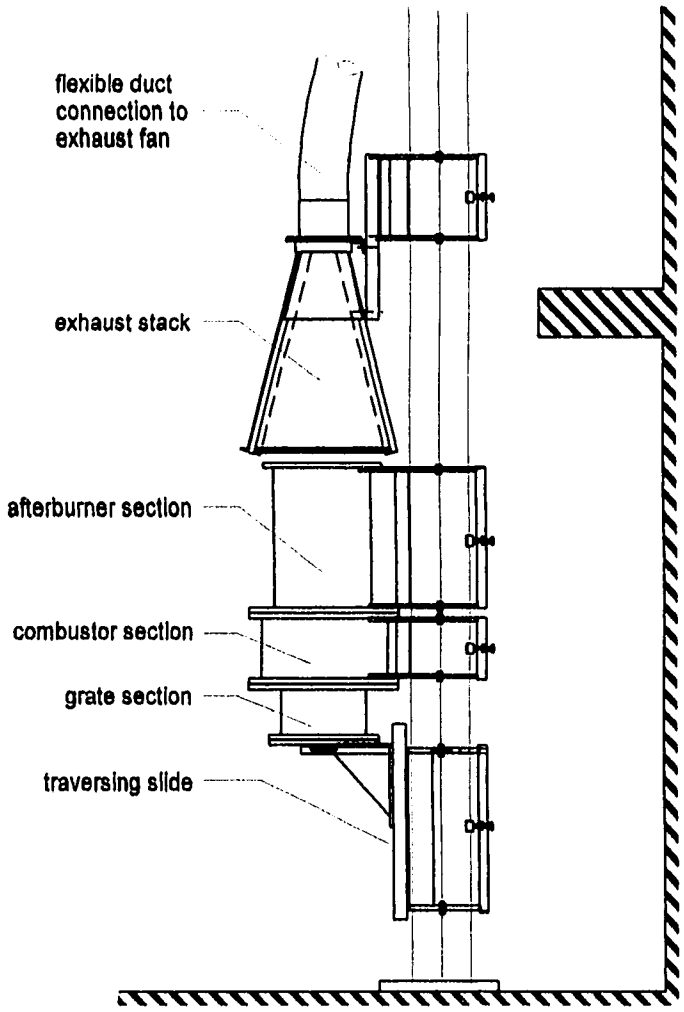

Figure 4.1 Schematic of the experimental apparatus.

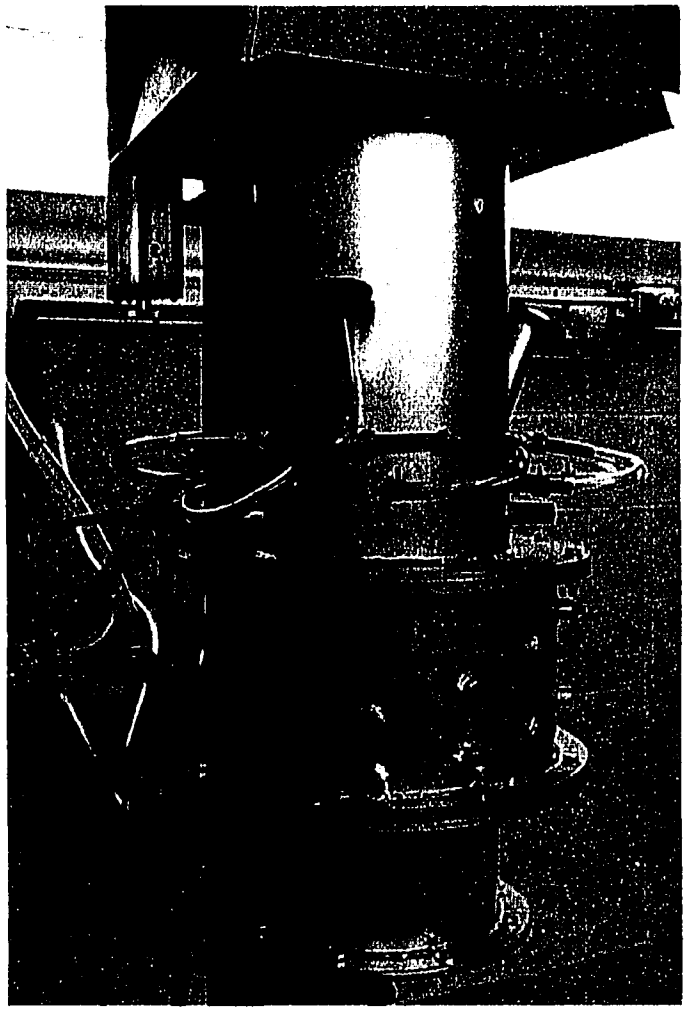

Figure 4.2 Photograph of the experimental apparatus.

section is 41 cm high with a 23 cm inner diameter. A 2.5 cm thick cooling jacket encircles this section (this provides a cold wall radiative boundary for the model). Eight overfire air jets, constructed of 1 cm steel tubes with a 90° upward bend at the end, are inserted radially into this section. There are four additional ports in the afterburner section, two for viewing, one for a gas sampling probe and one for a gas temperature thermocouple. The top section of the apparatus consists of an exhaust hood which removes products and dilutes them with ambient air. The hood's sides are doors which allow for access to the top of the bed for fuel feeding. An exhaust fan removes the products.

Primary air and overfire air are supplied from a compressed air system. The air flowrates are measured by rotameters; a thermocouple and pressure gauge in the air line are used to correct for air density changes. An in-line filter removes water and oil from the air. A switching system allows for air or nitrogen to be injected into the bottom of the reactor. The cooling water supplied to the afterburner and the gas sampling probes is circulated in a closed loop through a radiator to disperse the heat. Three rotameters control the water flow to the afterburner, the vertical and horizontal sampling probes. Mains water can also be injected into the cooling water system should the pump fail or the cooling water get too hot. A photograph of the experimental apparatus is shown in Figure 4.2.

4.2 Instrumentation

During the experiments two types of measurements were taken: gas samples and temperatures. The following section describes the probes used to obtain these measurements

and the methods used to ensure accurate and representative readings were obtained. The features of the apparatus including measurement and analysis devices are shown in Figure 4.3.

4.2.1 Concentration Measurements

4.2.1.1 Gas Sampling Probes

Two sampling probes were designed based on the convection probes of Bilger (1976): a vertical probe for sampling the gases within the bed (see Figure 4.5) and a horizontal probe for sampling the gases above the bed. A convection-style quench probe was chosen, as a mixing quench probe would have required additional instrumentation for the metering of the inert gas and an expansion quench probe would have required a small sample tube diameter which could have easily gotten plugged with fine fuel or ash particles.

With convection quench probes, the desired sudden temperature drop to quench the reaction is obtained through the sizing of the sample passage as well as the amount and temperature of the cooling water. Thus, the sample tube should be made as small as possible yet large enough to prevent clogging with fine fuel or ash particles. Taking the above-mentioned points into consideration, the sample tube was made out of 1.6 mm ID brass tubing. To ensure that the reactions were being quenched effectively, the sample probe passage was modelled as a non-isothermal plug flow reactor with heat exchange. The conversion of CO to CO_2 along the length of the "reactor" was investigated. The mole and energy balances were solved using MATLAB. The resulting temperature and conversion profiles for a gas with inlet conditions of 1600 K and 12.1% O_2, 8.5% CO_2 and 1.2% CO

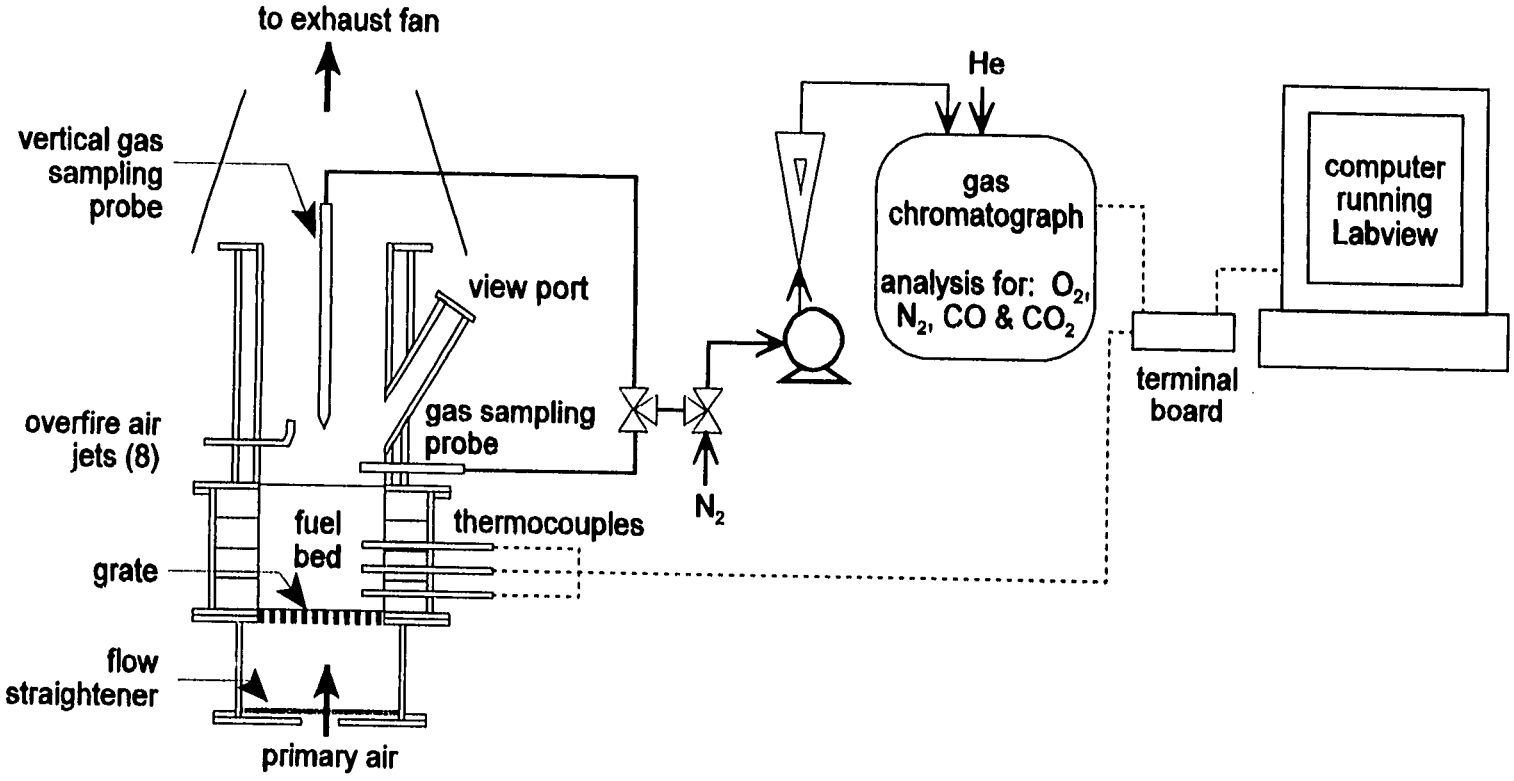

Figure 4.3 Section through of the experimental reactor and the measurement and analysis devices.

(these inlet conditions are typical model predictions in the oxidation zone) are plotted in Figure 4.4. The fast temperature drop and corresponding limited conversion (<6%) indicates that a probe with a 1.6 mm sample tube provides adequate quenching. Also, heat transfer calculations show that this size of tubing produces a cooling rate of $2.3 \cdot 10^6$K/s which is close to the rate of $2 \cdot 10^6$K/s quoted by Bilger (1976) for convection probes. Due to the limitations of the sampling train, the sample tube diameter is enlarged to 2.2 mm after a distance of 12.7 cm to reduce the pressure drop. This distance was chosen to ensure that the sample had adequate distance to reach 1000K (see Figure 4.4): Becker (1993) states that effective quenching requires a fast drop to 1000K, after which slower cooling is permissible.

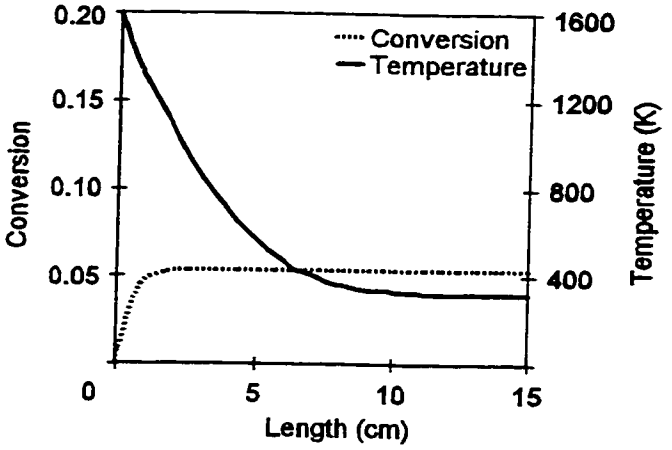

Figure 4.4 Conversion and temperature profiles of the first 15 cm of the probe sampling tube.

The size of the cooling water tube was based on the amount of cooling water required. The coolant's purpose is twofold: to quench the gas sample and to prevent burn-out of the probe. Therefore, heat from the sample and the bed had to be accounted for. Heat transfer and pressure drop calculations showed that a tube with a diameter of 3.2 mm would be sufficient. The criteria for the outer dimensions of the probe were to make the probe as small as possible (to minimize the thermal effects on the bed) but at the same time make it durable (the probe has a vertical length of 66 cm so it can not be too unwieldy). Calculations

indicated that the probe's outer diameter would have to be at least 1.3 cm (due to the dimensions of the sampling and cooling water tubes). This diameter also corresponded approximately to the size of the fuel particles. Thus, when inserted into the bed, the vertical probe does not overly disturb the gas flow, but appears in the transverse plane as another particle. A radiation shield is fitted around the first 20 cm of the vertical probe to reduce heat loss from the bed, increasing the size of the probe to 1.7 cm in diameter. To improve the sample cooling, the probe tips are machined from brass. Numerical heat conduction calculations were performed on the vertical probe tip to check the temperature profile and ensure that it remained cool. The vertical probe has a pointed tip to facilitate movement into the bed, whereas the horizontal probe has a blunt tip. The vertical probe is attached to a traversing slide to obtain samples at any vertical position in the bed. Figure 4.5 shows a schematic of the vertical probe.

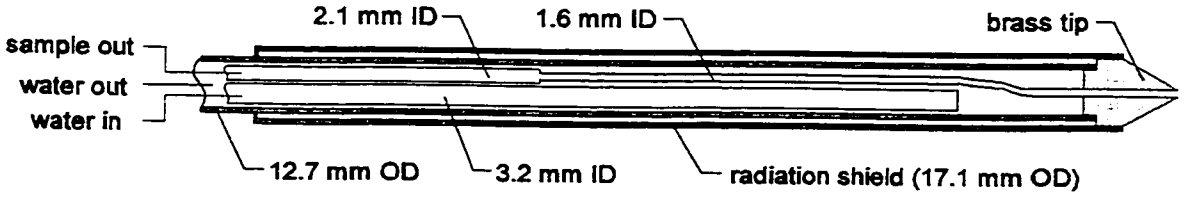

Figure 4.5 Vertical water-cooled gas sampling probe.

4.2.1.2 Isokinetic Sampling

As mentioned in section 2.2.1, there was no criterion in the literature for determining the proper sampling rate in a packed bed. If the sampling rate is too low, the probe will behave like a particle and the gas will flow around it with minimal disturbance to the system. However, if the sampling rate is too high, gas samples will not only be drawn from the desired

area, but also from the surrounding area. Gas samples will thus undergo additional reaction as they are drawn towards the probe, resulting in inaccurate concentration measurements. Thus, the object is to obtain a sample without disturbing the flow in the bed or biasing the sample. In a gas flow, this condition is met by isokinetic sampling: the sampling velocity is made to equal the local gas velocity. In a packed bed, this is impractical, because the local gas velocity depends on the geometry of the fuel particles bounding the interstice that is being sampled, and hence can vary widely and randomly from point to point in the bed. It was decided instead to set the sampling rate such that the mass flow through the probe would equal the mass flow through the bed cross-section occupied by the probe. On the scale of the probe size, this ensures that the bed flow is not disturbed, even if there are local disturbances in individual interstices. The sampling rates were determined by first using the char combustion model to estimate the gas mass flow at a given height in the bed and then the above criterion was applied to determine the flow through the probe.

4.2.1.3 Gas Sampling Train

The gas samples are drawn through the probes by a diaphragm pump and forwarded to a gas chromatograph for analysis. Two filters remove particulates which may be entrained in the flow. The criterion for isokinetic sampling is met by using a rotameter to regulate the sample flow. A switching system allows for each of the probes to be connected to the gas chromatograph. High-pressure nitrogen can be back-flushed through the probes if they became blocked with fine particles.

Leak testing was performed on the sampling train prior to each experiment to ensure that no air was being drawn into the system through the fittings. The response factor calibration gas (see section 4.2.1.4) was blown over the tip of the probe and drawn into the gas chromatograph through the sampling train. The sample was then analysed for the presence of oxygen which would indicate a leak.

4.2.1.4 Gas Sample Analysis

Gas samples obtained were analysed by a gas chromatograph equipped with a thermal conductivity detector. The gas chromatograph was a Varian 3350 which used a Supleco column packed with 60/80 Carboxen-1000 to separate the sample. Carboxen-1000 separates nitrogen, oxygen/argon, carbon dioxide and carbon monoxide. It will not separate argon from oxygen; to do this lower temperatures are required.

The gas chromatograph oven was temperature programmable to speed up the component elution. The program suggested by Supleco was an initial oven temperature of 35°C for 3 minutes followed by a temperature ramp of 20°C/min to 225°C. This resulted in the desired components being eluted in 14 minutes. The gas chromatograph oven cool-down took 8 minutes, resulting in a sample analysis every 22 minutes. Due to the constantly changing bed conditions, caused by ash buildup, it was deemed desirable to increase the gas sample analysis rate. To decrease the analysis time, the carrier gas flow was increased from 30 mL/min to 60 mL/min, and the temperature program was changed to an initial oven temperature of 40°C for 4 minutes followed by a temperature ramp of 20°C/min to 200°C. These changes reduced the total analysis time to 17.5 minutes including cool-down.

Peak areas from a chromatograph trace provide information on the relative concentrations of the components analysed. However, with thermal conductivity detectors, the observed areas are not proportional to the weight percent of the components (Messner et al., 1959). Four principal methods are used to quantify peak areas: internal standard, external standard, standard addition and area normalization. The first three methods all require the weight of the sample analysed to be precisely known. As this was not feasible with the proposed apparatus, the quantification method used was area normalization. Use of the area normalization technique requires the following criteria to be met: all analytes must be eluted, all analytes must be detected and all analytes must have the same sensitivity (Miller, 1988). The gas chromatograph and column used met the first two criteria; however, as mentioned previously, with thermal conductivity detectors, different compounds have different responses. The third requirement can be met by using substance-specific response factors to correct the areas. Tables of response factors are available in the literature (Dietz, 1967 and Rosie and Barry, 1973).

However, in order to improve accuracy, response factors for this work were determined using a calibration mixture (Miller, 1988). A substance was chosen as the standard and its response factor, f_S, was given an arbitrary value. A known mixture, by weight, of the analytes was then chromatographed. The areas of the standard, A_S, and unknown, A_i, peaks were then measured. The substance specific response factor of the unknown, was then calculated by

$$f_i = f_s\left(\frac{A_s}{A_i}\right)\left(\frac{W_i}{W_s}\right) \qquad (4\text{-}1)$$

where W_i/W_S is the weight ratio of the unknown to the standard. Nitrogen was selected as the standard and given a response factor of 1.0. Two calibration mixtures were used, one being bottled air and the other a calibration mixture of 64 wt% N_2, 14 wt% CO and 22 wt% CO_2 which had an accuracy of ±1% of the component. The explosive nature of O_2 and CO mixtures made it necessary to use two mixtures to cover all of the components. The trapezoid rule was used to calculate the areas of the peaks. As Braithwaite (1996) suggests doing a series of at least five replicates to obtain acceptable precision, values for the response factors were determined by chromatographing each of the calibration mixtures five times. They are tabulated in Table 4.1. A literature value was used for the response factor of argon. The weight percent of each of the components in an unknown sample is then calculated by

Table 4.1 Response factors used to quantify the peak areas produced by the gas chromatograph.

Component	Response Factor ±1σ
N_2	1
Ar	1.420 (Dietz, 1967)
O_2	1.293 ±0.002
CO_2	1.298 ±0.010
CO	0.998 ±0.003

$$Y_i\% = \left[\frac{A_i f_i}{\sum\left(A_j f_j\right)}\right] \times 100 \qquad (4\text{-}2)$$

4.2.2 Temperature Measurements

The thermocouples used for these experiments were type B (Pt-30%Rh/Pt-6%Rh), which have a maximum temperature of 1820°C. They were housed in ceramic tubes to

provide durability. Catalytic heating is prevented by coating the metal leads using a non-catalytic coating. Initially the "flame-plating" method outlined by Kaskan (1956), Fristrom and Westenburg (1965) and Madson and Theby (1984) was attempted, as it has been shown to eliminate catalytic effects and was the most widely used in the literature. Propane was bubbled through hexamethyldisiloxane and then burned in a Meker burner. To coat the thermocouples, the leads were passed through the flame, rotating to obtain an even coating. The coating formed was very fragile; placing the thermocouple into a flame resulted in the coating flaking off. Kaskan (1956) and Madson and Theby (1984) indicated that the flame temperature must be 1800 K for this coating technique to work. Producing a flame with this temperature was attempted; however, a more durable coating was not obtained. As the conditions in the bed would be much more extreme then those in a flame, the "flame-plating" technique was abandoned. The method of Burton and Ladouceur (1992) was then attempted. Ceramabond 569 adhesive (made by Aremco) was applied to the thermocouples and fired according the manufacturers instructions. Again, the coating was tested by placing it in a flame. This coating survived the flame temperatures and microscopic examination showed no defects in the coating. Thus, the adhesive was found suitable as a coating, producing an even and durable coating without any cracks or pock marks.

The method used to coat the thermocouples using Ceramabond 569 was as follows. First, the thermocouples were washed in distilled water and then in methanol. The bead and approximately 1 cm of the leads were dipped into the liquid adhesive. Curing was performed according to the manufacturer's instructions: four hours at room temperature followed by two hours at 93°C. While the coating survived the bed conditions, the thermocouples often

broke owing to mechanical damage or slagging. To repair the thermocouples the coating was scraped off. The leads were then twisted together and the bead was reformed by sticking the thermocouple into an oxyacetylene flame. The thermocouples were then recoated using the above method.

4.2.3 Data Acquisition

The data acquisition system consisted of three components: a terminal board, a data acquisition computer interface board and the data acquisition software. A National Instruments SC-2070 terminal board was used to connect the thermocouples and gas chromatograph to the computer interface card. The terminal board included an onboard temperature sensor for thermocouple cold-junction compensation. The computer interface card, a National Instruments AT-MIO-16XE-50 data acquisition board, was configured to sample the analog voltages at a rate of 10 scans/second. LabView was the software used to run the data acquisition system. A program was written in the LabView G (graphical) programming language to collect the readings from the thermocouples and gas chromatograph, convert the thermocouple voltage readings into temperature values and convert the peaks produced by the gas chromatograph into component weight percents. This information was also displayed and recorded to file by the program. The amount and timing of fuel addition could also be saved to the file. The relationship for the calculation of temperature as a function of thermocouple electromotive-force was obtained from the ASTM Standard E 230-93 "Temperature-Electromotive Force (EMF) Tables for Standardized Thermocouples". Each temperature reading was an average of one hundred readings, as this

produces the best results (National Instruments, 1995). The areas of the peaks produced by the gas chromatograph trace were calculated using the trapezoid rule. Weight percents of each component were calculated using equation (4-2).

4.2.4 Measurement Accuracy

The accuracy of the temperature and concentration data are dependent on the accuracy of the measurement devices (thermocouples and gas chromatograph) and the accuracy of the probe locations. National Instruments (1995) states that typical thermocouple accuracies are in the order of ±2°C, this includes compensation, linearization, measurement and thermocouple wire errors. Errors in the position of the thermocouples above the grate should be limited to construction inaccuracies as the thermocouple ports are fixed; however, as noted in section 4.2.2, during some experiments the thermocouple sheaths broke and this may have resulted in measurements which were not at the expected location. No information was provided by the manufacturers of the gas chromatograph or column regarding accuracy; however, tests performed with gas mixtures of known composition showed good agreement. The location of the vertical gas sampling probe is measured using a fixed scale which can be read to the nearest mm. Prior to each experiment the zero reading (when the tip of the probe contacted the grate) was checked and noted.

4.3 Fuel and Ash Characterization

The following sections describe the fuel and explain the methods used to characterize the fuel and ash particles. Diameters, densities, shapes and void fractions of both the fuel and ash particles had to be determined, as these are required inputs for the computer model. As the amount of ash in the fuel is a model input, it was also determined.

4.3.1 Fuel

Metallurgical coke was used as the fuel as it is a source of nearly pure carbon. It was made from a blend of two low volatile and two high volatile bituminous coals and was kindly donated by the Metallurgical Fuels Lab of CANMET Energy Technology Centre, Natural Resources Canada. A proximate analysis of the parent coal and the coke is given in Table 4.2 and an ash analysis is presented in Table 4.3. (Note: The coke for which these analyses were performed was a batch that was used for preliminary tests. The data presented in section 5.1 were obtained with subsequent batches which were supposed to be identical to this analysis; in fact small differences in the ash contents were found, which are reported in section 5.1.3.) The ash softening temperature was estimated to be 1480°C using the method of Gauger (Singer, 1981) and the information in Table 4.2. Singer (1981) indicates that the ash should become liquid at approximately 1580°C.

Table 4.2 ASTM proximate analysis of the fuel (Gransden, 1997).

Component	Coal	Coke
Volatiles	27.55%	0.45%
Fixed carbon	67.17%	92.65%
Ash	5.28%	6.9%

As mentioned in section 3.2, the pore structure affects the reactivity of the coke, thus values for the particle void fraction and internal specific surface and tortuosity are required as inputs for the pore diffusion model. Gransden (1997) indicated that internal surface area is approximately 0.1 m^2/g which is smaller than the values found in the literature. During the coking process, the coal fuses together, eliminating small pores, while larger ones are formed by volatiles bubbling through the plastic mass, resulting in a smaller internal surface area than in chars from "normal" coal combustion (Gransden, 1997). The internal void fraction is approximately 0.5 (Gransden, 1997). No value for the tortuosity was available so it was assumed to be 2. Calculations have shown that the tortuosity does not significantly affect the model predictions.

Table 4.3 Ash analysis (Gransden, 1997)

Component	wt %
SiO_2	51.1
Al_2O_3	29.16
Fe_2O_3	8.05
TiO_2	1.54
P_2O_5	0.25
CaO	2.37
MgO	1.09
SO_3	1.56
Na_2O	0.86
K_2O	2.23

To obtain the desired particle size, the coke was crushed in a jaw crusher, and the crushed coke then screened, using Tyler standard screens. Two size fractions of coke were used in the experiments (the Tyler Standard Equivalent mesh is given in brackets): 13x9mm (0.525x0.371) and 9x7mm (0.371x3), although of course only one fraction was used for any particular experiment.

4.3.2 Particle Diameter Determination

An average diameter for the coke was calculated by using the method outlined by Geldart (1990). The average diameter of an individual particle was determined by weighing, W, and counting a sample of particles, n,

$$d_{PC} = \left(\frac{6W}{\pi \rho_C n} \right)^{\frac{1}{3}} \tag{4-3}$$

where ρ_C is found as ρ_S in section 4.3.3. The average diameter for the 13x9mm fraction was calculated to be 10.2 mm and for the 9x7mm fraction, 7.6 mm

The ash produced was screened using Tyler standard sieves. The following increments were used (the Tyler Standard Equivalent mesh is given in brackets): 19x9mm (0.742x0.371), 9x5mm (0.371x4), 5x2mm (4x8), 2x1mm (8x14), 1x0.6 mm (14x28), 0.6x0.3mm (28x48), 0.3x0.15mm (48x100) and 0.15x0.07mm (100x200). The two largest size ranges were omitted from the diameter calculations as the particles in these increments were mainly agglomerates (see section 5.1.2). The average ash particle diameter was calculated using the volume-surface mean (McCabe et al., 1993, see also equation 3-43)

$$d_{PA} = \left(\sum_{i=1}^{N} \frac{X_i}{d_{PAi}} \right)^{-1} \tag{4-4}$$

where X_i is the volume fraction in an increment and d_{PAi} is the average particle diameter in an increment.

4.3.3 Void Fraction, Bulk and Particle Density Determination

The techniques for determining the void fraction and densities were combined, and used a modified version of the ASTM Standard D 167-93 "Test Method for Apparent and True Specific Gravity and Porosity of Lump Coke". The determination was done in a cylindrical container with a diameter of 17.5 cm, ensuring that the effect of the void fraction anomaly at the wall would be similar to that of the experimental reactor. The volume V_{TOTAL} of the container was measured by filling it with water and weighing it. Particles were added to the container until level with the top and weighed, $W_{PARTICLES}$. The bulk density is given by:

$$\rho_B = \frac{W_{PARTICLES}}{V_{TOTAL}} \tag{4-5}$$

Water was then added to the container filling it to the top. As per the ASTM standard, the particles were soaked for 15 minutes. The water was drained for 1 minute by inverting the container over a wire screen. The "wet particles" were weighed, ($W_{WETPARTICLES}$) and the container was refilled with water and weighed ($W_{WETPARTICLES+H2O}$). The void volume is given by

$$V_{VOID} = \frac{W_{WETPARTICLES+H_2O} - W_{WETPARTICLES}}{\rho_{H_2O}} \tag{4-6}$$

The bed void fraction is calculated as

$$\varepsilon = \frac{V_{VOID}}{V_{TOTAL}} \tag{4-7}$$

and the particle density is then

$$\rho_S = \frac{\rho_B}{(1-\varepsilon)} \tag{4-8}$$

The reasoning behind soaking the particles is to impregnate the porous material with the water so that the void fraction obtained is that of the bed alone (not the internal voids of the particles).

The above method proved effective for calculating the void volume of the coke particles. However, with the ash particles it was found that not all of the water would drain from the bed of particles, falsifying the value of $W_{WETPARTICLES}$. Microscopic inspection of the ash particles showed them to be not obviously porous; however, the small particles did have a dendrite ("snowflake") structure which retained water by capillary action. Hence, the step of soaking and removing the water was not used in the void volume determination of the ash. The void volume of the ash is calculated as

$$V_{VOID} = \frac{W_{WETPARTICLES+H_2O} - W_{PARTICLES}}{\rho_{H_2O}} \tag{4-9}$$

4.3.4 Sphericity Determination

Permeametry was used to determine the sphericity, ψ, of the particles. In the case of the coke particles, the reactor was used as the "container". For the ash particles a 10 cm diameter column was used. The aspect ratios of these "containers" are approximately 22:1, therefore wall effects are significant. The pressure difference between a pitot tube inserted at the bottom of the bed and the pressure above the bed was measured using a differential pressure transducer. Air flowrates passed through the bed were measured using rotameters. The Ergun equation written as follows was used to describe the pressure drop through the packed bed

$$\frac{\Delta P}{L} = \frac{150\mu v}{\psi^2 d_P^2}\frac{(1-\varepsilon)^2}{\varepsilon^3} + \frac{1.75\rho_G v^2}{\psi d_P}\frac{(1-\varepsilon)}{\varepsilon^3}M \qquad (4\text{-}10)$$

where ΔP is the measured pressure difference, L is the height of the bed, μ is the viscosity, v is the air velocity and ρ_G is the air density. M is the correction factor of Mehta and Hawley (1969) which accounts for "wall effects" and is given by

$$M = 1 + \frac{4d_P}{6d_B(1-\varepsilon)} \qquad (4\text{-}11)$$

4.3.5 Ash Content

The ASTM Standard D 3174-93 "Standard Test Method for Ash in the Analysis Sample of Coal and Coke from Coal" was used to determine the ash content of the fuel. A

weighed sample of fuel, which was approximately 1 g, is placed in a porcelain capsule of known weight. The capsule was then placed in a tube furnace at 750°C. The furnace was fanned at intervals as the ashing test is supposed to be under oxidizing conditions. After four hours, the capsule is removed from the furnace and weighed. The ash in the sample is calculated as follows

$$\alpha\% = \left(\frac{W_{CAPSULE+ASHRESIDUE} - W_{EMPTYCAPSULE}}{W_{FUELSAMPLE}} \right) \times 100 \qquad (4\text{-}12)$$

4.4 Experimental Procedure

In each experiment the thermocouples were inserted 6.4 cm into the bed. This distance was chosen to ensure that the thermocouple measurements were not affected by the water-cooled probe in the centre of the bed and heat loss at the wall. The vertical placement (height above the grate) of the thermocouples depended on the thickness of the bed. An experiment was started by igniting 200 g of 1 cm square wood blocks with a propane torch. Wood contains less than 1 % ash and only about 15% fixed carbon (char), so it had a negligible affect on the bed. The primary air rate was then set and the data acquisition system started. Once the wood fire was going, the coke required for the desired bed height was slowly added. The bed was then left to reach steady state. The time depended on the air rate and bed thickness (20 to 60 minutes). Throughout each test, coke was added at timed intervals to maintain the bed height, and the bed was tamped often to ensure that a uniform

bed height and packing was maintained. Once the thermocouples indicated the bed temperatures had leveled off at steady state, gas sampling was started. The probe was lowered into the bed and gas samples were taken at various bed depths. To ensure that the point being sampled had not been disturbed by the water-cooled probe, the probe was lowered into the bed with points at the top of the bed being sampled first rather than being pulled up through it. The sampling train pump was run for at least three minutes before each sample was taken to allow for any residual gases to be flushed out of the sampling train. If the probe became clogged during sampling (a frequent occurrence), it was backwashed with compressed nitrogen. At the end of an experiment, nitrogen was injected to "freeze" the bed conditions. The bed was then sectioned into slices by lowering the grate section a measured distance using the traversing slide. A steel slide was then inserted into the bed, slicing off a bed sample of a given height. This procedure was then repeated for the remaining bed and is illustrated in Figure 4.6.

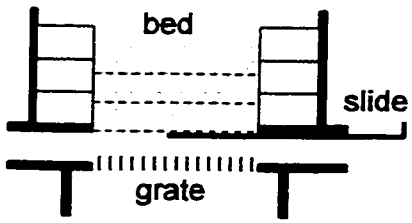

Figure 4.6 Sectioning of the bed into measured slices.

4.4.1 Bed Sample Analysis

Analysis was done on each slice for composition (% coke and % ash) and particle size distribution. The determination of the composition was done by sorting and weighing the coke and ash particles. An ASTM ashing test (see section 4.3.5) was also done on the ash to determine how much carbon was "in" the ash phase. The size distribution was obtained by screening the samples (see section 4.3.2).

5.0 RESULTS AND DISCUSSION

In this chapter the data obtained from the fuel bed experiments is presented, including the observations of ash behaviour used to develop the ash sub-model. Model predictions are used to illustrate the effects of the ash build up in a fuel bed. Validation of the char combustion model is presented in two parts: a sensitivity analysis to check the reliability of the heat and mass transfer correlations and reaction rates and to determine optimal kinetic and transport parameters followed by a comparison of the model predictions with the data acquired from the fuel bed experiments. Finally, the experimental data and model predictions are used to study the effect of operating conditions on the structure of fuel beds.

5.1 Fuel Bed Experiments

A total of seven different fuel bed experiments using different operating conditions are reported here. The operating conditions for these experiments are listed in Table 5.2. The length of each experiment depended on the time required to obtain a detailed concentration profile over the entire bed. Test 05A191L was run longer to study extinction of the bed. The concentration and temperature profiles obtained from these experiments are presented in Figures 5.16-5.22.

Table 5.2 Experimental operating conditions

Test #*	Bed height (cm)	Particle size (cm)	Air mass flux (kg/m^2hr)	Measured average burning rate (kg/m^2hr)	Test duration (hr)
05A191L	5	1.02	191	9.7	7
05A263L	5	1.02	263	21.1	4.8
05A520L	5	1.02	520	53.9	3.2
10A343L	10	1.02	343	46.1	3.3
15A168S	15	0.76	168	19.5	4.6
15A236S	15	0.76	236	27.2	4.1
15A327S	15	0.76	327	49.9	4

* key to Test numbering: ## (bed height cm), A### (air mass flux kg/m^2hr), S or L (particle size - S = 0.76 cm and L=1.02cm)

5.1.1 Fuel Properties

Table 5.1 summarizes the physical properties of the coke determined by the methods outlined in section 4.3. These values were assumed to be the same for the two different batches of coke used in the experiments.

Table 5.1 Physical properties of the coke as determined by the characterization experiments.

Property	Value $\pm 1\sigma$
Diameter (cm)	0.76 ±0.02 1.02 ±0.02
Particle density (kg/m^3)	880 ±2
Void fraction	0.500 ±0.002
Sphericity	0.50 ±0.01

5.1.2 Experimental Observations of Ash Behaviour

Sectioning of the bed into slices provided information on the behaviour of the ash. The following observations are based on inspection and analysis of the bed slices using the procedure outlined in section 4.4.1. Ash particles were found to segregate completely from the fuel particles. As seen in Figure 5.1, there is no evidence of an ash layer adhering the surface of the fuel particles. Visual inspection and screening of the ash particles indicated that the ash is produced as small particles. This can be observed in Figures 5.1 and 5.2. In Figure 5.2, the two larger particle sizes are not single particles, but agglomerations of individual particles sintered together. These agglomerates were only

Figure 5.1 Photograph of a bed sample illustrating the complete segregation of the ash from the char.

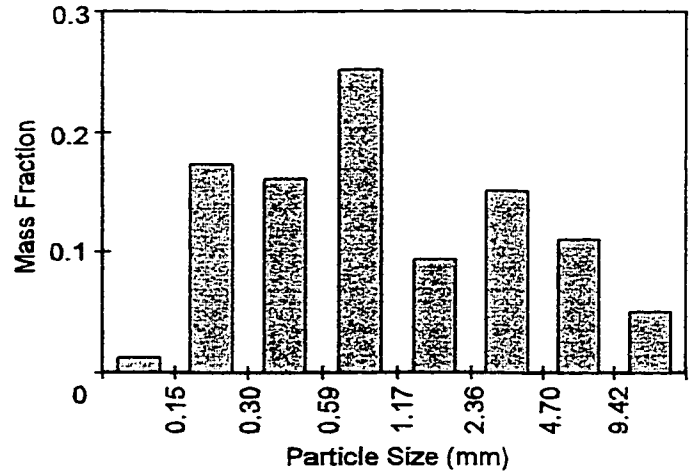

Figure 5.2 Particle size distribution of the ash produced during Test 05A191L.

observed near the wall and the thermocouples in most experiments. It is suspected that the wall refractory and thermocouple insulators reacted with the ash. Ash has been shown to have a damaging effect on refractories (Reid, 1981). Ash sintering was observed throughout the bed in experiments which produced high temperatures (high combustion rates and/or thick beds). Under these conditions, the sintering was caused by the solids temperature reaching the ash softening temperature. The agglomerates produced were open and friable with a structure similar to a bed of unsintered ash particles. Thus, the agglomerates were excluded in the calculation of the average ash diameter. Screening results of each slice, from a given experiment, showed similar particle size distributions (see Figure 5.3) and mean diameters. This indicates that the ash production mechanism is similar throughout the bed and that once produced, the ash particles do not undergo further changes except for sintering. Ash particles appeared to move down through the bed with the fuel particle which generated them, finally accumulating in a layer on top of the grate. The bed retained most of the ash formed as the

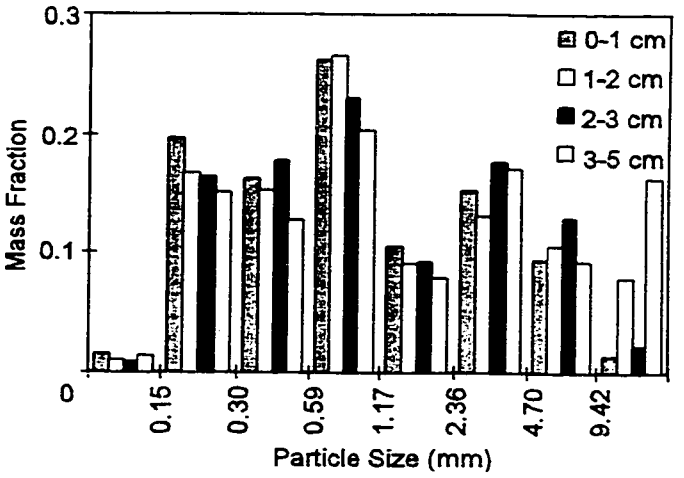

Figure 5.3 A comparison of the ash particle size distribution in each layer of the Test 05A191L fuel bed.

smaller ash particles were trapped in the interstices between the larger fuel particles. Some fine particles fell through the grate into the ashpan while others may have been elutriated. However, comparisons of the actual amount of ash produced and the theoretical amount showed the amount lost to be negligible. The increasing concentration of ash from the top to bottom of the bed, as shown in Figure 5.4, is indicative of the downwards movement of the ash.

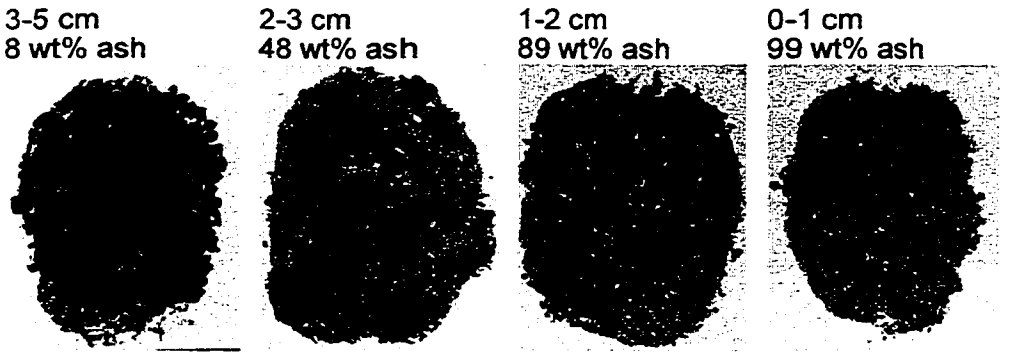

Figure 5.4 Comparison of the ash concentrations in successive layers of the Test 05A191L fuel bed.

While ash formed in a given experiment was similar throughout the bed, there was a significant difference in the ash produced by experiments run under different operating conditions. As mentioned previously, more sintering was encountered with an increase in the solid temperature. Also, the average particle size, density and void fraction of the ash particles changed significantly. This was expected as the physical properties of ash are known to be dependent on combustion conditions. A comparison of the ash produced from Tests 05A191L and 15A236S is shown in Figures 5.5 and 5.6. Figure 5.5 shows the difference in the particle size distribution; the average ash particle diameter for Test 15A236S was 0.8 mm

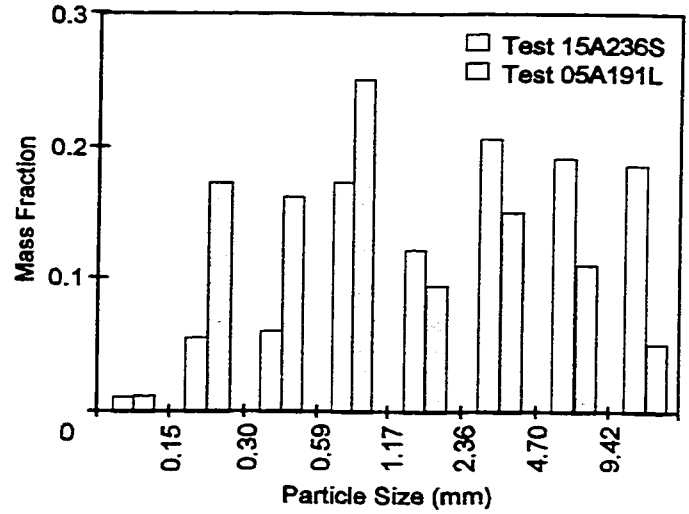

Figure 5.5 Difference in the ash particle size distribution caused by different operating conditions.

and for Test 05A191L 0.5 mm. Figure 5.6 illustrates the difference in the physical properties of the ash produced during the two tests, particularly in the density. The difference in the ash densities is related to the effect that the bed temperatures have on the ash structure. The low density ash produced during Test 05A191L was "fluffy", whereas the higher density ash produced during Test 15A236S, was more compact and had larger sized particles. Test 05A191L had temperatures which were on average 100°C lower than Test 15A236S. The "fluffy" ash represents the ash as it was first formed, while the denser ash results from some sintering and/or fusion of the "fluffy" ash into larger and denser particles. The difference in the colour indicates that different transformations of the mineral matter into ash have occurred, as the colour of the ash is representative of the chemical composition (Benson et al., 1993).

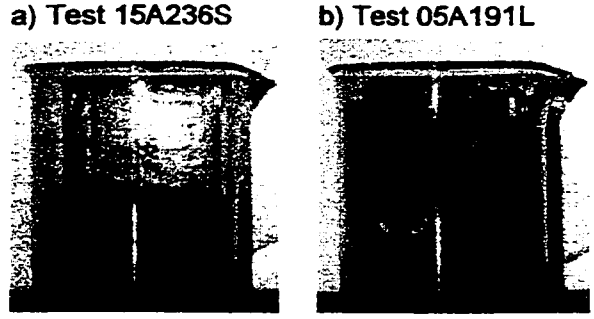

Figure 5.6 Illustration of the difference in ash properties caused by different operating conditions. Each beaker contains 15 g of ash.

5.1.3 Ash Properties

Table 5.3 summarizes the ash properties determined using the methods outlined in section 4.3. As was discussed in the previous section and seen in Table 5.3, the properties of the ash varied significantly from experiment to experiment. During the early experimental runs, the significant effect that the ash properties have on the model predictions was not realized and as a result not all of the ash properties were measured after the experiments. In these cases, ash properties from experiments run under similar operating conditions were used as model inputs. The values having an asterisk in Table 5.3 are ones which were not actually measured on the ash produced during that particular experiment, but were used as model inputs. The dendrite structure of the ash (noted in section 4.3.3) and the highly irregular shapes of the agglomerates were the cause of the very small ash sphericity.

Table 5.3 Physical properties of the ash as determined by the characterization experiments.

Test #	Average particle size (cm)	Density, ρ_A (kg/m^3) $\pm 1\sigma$	Void fraction $\pm 1\sigma$	Sphericity $\pm 1\sigma$	% ash in coke $\pm 1\sigma$
05A191L	0.05	1648 ±25	0.75 ±0.01	0.18*	7.61 ±0.10
05A263L	0.07	1637 ±57	0.73 ±0.01	0.184 ±0.004	7.61 ±0.10
05A520L	0.1	2079 ±68	0.70 ±0.01	0.18*	6.40 ±0.02
10A343L	0.1	2079*	0.70*	0.18*	6.40 ±0.02
15A168S	0.06	1637*	0.73*	0.18*	6.40 ±0.02
15A236S	0.08	1810 ±37	0.65 ±0.01	0.179 ±0.004	7.61 ±0.10
15A327S	0.08*	1810*	0.65*	0.18*	6.40 ±0.02

* assumed values based on ash properties from similar experiments

5.2 Char Combustion Model

Figure 5.7 shows a typical model prediction of the temperature and concentration profiles in a combustor bed. The O_2 is consumed in the first couple of centimetres in the high temperature oxidation zone, being converted primarily to CO_2. Once all of the O_2 is consumed, the CO_2 is converted to CO by the endothermic reduction reaction. This is highly endothermic, which results in the solid temperatures being lower than the gas temperatures. The presence of an inert ash layer on top of the grate is evident from the atmospheric oxygen concentration and low temperatures in the first 1.5 cm of the bed.

5.2.1 Ash Model

5.2.1.1 Effects of Heat and Mass Transfer Correlations on Model Predictions

The changes to the model predictions caused by the modifications made to account for ash in the heat and mass transfer correlations (see section 3.3.3) can be observed in Figure 5.8. These two changes - and therefore the ash itself - have a significant effect on the model predictions. In Figure 5.8a a comparison of the model predictions including the changes to heat and mass transfer to those with no change to mass transfer is shown. If the mass transfer modification is included, the mass transfer is reduced as the ash particles fill the voids between the fuel particles. As seen in Figure 5.8a this results in the oxygen moving further into the bed before it is completely consumed. Figure 5.8b shows a similar comparison, but without the changes to the effective solid thermal conductivity. The inclusion of the ash phase in the calculation of the effective solid conductivity results in a decrease in the effective solid conductivity, since the ash particles act as radiation shields and reduce interparticle radiation. This results in the particles at the bottom of the bed being kept cooler by the incoming air and consequently the reaction zones occur further from the grate, as seen in Figure 5.8b. Omission of both changes results in the reaction zones occurring even closer to the grate. Without the heat and mass transfer models it was impossible to get agreement between the experimental and model predictions, because the model predicted that oxygen depletion would occur too low in the bed.

5.2.1.2 Effects of Ash Layer Buildup on Model Predictions

The effect of the accumulation of ash in the bed can be observed in Figures 5.9 and 5.10. The 5 hour prediction in these figures represents conditions shortly before extinction occurs. As time progresses, ash is retained on the grate in a layer of increasing thickness, causing the model predictions to continuously change. A comparison of Figure 5.9a and b shows how ash accumulation shifts the reaction zones higher in the bed and effectively creates a progressively thinner bed. The concentration and temperature profiles show how ash accumulation divides the bed into an active layer and an inert ash layer. A model prediction of the ash layer buildup over time is shown in Figure 5.10. The predicted percent of unburnt carbon, defined as d_{PC}^3 / d_{PC0}^3, and the solid temperature are also given. From this figure, it can be observed that the growing ash layer increasingly chokes off combustion, resulting in an unburnt carbon residue within the ash layer. Eventually, the whole bed extinguishes with significant carbon residues at the top.

The thickness of the ash layer and the rate of its buildup are directly proportional to the amount of ash in the fuel, but they are also strongly dependent on the ash properties. Figure 5.11 shows the effect of ash properties on the concentration and gas temperature profiles. In Figure 5.11a, b and c, the ash particle diameter, d_{PA}, void fraction, ε_A, and density, ρ_A, were individually changed from the ash properties of Test 05A520L to the ash properties of Test 05A191L. The profiles show how the ash properties influence the thickness of the ash layer and how this in turn influences the profiles in both the oxidation and reduction zone. Changes to the ash particle diameter affect the heat transfer: smaller particles

have a larger specific surface area, and at the bottom of the bed they will be cooled more by the incoming air, as seen in Figure 5.11a. Smaller ash particles also give a lower effective solid conductivity, which appears to give a slightly steeper temperature gradient in the oxidation zone. As seen in Figure 5.11b and c an increase in the ash phase void fraction or a reduction in the ash density gives a proportional increase in ash volume. Changes to the ash sphericity did not significantly influence the model predictions.

5.3 Model Verification

Concentration measurements at different heights in the bed were taken at widely differing times due to the long cycle time of the gas chromatograph (see section 4.2.1.4). Also, because the bed conditions were continuously changing it would be meaningless to compare the experimental data with model predictions at one given time. Thus, the Figures 5.12-5.22 show "composite" model curves, in which the model prediction plotted at a particular height above the grate is that which corresponds to the time at which the nearest gas sample was obtained. Since the probe was always pushed downwards in the bed, concentration points at the top of the bed were taken near the start of a test, and those nearer the grate were recorded later.

5.3.1 Sensitivity Analysis

The char combustion simulation can be run using a number of options for the fluid-to-particle mass and heat transfer and for the char oxidation and reduction reaction rates. The

effect that these choices have on the agreement between model predictions and experimental data is analysed in the following sections. To determine which options produce model predictions which best represent the experimental data, the model predictions for each option are compared with the experimental data of Test 05A520L. This test was chosen as it was performed with a bed thickness typical of a combustor and it has a detailed concentration profile in both the oxidation and reduction zones. The one drawback with using this data is that only two thermocouples penetrated the 5 cm bed due to the limitations of the apparatus. However in packed beds, concentration profiles are considered to be a better indicator of model accuracy than temperature profiles, as it is uncertain which temperature (solid or gas) the thermocouple measurements actually represent.

5.3.1.1 Heat and Mass Transfer Correlations

Fluid-to-particle heat and mass transfer correlations are an area of uncertainty in packed bed combustion modelling as there are no specific experimental data available (Hobbs et al., 1993). All of the correlations investigated by Cooper (1996) were obtained from experiments which were performed at temperatures of approximately 300 K and in non-reactive systems (very different from a combustor); thus, their applicability was questionable. The model developed by Cooper (1996) can be run with three of the most suitable correlations: Chu et al. (1953), Yoshida et al. (1962) and Battacharyya and Pei (1975).

Cooper (1996) found that the correlation of Yoshida et al. (1962) produced model predictions which best compared with the experimental data of Nichols (1935); however, during the conversion of the model to include non-spherical particles, it was found that this

correlation contained discrepancies regarding the use of particle sphericity. Since Cooper (1996) found the correlations of Yoshida et al. (1962) and Chu et al. (1953) to have similar transfer rates, only the correlations of Chu et al. (1953) and Bhattacharyya and Pei (1975) were investigated in this study.

As seen in Figure 5.12, model predictions calculated using the correlation of Chu et al. (1953) do not agree with the experimental data at all. The model predicts a reduction zone which starts too low in the bed and reaction rates which are too fast, indicating that the heat and mass transfer rates are too high. The model prediction of a sharp decrease in the O_2 concentration in the oxidation zone is a result of too high a mass transfer rate.

Cooper (1996) found that the correlation of Bhattacharyya and Pei (1975) predicts lower heat and mass transfer rates than that of Chu et al. (1953). As a result, the use of the Bhattacharyya and Pei (1975) correlation markedly improved the agreement between model predictions and experiment data as seen in Figure 5.13. This figure shows that the model predicts a more gradual depletion of the oxygen, which is more in line with the experimental oxygen profile than the sharp decrease predicted using the Chu et al. (1953) correlation. The predicted and experimental maximum CO_2 concentrations also compare better in Figure 5.13 than when using the Chu et al. (1953) correlation (which greatly underestimates the CO_2 concentration). An improvement in the agreement between the predicted and experimental temperatures in the reduction zone can also be observed in Figure 5.13.

A comparison of Figure 5.12 and 5.13 clearly indicates that the experimental data correspond much better to the model prediction using the lower transfer rates of Bhattacharyya and Pei (1975) than those of Chu et al. (1953), and therefore the remaining

model predictions use the correlation of Bhattacharyya and Pei (1975) to calculate the heat and mass transfer coefficients. Once the appropriate reaction rate parameters for the CO_2 reaction are determined (see section 5.3.1.2) the model predictions using the correlation of Bhattacharyya and Pei (1975) will be seen to fit the experimental data very well. The same conclusion was drawn when the heat transfer correlations were reviewed after "fitting" the CO_2 kinetics. It should be noted that no adjustments had to be made to the transfer correlation to "fit" the experimental and model data. This is contrary to the experience of Hobbs et al. (1993) who claimed that to obtain good agreement between experimental and predicted results, one has to assume smaller fluid-to-particle heat transfer than in a non-reactive system. The fixed-bed model of Hobbs et al. (1992) requires a fluid-to-particle heat transfer correction factor, with a value of 0.02-0.1, to "fit" the predicted solid temperatures to data - a massive change in heat transfer physics.

5.3.1.2 Reaction Kinetics

As described in section 3.2, the simulation was modified to include the effects of diffusion and reaction in the pores. The effect of including the pore diffusion model in the determination of the char oxidation and reduction rates can be seen by comparing Figures 5.13, 5.14 and 5.15 and is described below.

A) Char Oxidation Reaction

Figures 5.13 and 5.14 show the model predictions in which the char oxidation rate is calculated using the Field's expression (equation 3-17) and the pore diffusion model (equation 3-19), respectively. The reduction reaction was not modified and used the rate parameters

for subbituminous coal char of Goetz et al. (1982). As expected, the model predictions in these two figures show virtually no difference in the concentration or temperature profiles, even though the use of the pore diffusion model decreases the rate of the char oxidation reaction by a factor of four. Inspection of the numerical values showed that the oxygen concentration varies by less than 1% and the temperature by less than 50 K (at a given bed location). This lack of effect that changes to the kinetics have on the concentration and temperature profiles, indicates that the char oxidation reaction is diffusion-controlled, as has also been concluded by others (Cooper, 1996 and Hobbs et al., 1992). The rate expression of Field was thus deemed adequate for calculating the char oxidation reaction rate and is used in the remaining model predictions.

B) CO_2 Reduction Reaction

The rate of the CO_2 reduction reaction at the char surface is known to vary with char type; however, values for the kinetic parameters were not available for the fuel used. Thus, initially published rate coefficients were used for both the effective, K_{CO2}, and the intrinsic, K_{ICO2}, reaction rates. Goetz et al. (1982) gave rate parameters for chars from four different coals, of which those for subbituminous coal char (A = 102.6 kg /m^2 s kPa and E = 177700 kJ /kmol) were found to give model results most closely approximating the present data and those of Nichols (1935). Figures 5.13 and 5.15 show predictions obtained from a simulation using these coefficients with and without the inclusion of the pore diffusion model, respectively. Inspection of the two figures shows that by including diffusion and reaction in the pores, the char reduction rate is increased. This is discernible from the higher CO concentrations exiting the bed (29% compared with 24%) and the lower temperatures in the

reduction zone. The increase in the depth of the ash layer is also an indication of an increase in reaction rate, as more of the carbon has been consumed, thus producing more ash. This effect was found to be even more pronounced in thicker beds. As pore diffusion and reaction affects the model predictions and the inclusion of pore diffusion is more realistic, the remaining simulations are run with the pore diffusion model included in the calculation of the CO_2 reduction rate.

The overprediction of the ash layer depth and the CO concentration as well as the underprediction of the temperatures in the reduction zone indicates that the rate parameters of Goetz et al. (1982) result in a reduction rate which is too fast. As there is no intrinsic reaction rate data in the literature for the reduction reaction, the pre-exponential was altered until the best reproduction of the experimental concentration profiles was obtained. The model predictions shown in Figure 5.16 were obtained using the following intrinsic reaction rate expression (in kg/m^2skPa):

$$K_{ICO_2} = 0.05 \exp\left(\frac{-177700}{RT_S}\right) \tag{5-1}$$

The activation energy was unchanged. This expression was found to fit the experimental data from the seven tests the best. The "fitting" of this expression was done by eye, no least squares analysis was performed.

5.3.2 Comparison of Model Predictions with Experimental Data

To verify the char combustion model, the seven experiments listed in Table 5.2 were simulated using the model. For the different simulations, a number of the model inputs varied including the operating conditions in Table 5.2 (fuel particle diameter, bed height and primary air flow). Also, as the ash properties are dependent on the operating conditions, each simulation used different inputs for the ash properties. The runs and corresponding properties are listed in Table 5.3. The coke properties entered into the model remained the same for each simulation (see Table 5.1 and section 4.3.1). Optimal transport coefficients and reaction kinetics, as determined in the previous section, were used and were the same for all of the simulations.

To determine the validity of the model predictions, comparisons between experimental and model data are presented and discussed in the following sections. They include bed temperature and gas concentration profiles, burning rates, bed solids composition at the end of a run, and transient profiles (ignition and extinction).

5.3.2.1 Concentration and Temperature Profiles

Figures 5.16-5.22 compare experimental gas concentration and temperature profiles with the model predictions. A good agreement between model and experiment can be observed for both temperature and concentration profiles with all of the trends properly predicted. The good fit of the oxygen consumption and the lowest thermocouple measurement indicates that the ash layer build up is accurately modelled. Observed deviations can be attributed to two main causes: the modelling of the ash in the bed and the CO_2

reduction rate expression. Also, while every attempt was made to prevent channeling in the bed by tamping the bed regularly, channeling may have contributed to the observed differences.

A comparison of the Figures 5.16-5.22 shows that Test 15A168S has the worst fit. This test was done at a low velocity and gave rise to a Reynolds number close to the transition value. Thus, the heat and mass transfer correlations which assume turbulent flow may be less accurate here.

As mentioned in section 2.4, mineral matter undergoes many complex transformations as it is converted to ash and the ash itself undergoes phase changes as it moves downwards through the different combustion zones. This results in the ash having different properties at different points in the bed; however, these transformations have not been included in the ash sub-model. As the ash properties were found to have a considerable influence on the model predictions (see section 5.2.1.2), this may contribute to the discrepancies. The properties of the ash used as model inputs (see Table 5.3) are its properties at room temperature and are assumed by the model to be the same throughout the bed, though this is not likely. For example, during some of the experiments the thermocouples measured temperatures greater than 1600°C, at which point any ash present would be liquid, as this is above the ash melting point (see section 4.3.1). This liquid ash (slag) would have very different properties and effects on the fuel bed than solid ash particles. Also, the presence of ash agglomerates in all of the tests indicates that softening, if not melting, of the ash did occur.

The deviations of the concentration profiles in the oxidation zone can be attributed to the presence of the ash. Ash has the greatest affect on the data points in the oxidation zone

because ash concentrations are the highest at the bottom of the bed and these data were obtained later in the run when a larger quantity of ash was present in the bed. By looking at the model predictions for the thin beds (Figures 5.16-5.18), it can be seen that the consumption of the oxygen is modelled accurately closest to the grate where the temperatures are low; however, higher up in the bed the model predicts an oxygen consumption rate which is too high. One explanation is that in the cooler regions of the bed the ash properties are most likely to be similar to the model inputs. As the oxygen concentration approaches zero, the bed temperatures reach a maximum, at which point the ash may have softened or liquefied, giving it different properties. Another factor which may have resulted in the further penetration of the oxygen is the radially inserted thermocouples. During sampling of the bed, it was often found that the thermocouple sheaths (especially those lower in the bed where ash concentrations were the highest) were covered with large crusts or agglomerations of ash. These may have prevented the fuel and ash from sliding down easily, resulting in the formation of cavities in the bed which would have allowed oxygen to penetrate further into the bed. Kreisinger et al. (1916) noted that this was found to be a problem during their experiments.

As seen in Figures 5.19-5.22, the fitted model prediction overpredicts the reduction rate for thicker beds. This is physically reasonable, as it has been shown that pore diffusion and reaction occur in the reduction zone (see section 5.3.1.2). The reaction in the pores will enlarge the pores, reducing the internal specific surface area, which would in turn reduce the reaction rate. Smoot and Smith (1985) state that to accurately model pore diffusion and reaction, variations of the internal pore structure with time should be included. In thick beds,

the particle residence time in the reduction zone is much longer than in thin beds, so this effect would be more pronounced. Thus, reaction rates which fit concentration profiles for thinner beds would be too fast for thicker beds. The reason that the simulation of Test 15A236S compares better with the experimental values may be due to the use of a different batch of coke for this test, which may have had a slightly higher reactivity than the coke used for Tests 15A327S and 10A343L. It should be noted that the fit could have been improved by adjusting the reduction reaction for each individual run, but this was not done.

It should also be noted that in all of the measurements, there is a degree of stochastic variation, owing to the irregularity of the coke particles. The detailed geometry of the bed near the probe is continuously varying, and this will cause variations in measured concentrations.

It is uncertain which temperature (gas or solid) the thermocouple measurements represent, as the thermocouple bead could be in contact with a fuel particle or in the interstice between two particles. However, due to the high radiant fluxes between particles in the bed (Yagi and Kunii (1957) state that in packed beds most of the heat transfer is via radiation), the thermocouples would tend to approach the solid temperature rather than the gas temperature. The predicted temperature profiles agree well with the limited experimental data. The one exception is the lowest thermocouple in Test 05A191L. This large discrepancy in the temperature while concentration profiles showed good agreement was probably caused by the fact that the sheath of this thermocouple broke during the test. The downwards movement of the fuel and ash would have carried the thermocouple along with them and the temperature measurements would be of the cooler ash layer.

5.3.2.2 Burning Rates

A comparison of the measured and predicted burning rates is presented in Table 5.4. The values presented are averaged over the entire experimental run and corresponding model simulation, as the burning rates change as the bed fills with ash. A major source of uncertainty in this comparison is the starting conditions of the bed. During some of the experiments, the bed took a long time to fully ignite, particularly at low air flow rates. A comparison of the values shows agreement to within 30%, except for Test 05A191L. The deviations are in the expected directions: for Test 05A520L the model underpredicts the CO reduction reaction, thus the burning rate will also be less, whereas for Test 15A168S the model overpredicts the CO reduction reaction with a consequent higher burning rate prediction. Test 05A520L has the worst agreement between the model and experimental values because the test was run until the bed extinguished itself and it has been found that the model does not accurately predict extinction of the bed (see section 5.3.2.4).

Table 5.4 Comparison of measured average burning rates and the average burning rates predicted by the model.

Test #	Average Burning Rate (kg/m^2hr)	
	Measured	**Predicted**
05A191L	9.7	18.3
05A263L	21.1	25.3
05A520L	53.9	48.2
10A343L	46.1	46.4
15A168S	19.5	23.9
15A236S	27.2	35.3
15A327S	49.9	49.5

5.3.2.3 Bed Composition

A comparison of the predicted distribution of ash in the bed and the results of bed sampling performed at the end of the run is presented in Figures 5.23 and 5.24. Figure 5.24 shows only the first 5 cm of the 15 cm bed. The predicted percent unburnt carbon and solid temperature are also given. Considering that is difficult to cut the bed along precisely defined planes the agreement is good. For the two sets of results presented, it can be observed that the model underpredicts the carbon consumption near the grate, especially for the thin bed. The model predicts a much lower ash concentration than what was observed experimentally (70% compared with 97%). A possible cause for this discrepancy is that although the carbon oxidation reaction is diffusion-controlled in the active part of the bed, chemical kinetics may be important in determining the carbon consumption in the ash layer due to the lower temperatures. Inspection of the solid temperatures in the two beds shows that the thicker bed has higher temperatures in the "ash layer". This would keep the reaction diffusion-controlled for longer, resulting in more of the carbon being consumed as observed in Figure 5.24. The model and experimental results show the presence of small amounts of unburned carbon within the ash layer: as coke particles burn away they are surrounded by increasing concentrations of ash, resulting in a dilution of the combustion heat release and eventually the extinction of the particles. The ash agglomerates were also found to contain small amounts of carbon - about 1% by weight - which would be largely inaccessible to oxygen.

5.3.2.4 Ignition and Extinction

Test 05A191L was used to investigate extinction of the bed and check the transient behaviour of the model. This test was run until the bed was extinguished by the buildup of ash. It took 6.2 hours for there to be no visible glowing in the bed; however, prior to this, most of the bed had already been extinguished. By 4.2 hours, the bed near and in contact with the reactor walls was no longer glowing. Also, for the last hour of the run, no fuel feeding was performed, as the burning rate was low enough not to require any feed to maintain the bed height.

Figure 5.25 shows the comparison of the solid temperature profiles predicted by the simulation and the temperature measurements obtained experimentally over the course of the entire run (from ignition to extinction). Figure 5.25 shows that the model had a faster temperature rise indicating a quicker ignition time. The model does not represent the exact method used to ignite the bed: it assumes that the required amount of fuel is in the reactor and is heated and ignited by a hot layer on top of the grate, whereas experimentally, once the wood fire is going, the coke is slowly added to the bed until the desired bed depth is obtained. Considering these differences, the agreement is reasonable. It is important that the experimental and model ignition times correspond fairly closely due to the effect that the buildup of ash has on the bed.

The model predictions of bed extinction do not compare well with the experiment. An extinction time of 7.6 hours is predicted by the model and as seen in Figure 5.25, combustion continues in most of the bed for much longer (as shown by the temperatures) than in reality. This is the cause of the big discrepancy in the burning rates in Table 5.4. One

cause of these discrepancies is that during extinction, the bed temperatures are much lower, resulting in a kinetically-controlled oxidation zone. It is possible that the oxidation kinetics used may then lose their validity. Another cause of these discrepancies is that the model is one-dimensional; however, from experimental observations, the bed does not remain one-dimensional as the ash layer becomes a significant portion of the bed. Heat losses to the wall increase, as observed by the extinguishing of the bed near the walls. Also, heat loss to the water-cooled probe will have an increased effect, resulting in temperature non-uniformities and subsequent combustion non-uniformities across the bed.

5.4 Effects of Operating Conditions on Fuel Bed Combustion

5.4.1 Air Flow

The effect of the air flow rate on fuel bed combustion can be observed by comparing the results from Tests 05A191L, 05A263L and 05A520L. These tests had a common bed height, 5 cm, but different primary air flow rates (see Table 5.2). While Table 5.2 shows that increasing the air flow increases the burning rate, a comparison of the concentration profiles in Figures 5.16, 5.17 and 5.18 shows virtually no difference (the small differences can be attributed to the difference in ash build up rate which is a function of the burning rate). Thus, fuel bed stoichiometry is independent of the air flow rate. This is the unique self-regulating nature of fuel beds which results in the combustion rates for a given bed depending solely on air flow. However, Figures 5.16, 5.17 and 5.18 show that changes in air flow rate do affect

the temperature profiles. Increasing the air flow decreases the gas residence time, which results in a corresponding decrease in the heat transfer between the two phases. A resulting increase in the temperature difference between the two phases is observed. Also, the overall bed temperature increases with an increase in airflow, as higher temperatures are required to radiate the additional heat release produced by the higher burning rates.

5.4.2 Bed Thickness

A comparison of the profiles of Tests 05A263L, 10A343L and 15A236S show how the stoichiometry of the bed is affected by the bed thickness. With a thin bed, as seen in Figure 5.18, the O_2 penetrates deep into the bed, allowing for most of the CO_2 produced to leave the bed before it can be reduced to CO. Figure 5.19 shows that doubling the bed thickness results in a thicker reduction zone and thus the CO_2 produced is converted to CO. Increasing the bed depth by another 5 cm (see Figure 5.21) results in almost all of the CO_2 produced in the oxidation zone to being converted to CO. As seen in the previous section, the stoichiometry is independent of air flow; thus, the only way to control the stoichiometry of a fuel bed is through the bed depth. Thin beds have lower temperatures than thick beds because heat losses from the bed by conduction and radiation become larger relative to the heat release. The temperatures leaving thin beds are much higher than thick beds as the reduction zone is not thick enough for the endothermic reduction reaction to significantly affect them. A comparison of the operating conditions of Tests 05A263L and 15A236S (see Table 5.2) indicates that for a given air flow, increasing the bed height also increases the burning rate. Thicker beds have more char available for consumption.

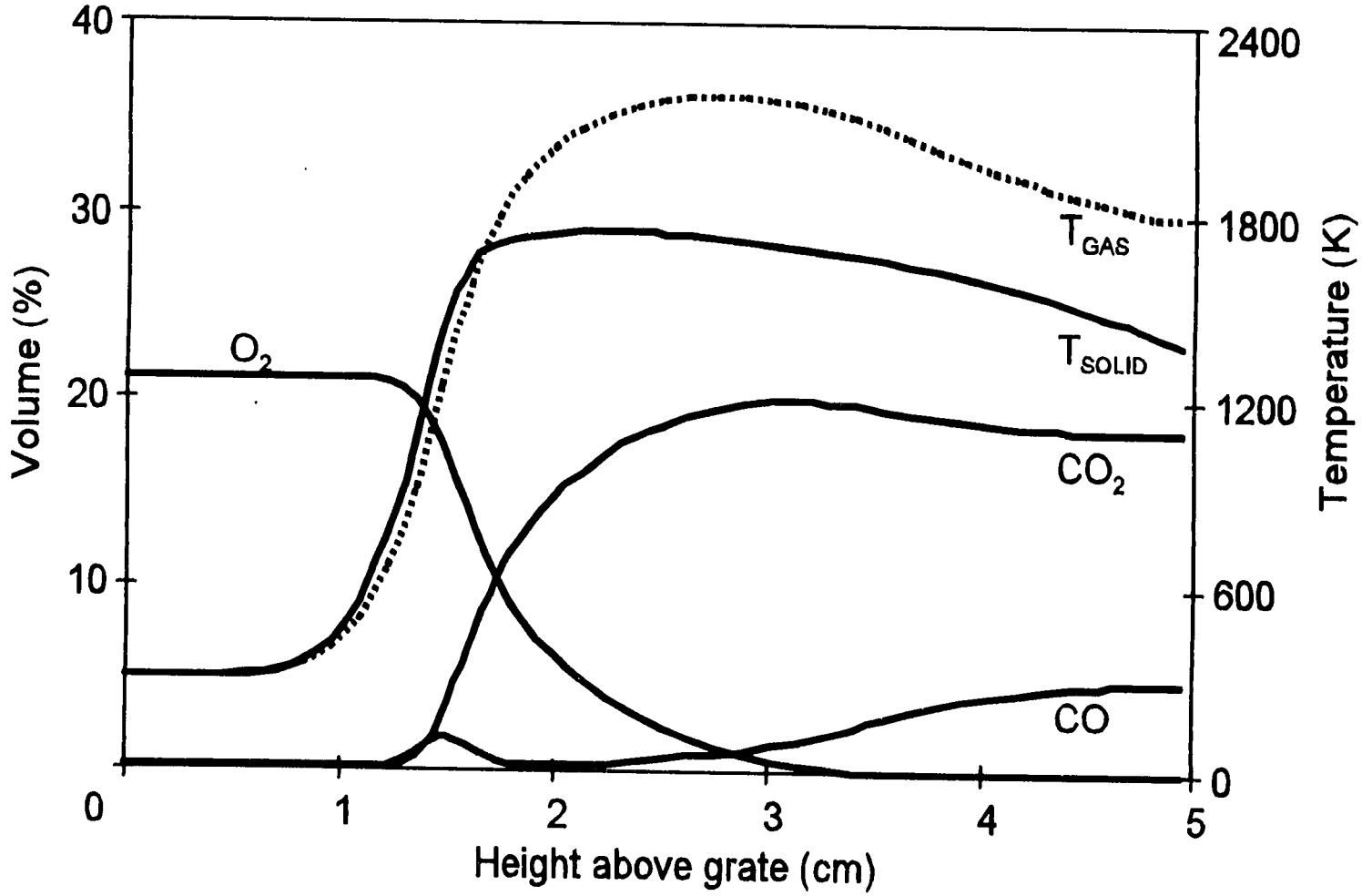

Figure 5.7 Predicted temperature and concentration profiles, using the operating conditions and particle properties of Test 05A520L, after 2 hours of operation. The simulation was run with the following model options: heat and mass transfer correlation - Bhattacharyya and Pei (1975), char oxidation reaction - Field (1969), and CO_2 reduction reaction - "fitted" rate parameters (see Equation 5-1) with the pore diffusion model.

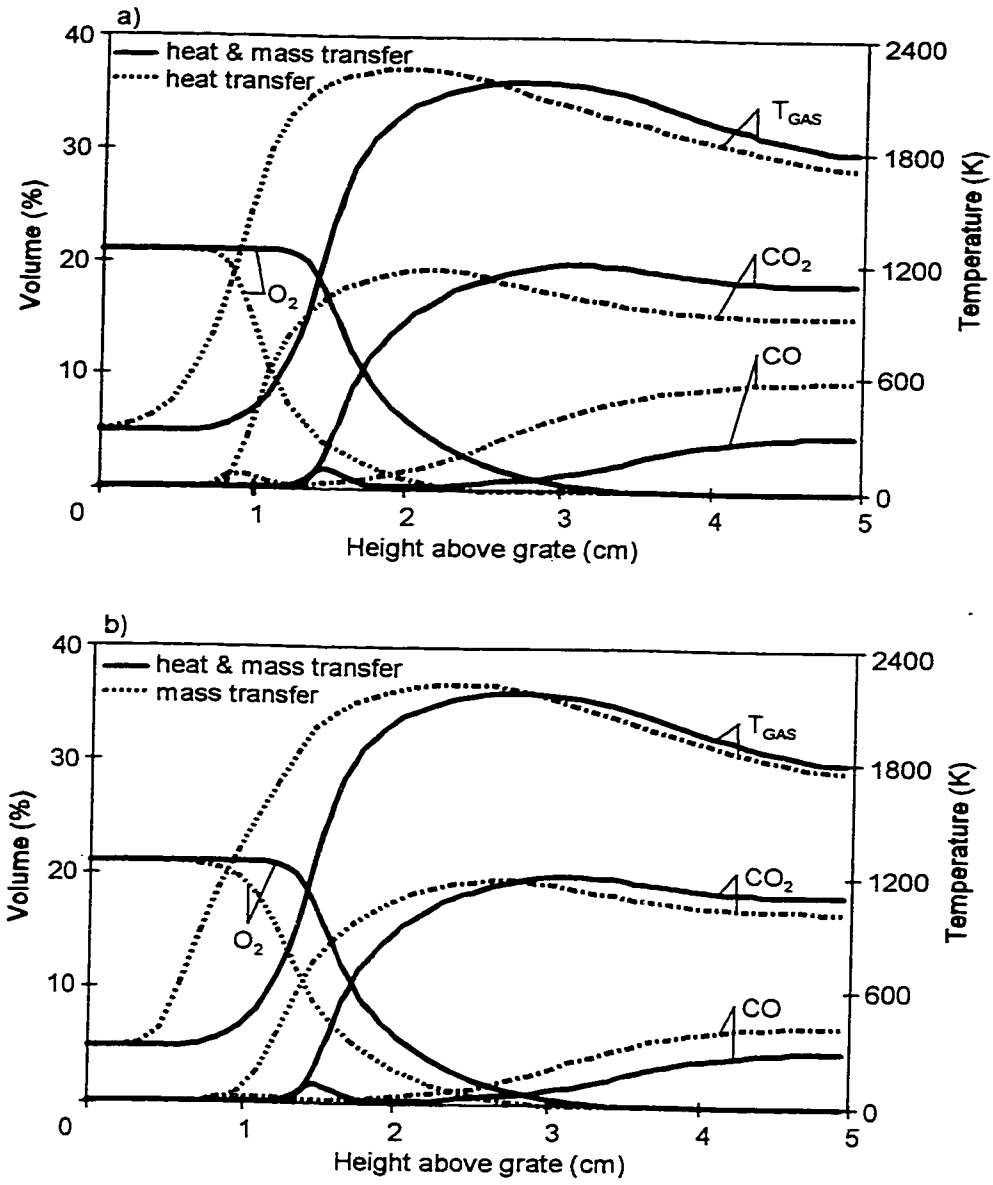

Figure 5.8 Results of the model modifications made to include the effects of ash on heat and mass transfer in the bed on the temperature and concentration profiles. Compared are the profiles when both the heat and mass transfer changes are included and when a) only the heat transfer change is included and b) only the mass transfer change is included. All other conditions remain the same as Figure 5.7.

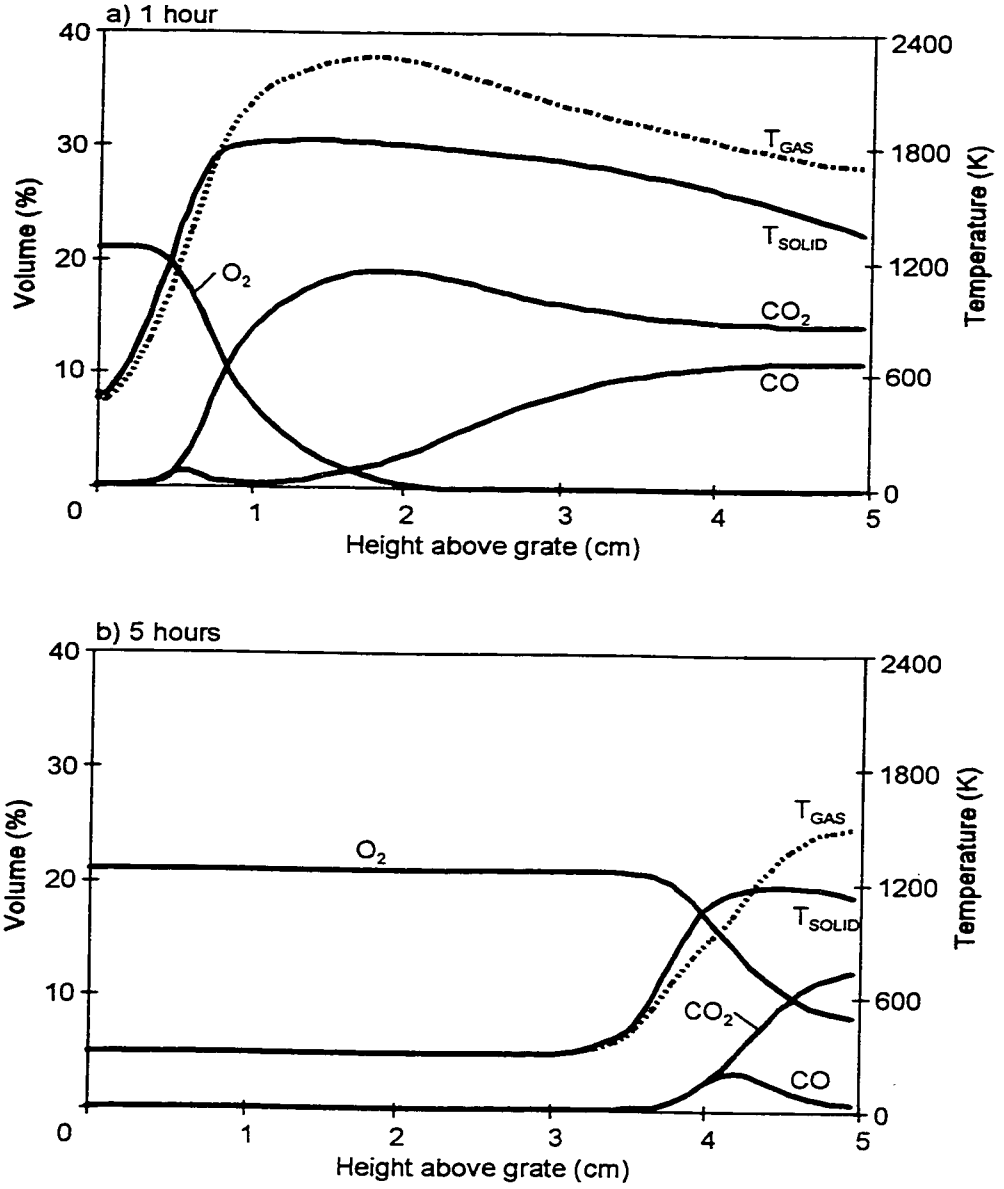

Figure 5.9 Predicted temperature and concentration profiles for the conditions of Figure 5.7 except after a) 1 hour and b) 5 hours of operation.

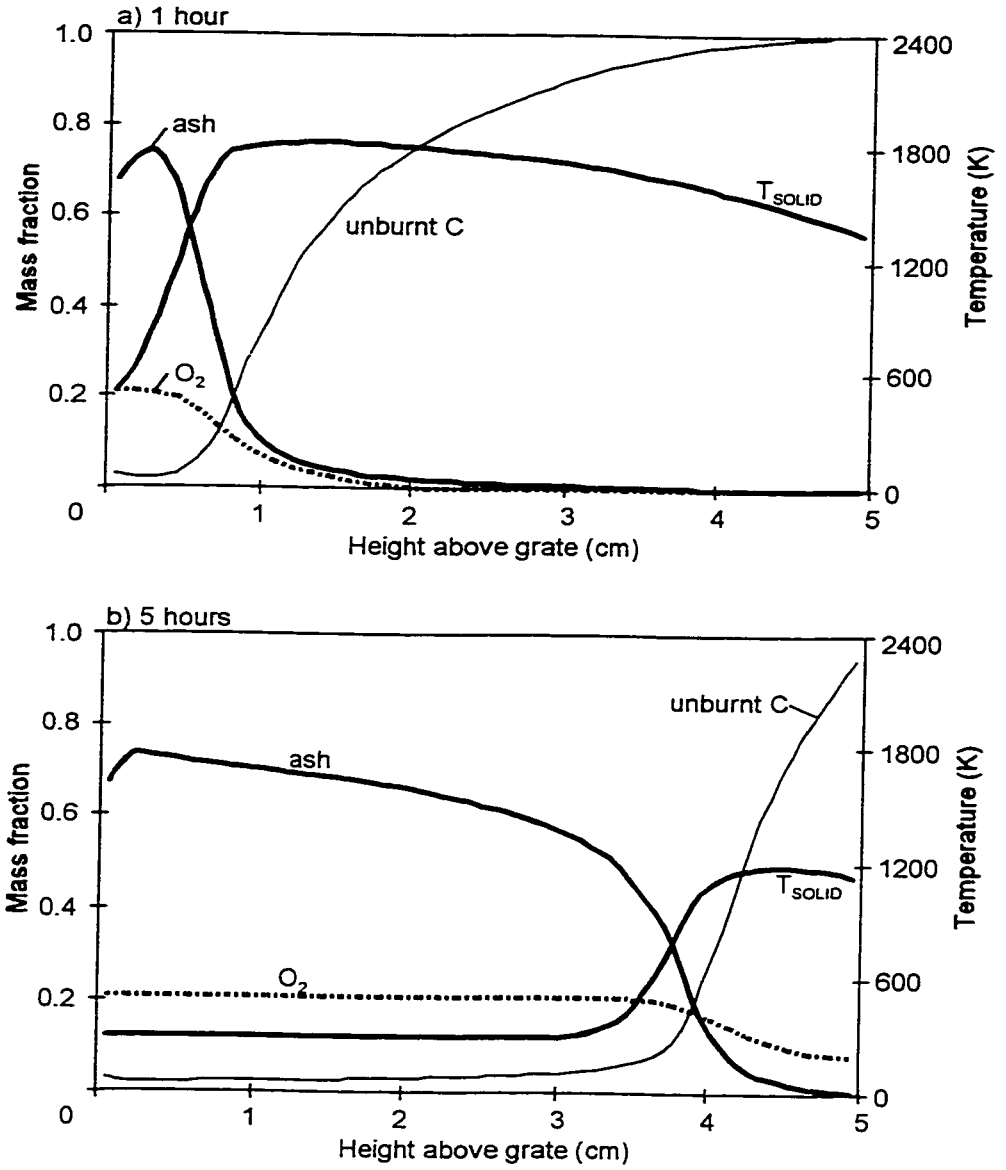

Figure 5.10 Predicted ash fraction, unburnt carbon fraction, O_2 fraction and solid temperature versus bed height for the conditions of Figure 5.7. a) shows the predictions after 1 hour of operation and b) after 5 hours of operation.

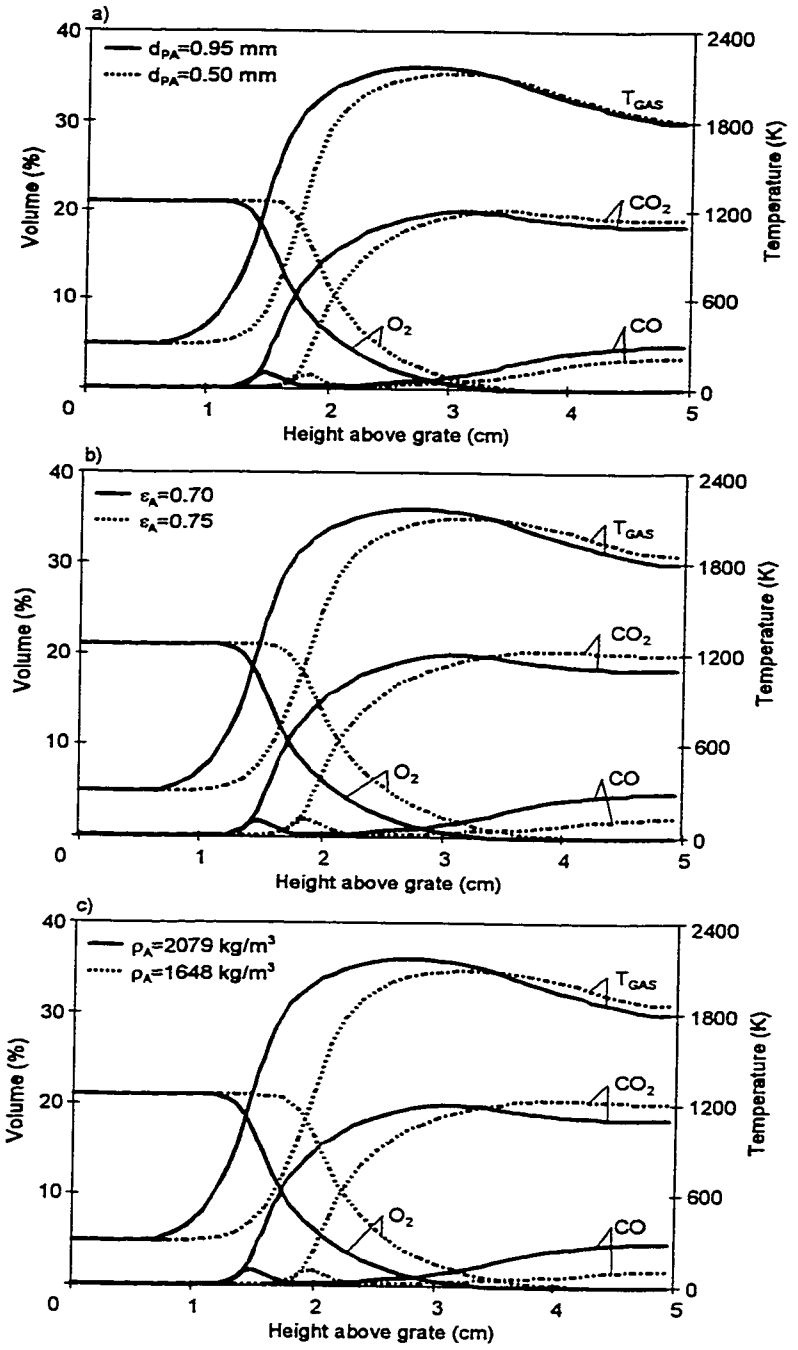

Figure 5.11 Effect of changing the ash properties on predicted temperature and concentration profiles for the operating conditions of Test 05A520L. The ash properties which are not changed in each graph are those of Test 05A520L and the simulation was run with the same options as Figure 5.7.

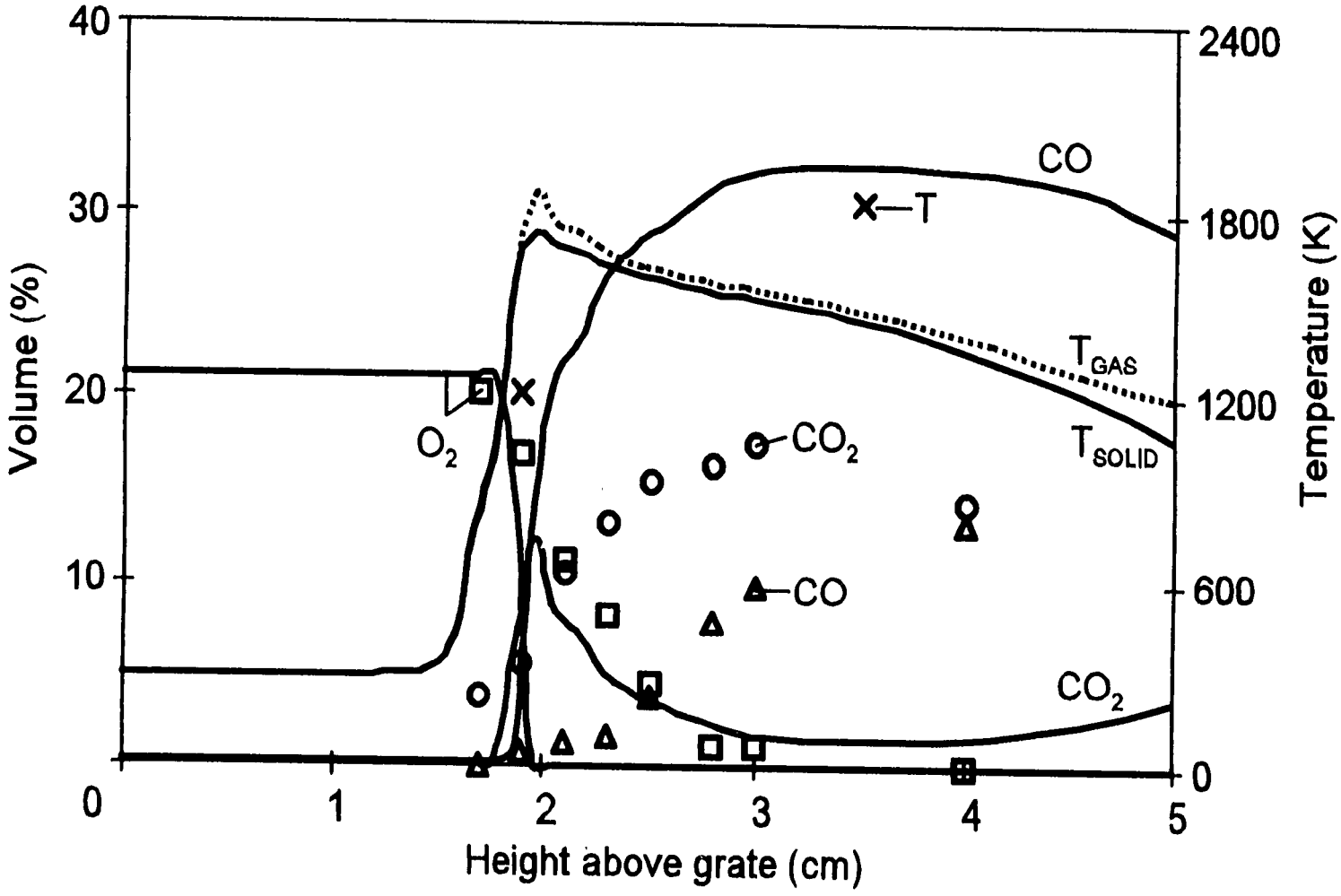

Figure 5.12 Composite graph comparing the experimental and predicted temperature and concentration profiles. The operating conditions and particle properties are those of Test 05A520L. The simulation was run with the following model options: heat and mass transfer correlation - Chu et al. (1953), char oxidation reaction - Field (1969), and CO_2 reduction reaction - subbituminous coal char (Goetz et al.,1982) without the pore diffusion model.

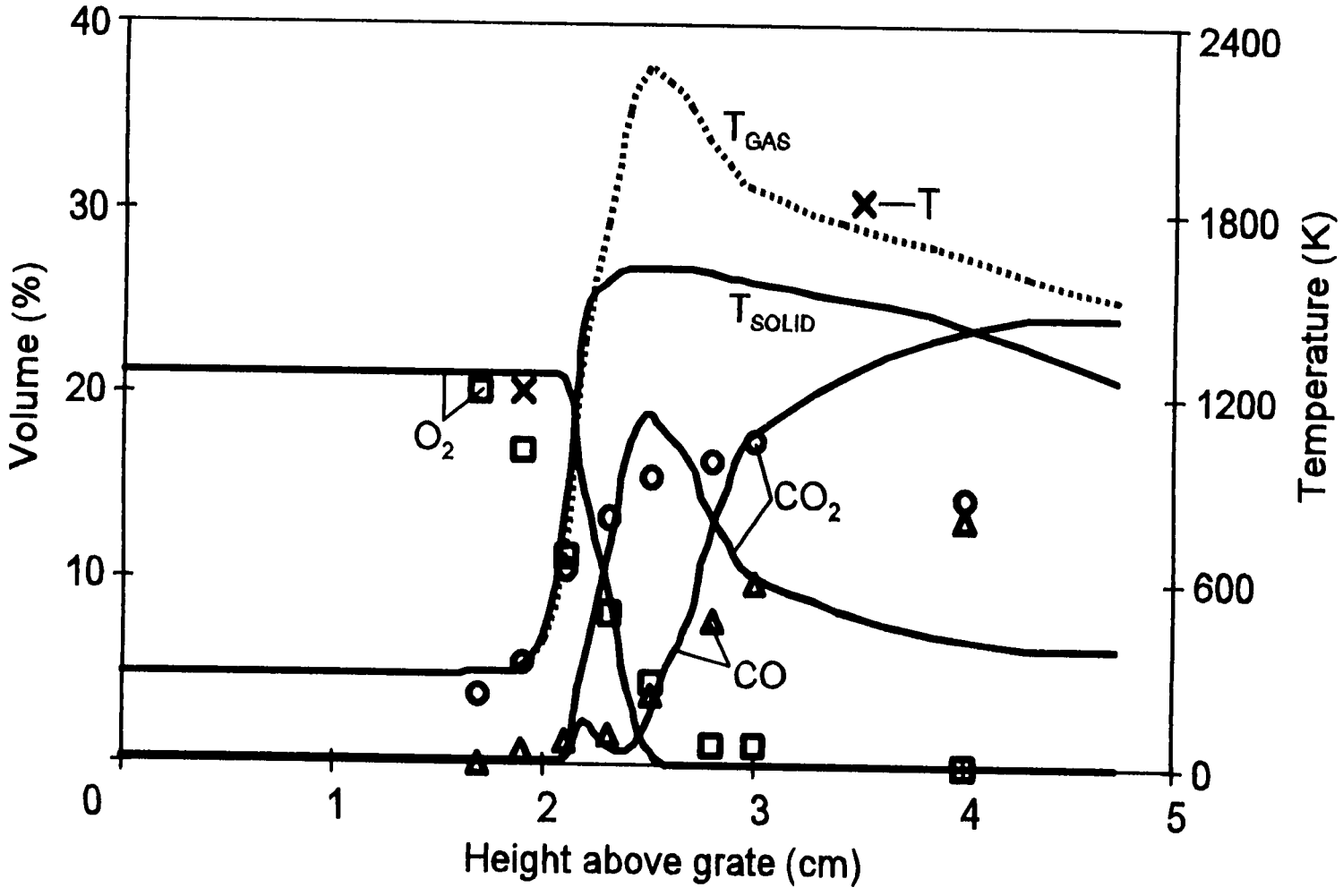

Figure 5.13 Composite graph comparing the experimental and predicted temperature and concentration profiles. The operating conditions and particle properties are those of Test 05A520L. The simulation was run with the following model options: heat and mass transfer correlation - Bhattacharyya and Pei (1975), char oxidation reaction - Field (1969), and CO_2 reduction reaction - subbituminous coal char (Goetz et al.,1982) without the pore diffusion model.

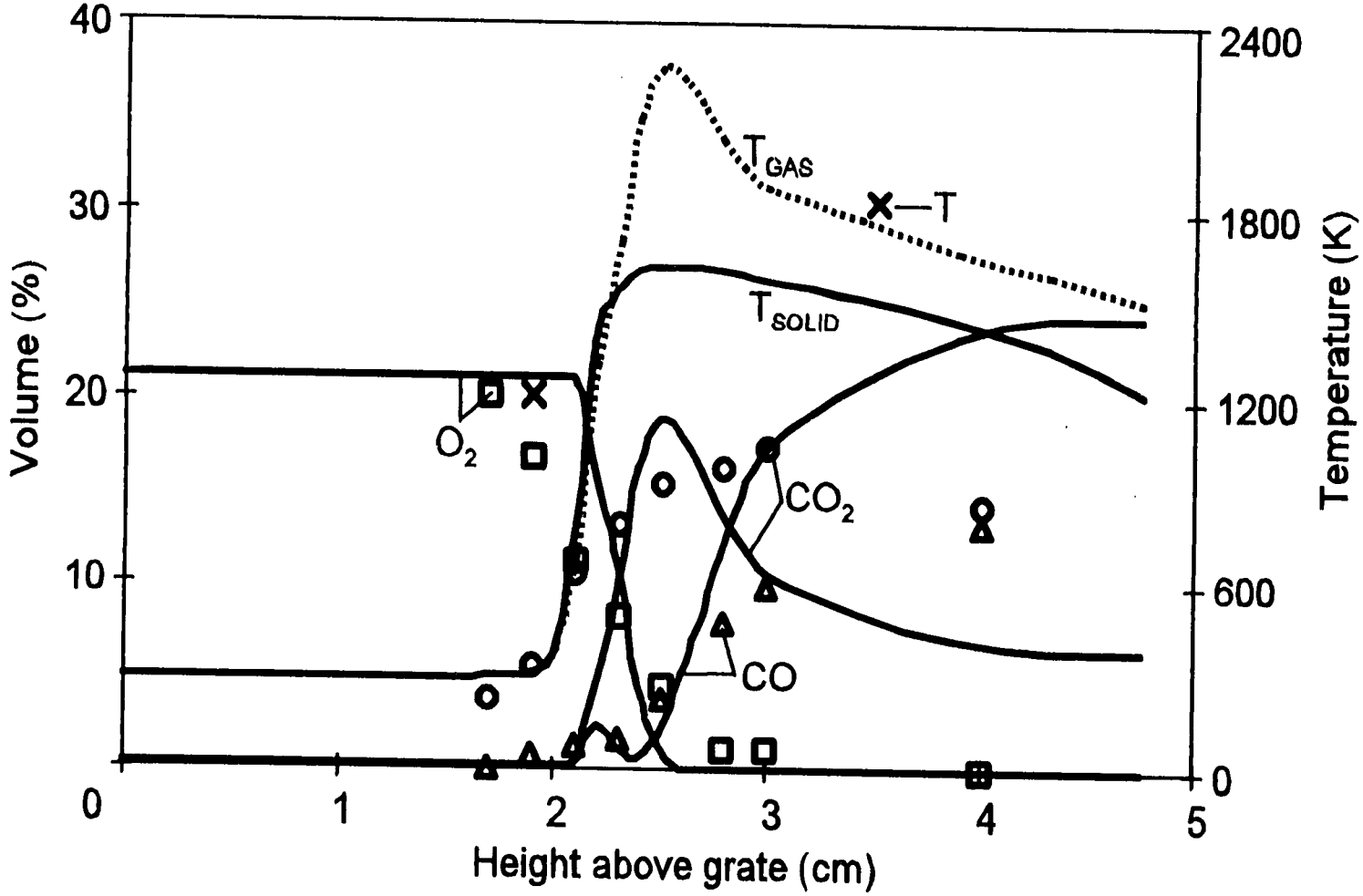

Figure 5.14 Composite graph comparing the experimental and predicted temperature and concentration profiles. The operating conditions and particle properties are those of Test 05A520L. The simulation was run with the following model options: heat and mass transfer correlation - Bhattacharyya and Pei (1975), char oxidation reaction - pore diffusion model, and CO_2 reduction reaction - subbituminous coal char (Goetz et al.,1982) without the pore diffusion model.

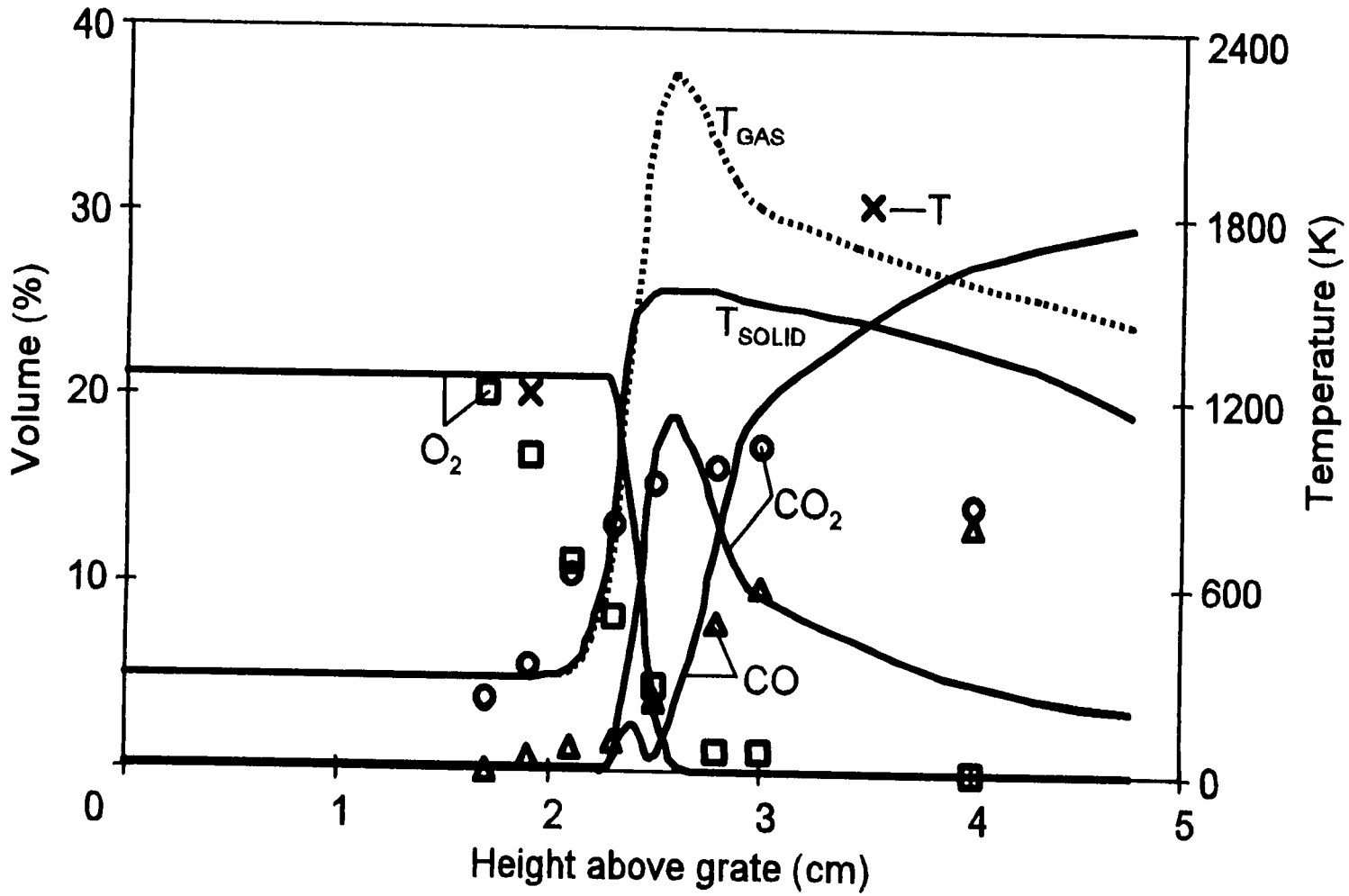

Figure 5.15 Composite graph comparing the experimental and predicted temperature and concentration profiles. The operating conditions and particle properties are those of Test 05A520L. The simulation was run with the following model options: heat and mass transfer correlation - Bhattacharyya and Pei (1975), char oxidation reaction - Field (1969), and CO_2 reduction reaction - subbituminous coal char (Goetz et al.,1982) with the pore diffusion model.

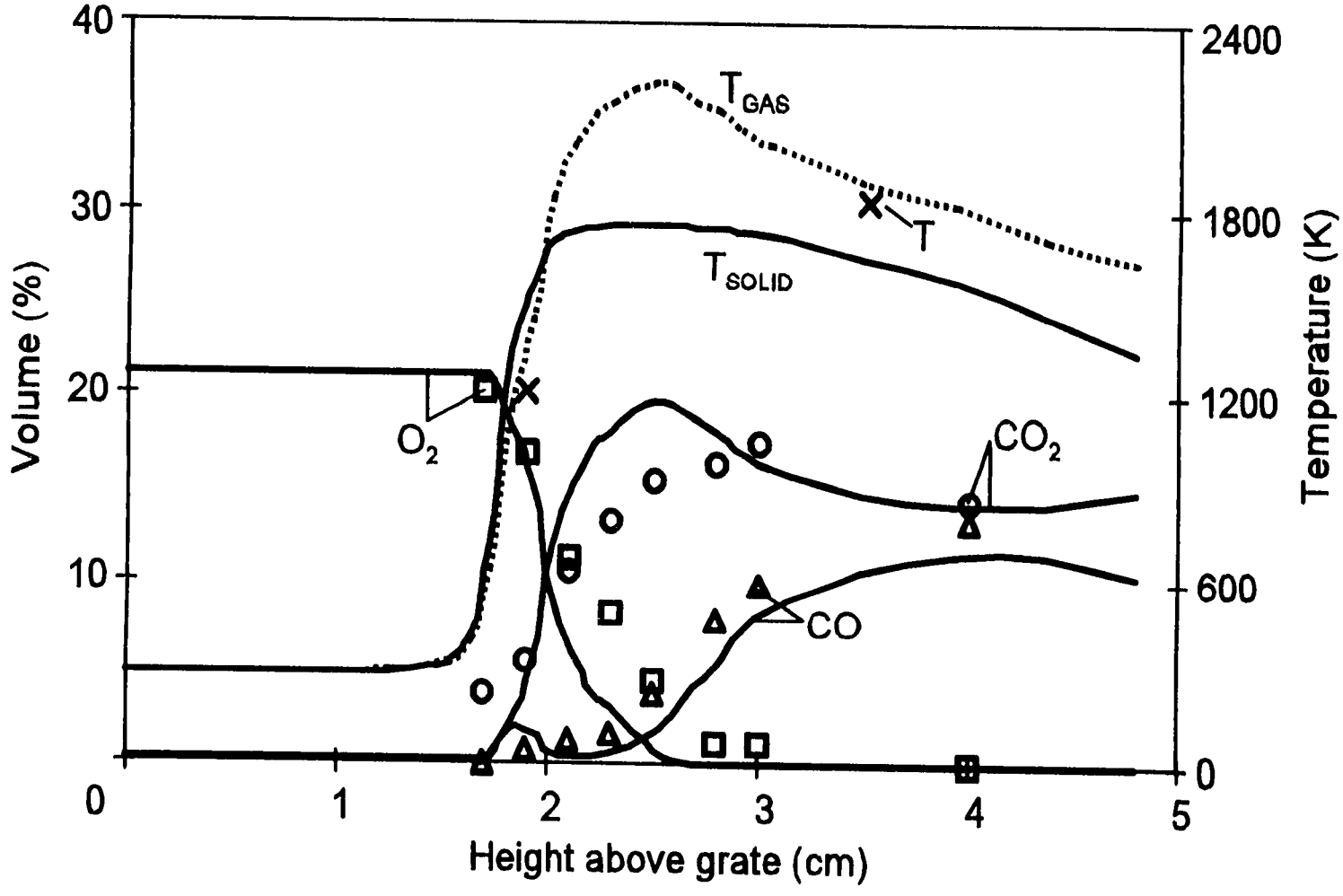

Figure 5.16 Composite graph comparing the experimental and predicted temperature and concentration profiles. The operating conditions and particle properties are those of Test 05A520L. The simulation was run with the following model options: heat and mass transfer correlation - Bhattacharyya and Pei (1975), char oxidation reaction - Field (1969), and CO_2 reduction reaction - "fitted" rate parameters (see Equation 5-1) with the pore diffusion model.

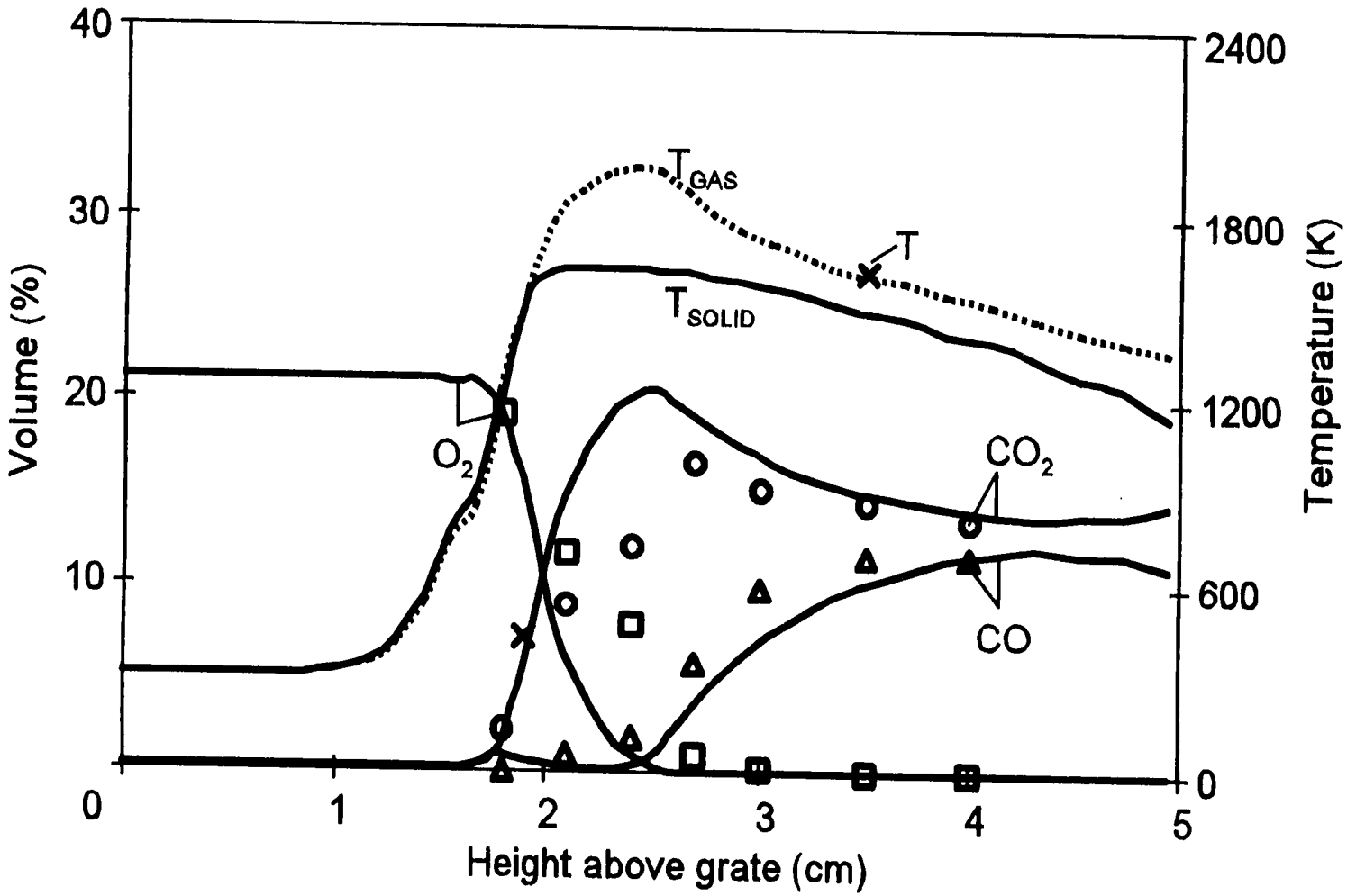

Figure 5.17 Composite graph comparing the experimental and predicted temperature and concentration profiles. The operating conditions and particle properties are those of Test 05A191L. The simulation was run with the following model options: heat and mass transfer correlation - Bhattacharyya and Pei (1975), char oxidation reaction - Field (1969), and CO_2 reduction reaction - "fitted" rate parameters (see Equation 5-1) with the pore diffusion model.

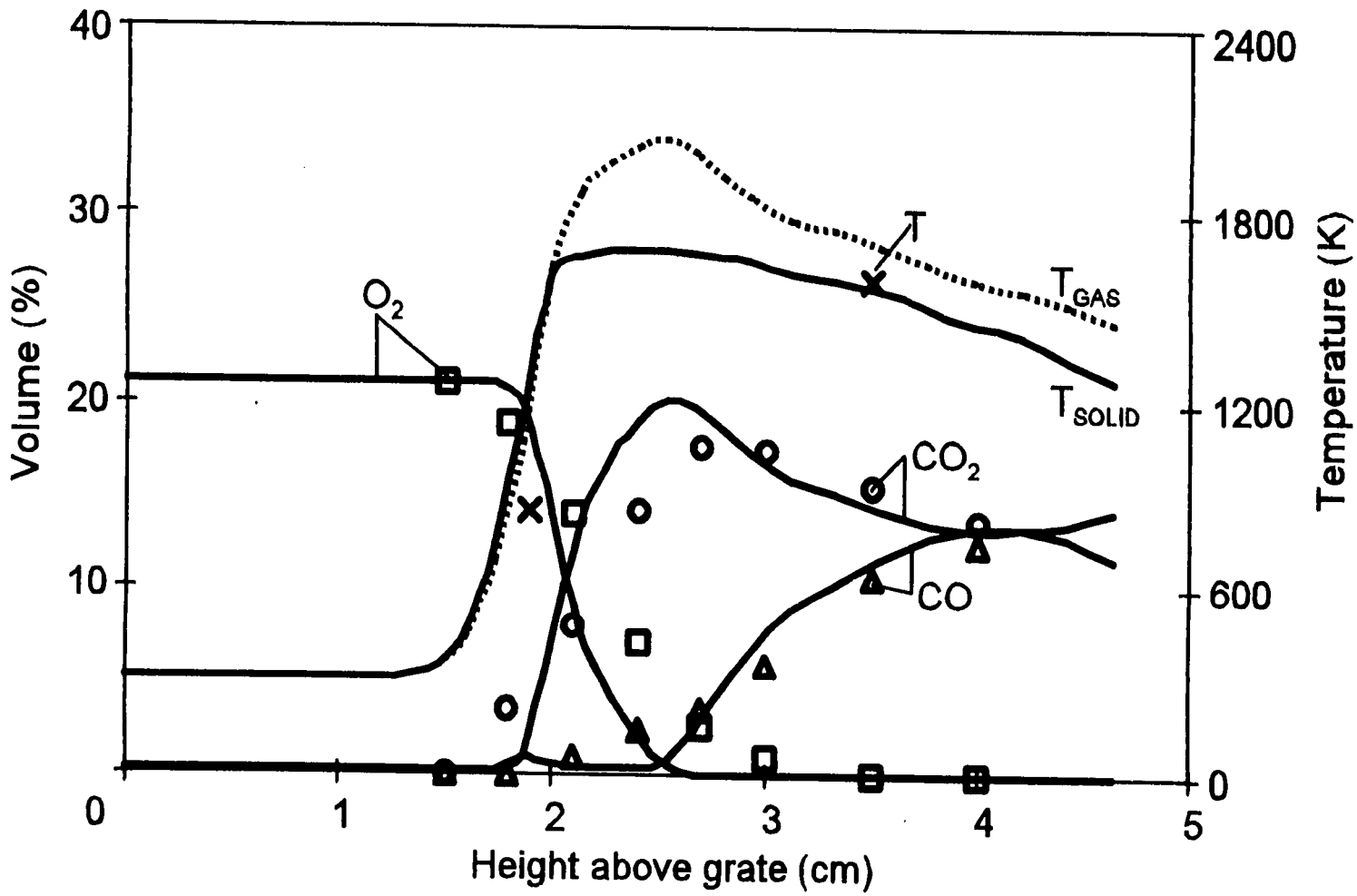

Figure 5.18 Composite graph comparing the experimental and predicted temperature and concentration profiles. The operating conditions and particle properties are those of Test 05A263L. The simulation was run with the following model options: heat and mass transfer correlation - Bhattacharyya and Pei (1975), char oxidation reaction - Field (1969), and CO_2 reduction reaction - "fitted" rate parameters (see Equation 5-1) with the pore diffusion model.

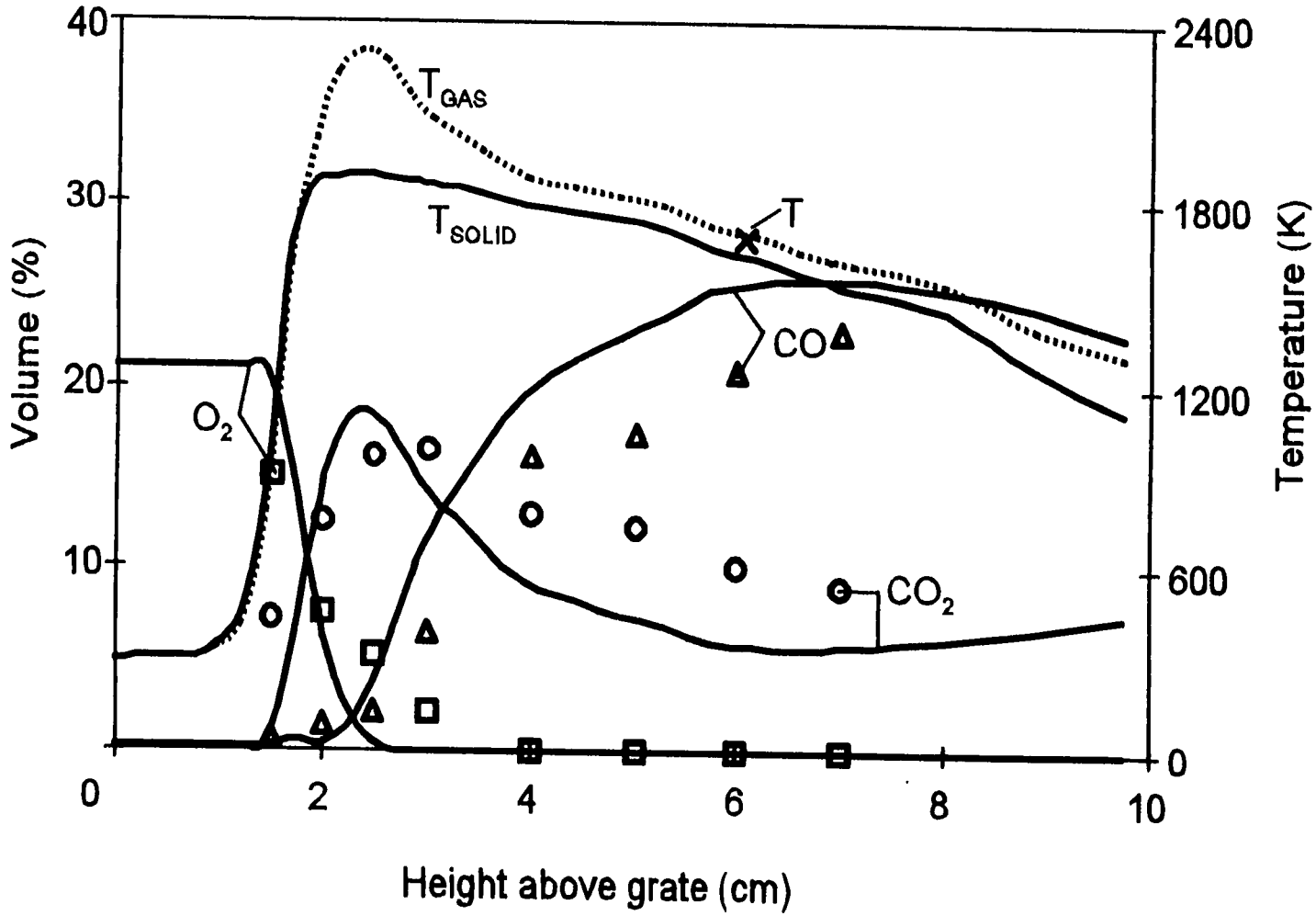

Figure 5.19 Composite graph comparing the experimental and predicted temperature and concentration profiles. The operating conditions and particle properties are those of Test 10A343L. The simulation was run with the following model options: heat and mass transfer correlation - Bhattacharyya and Pei (1975), char oxidation reaction - Field (1969), and CO_2 reduction reaction - "fitted" rate parameters (see Equation 5-1) with the pore diffusion model.

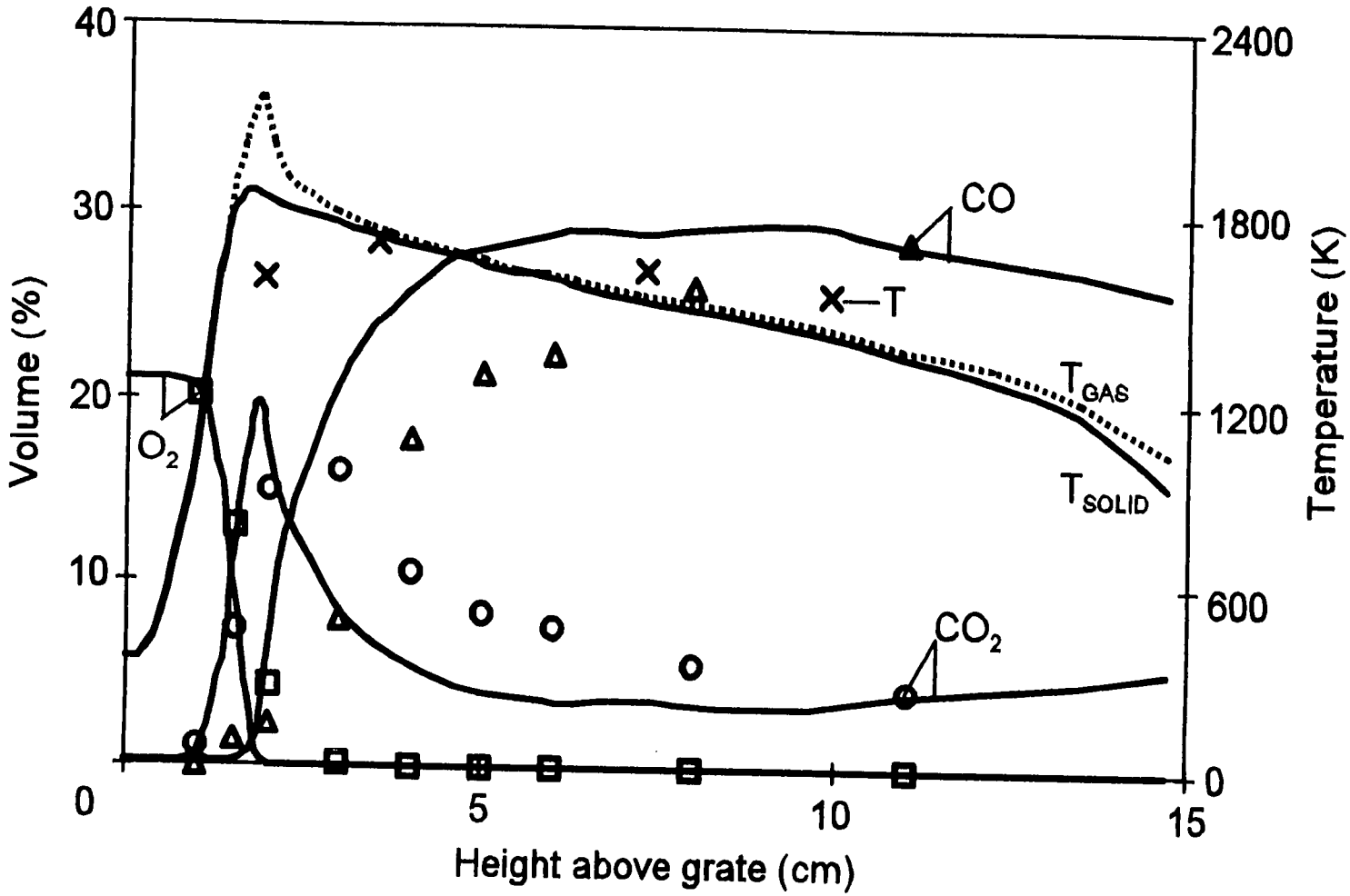

Figure 5.20 Composite graph comparing the experimental and predicted temperature and concentration profiles. The operating conditions and particle properties are those of Test 15A168S. The simulation was run with the following model options: heat and mass transfer correlation - Bhattacharyya and Pei (1975), char oxidation reaction - Field (1969), and CO_2 reduction reaction - "fitted" rate parameters (see Equation 5-1) with the pore diffusion model.

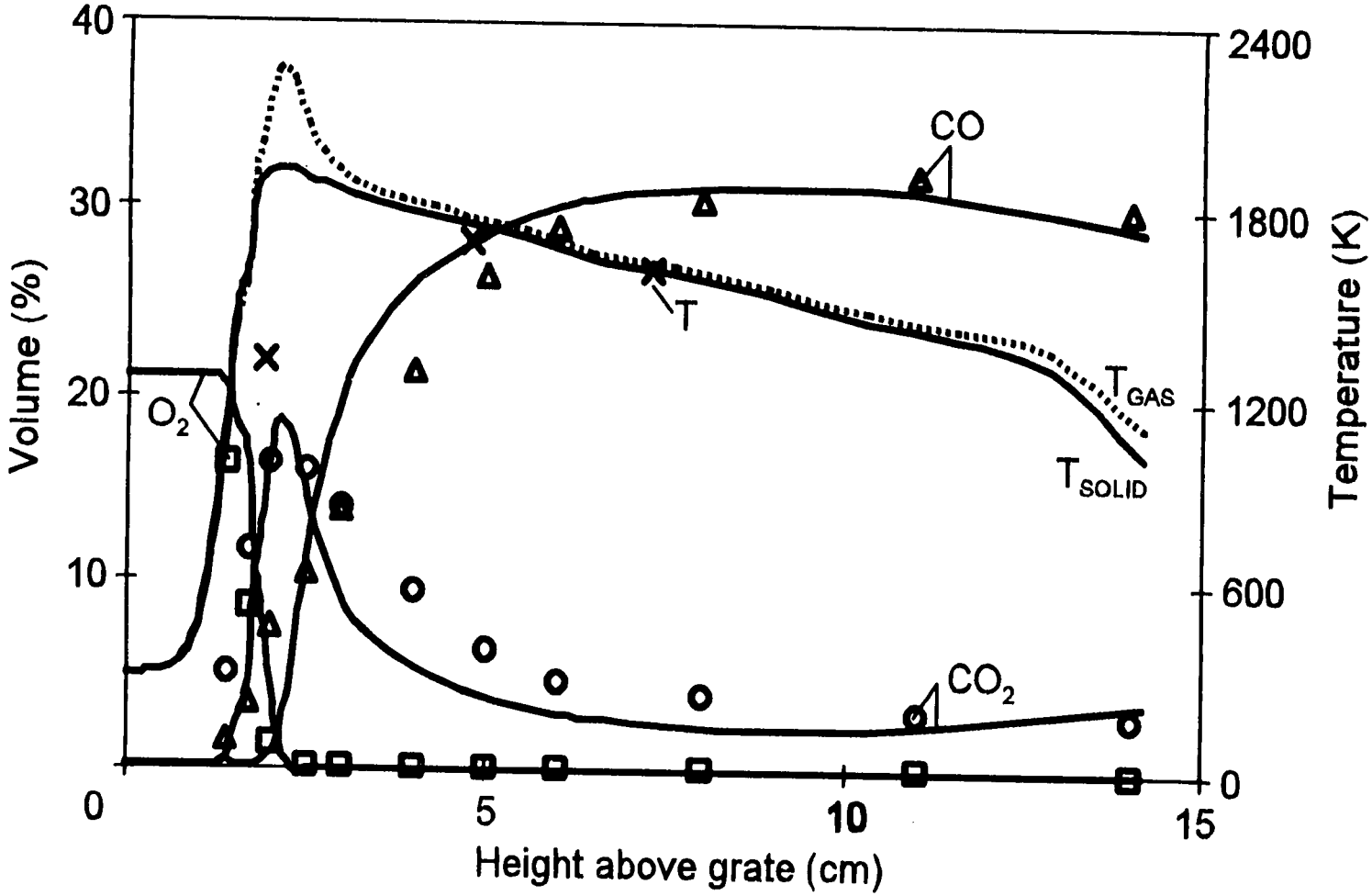

Figure 5.21 Composite graph comparing the experimental and predicted temperature and concentration profiles. The operating conditions and particle properties are those of Test 15A236S. The simulation was run with the following model options: heat and mass transfer correlation - Bhattacharyya and Pei (1975), char oxidation reaction - Field (1969), and CO_2 reduction reaction - "fitted" rate parameters (see Equation 5-1) with the pore diffusion model.

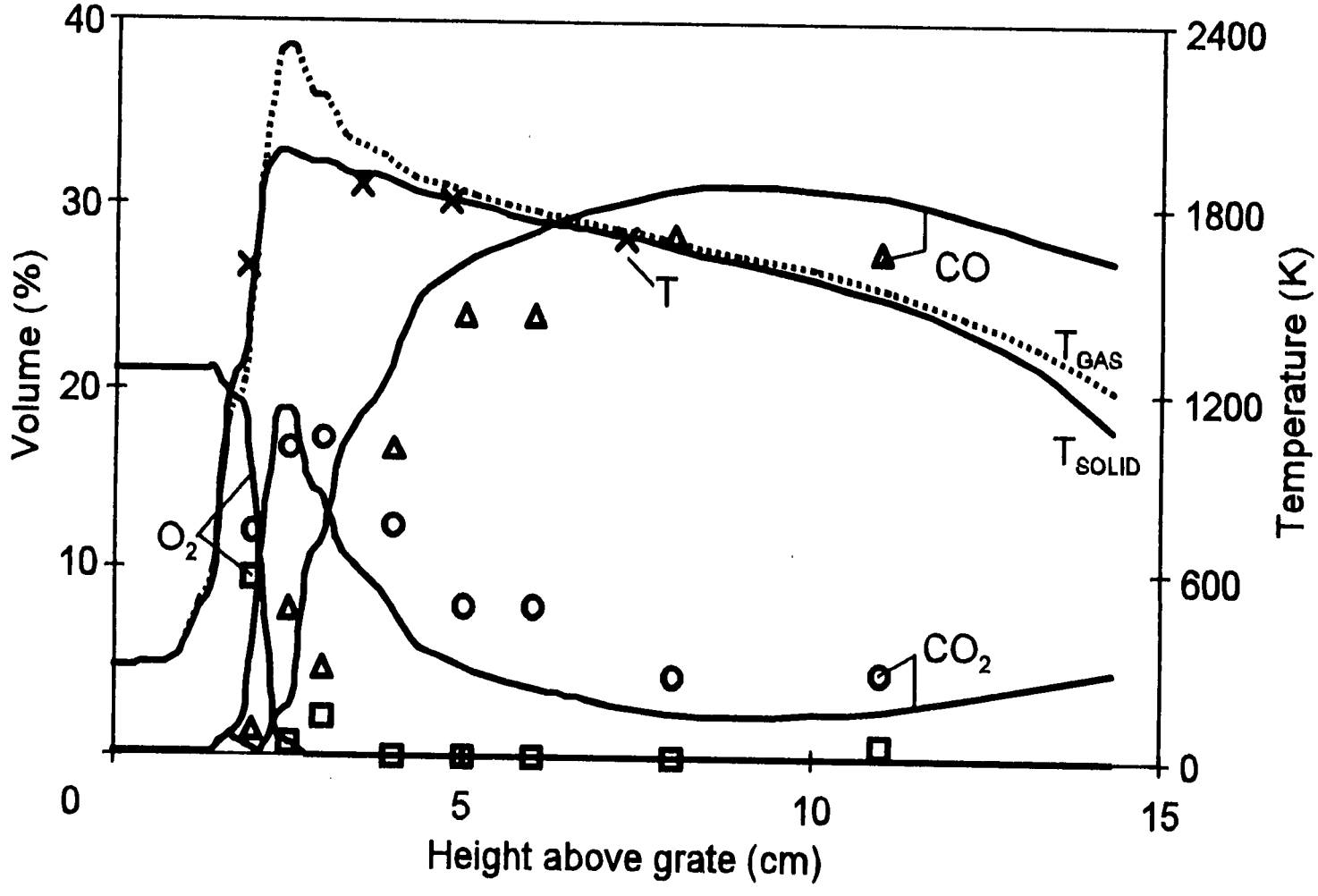

Figure 5.22 Composite graph comparing the experimental and predicted temperature and concentration profiles. The operating conditions and particle properties are those of Test 15A327L. The simulation was run with the following model options: heat and mass transfer correlation - Bhattacharyya and Pei (1975), char oxidation reaction - Field (1969), and CO_2 reduction reaction - "fitted" rate parameters (see Equation 5-1) with the pore diffusion model.

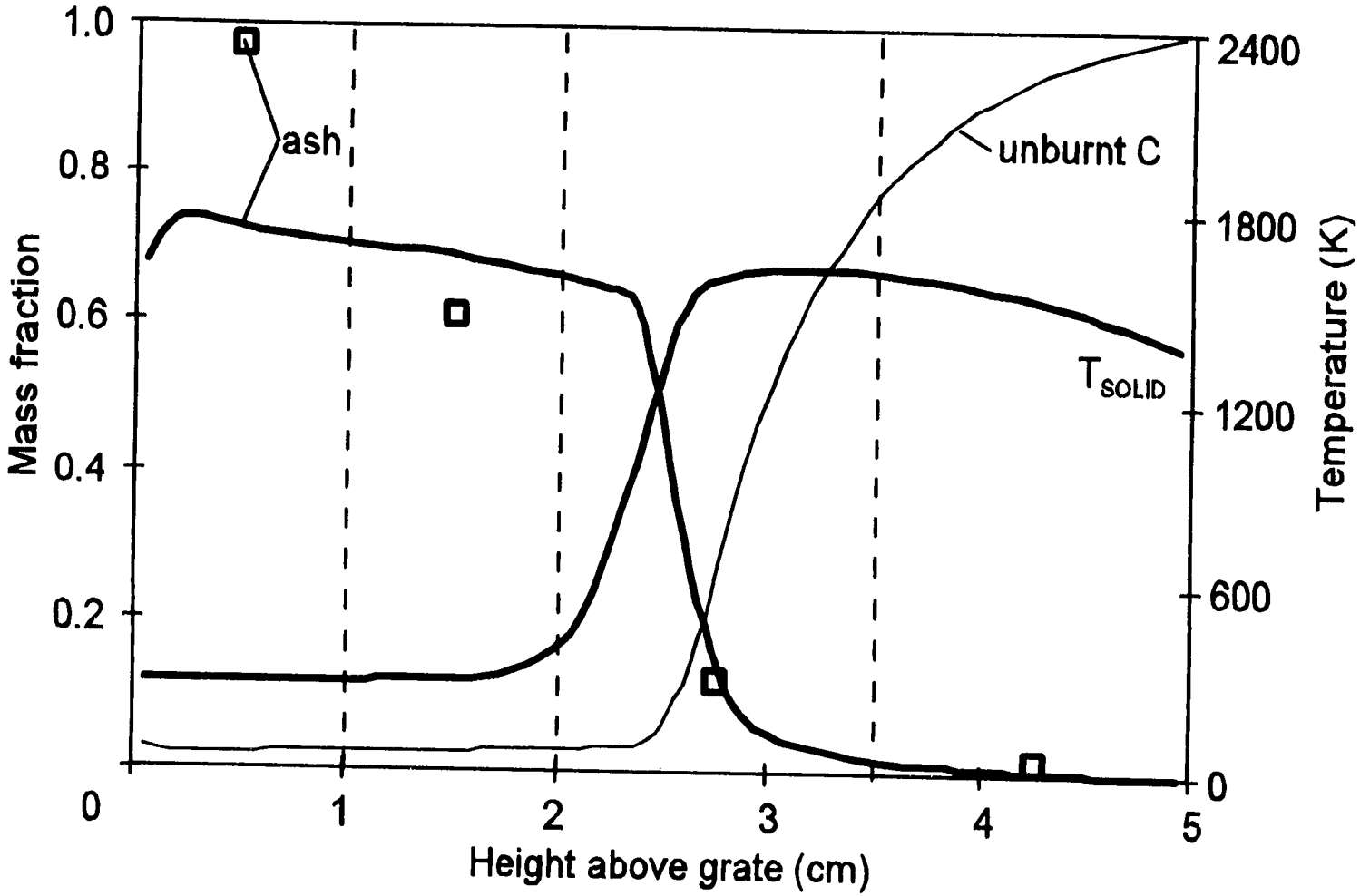

Figure 5.23 Comparison of the predicted and experimental ash mass fractions at the end (3.2 hours) of Test 05A520L. Vertical dashed lines indicate the boundaries of the sample slices for which the experimental points are averages. The model predictions of the unburnt carbon fraction and solid temperature are also shown. The simulation was run with the following model options: heat and mass transfer correlation - Bhattacharyya and Pei (1975), char oxidation reaction - Field (1969), and CO_2 reduction reaction - "fitted" rate parameters (see Equation 5-1) with the pore diffusion model.

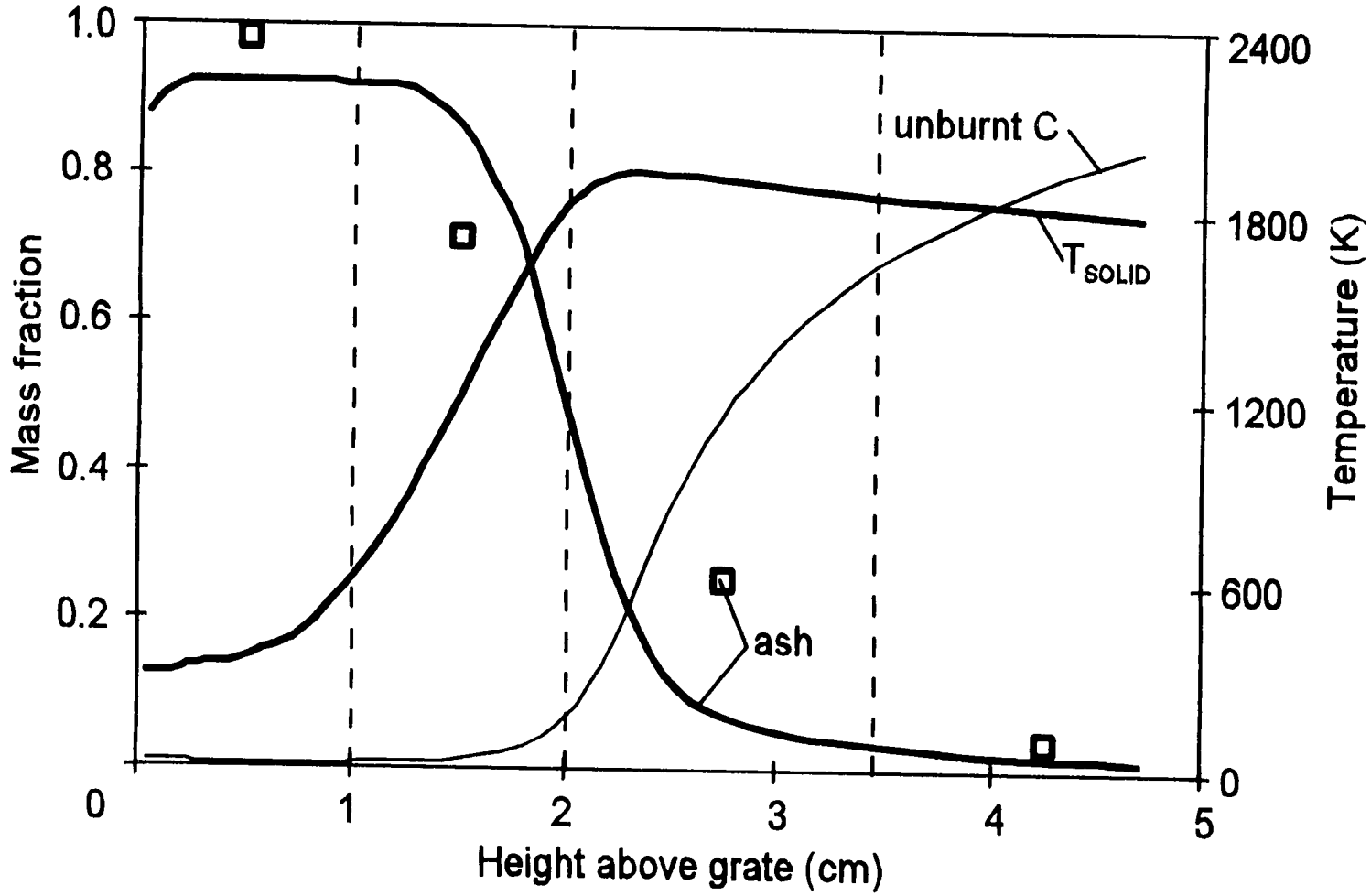

Figure 5.24 Comparison of the predicted and experimental ash mass fractions at the end (4.1 hours) of Test 15A236S. Vertical dashed lines indicate the boundaries of the sample slices for which the experimental points are averages. The model predictions of the unburnt carbon fraction and solid temperature are also shown. The simulation was run with the following model options: heat and mass transfer correlation - Bhattacharyya and Pei (1975), char oxidation reaction - Field (1969), and CO_2 reduction reaction - "fitted" rate parameters (see Equation 5-1) with the pore diffusion model.

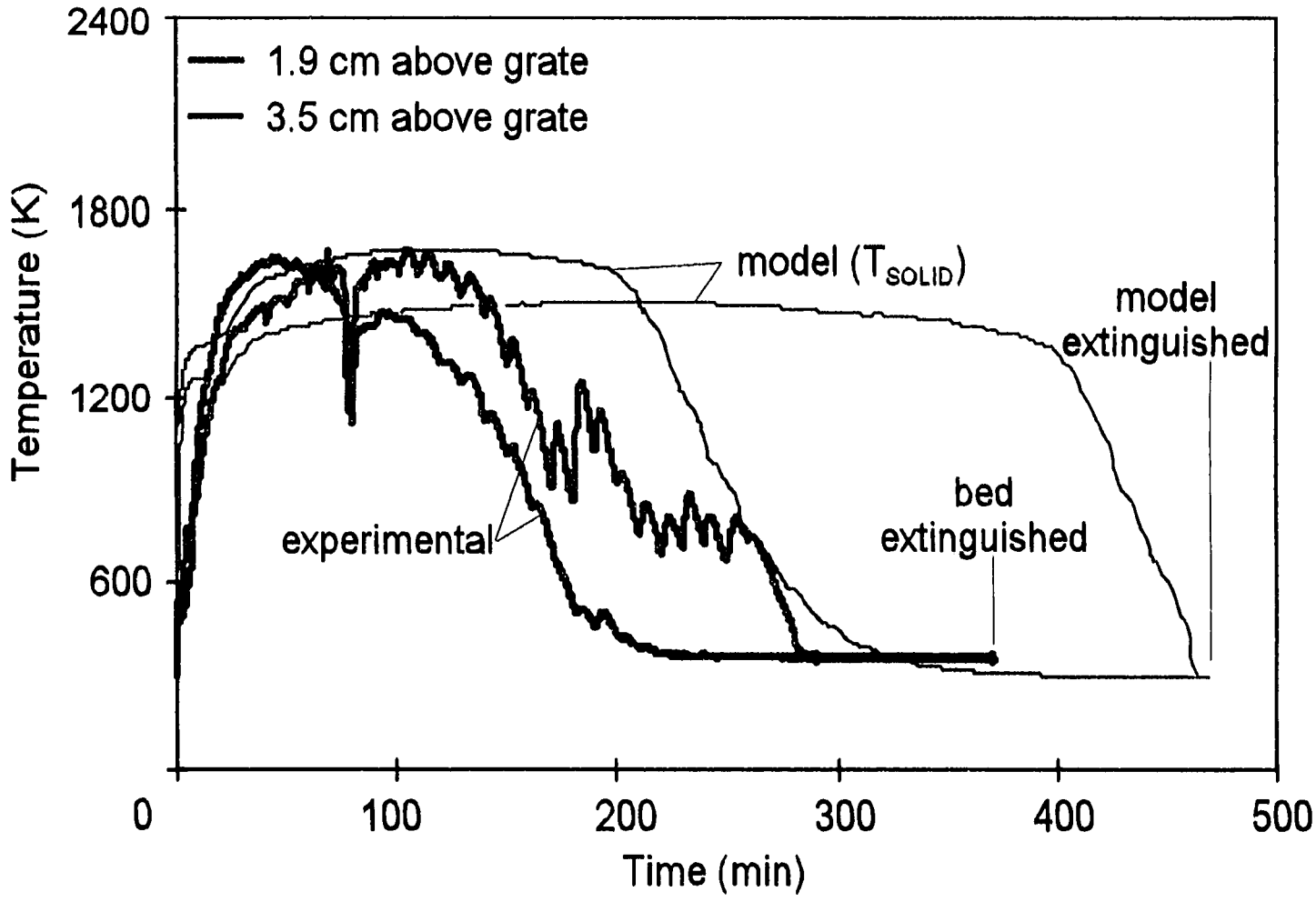

Figure 5.25 Comparison of the predicted and experimental temperatures of Test 05A191L over the entire experimental run. The simulation was run with the following model options: heat and mass transfer correlation - Bhattacharyya and Pei (1975), char oxidation reaction - Field (1969), and CO_2 reduction reaction - "fitted" rate parameters (see Equation 5-1) with the pore diffusion model.

6.0 CONCLUSIONS

This thesis has presented a series of experimental measurements on coke combustion in an overfeed packed bed, and has compared these to a detailed numerical model. A model for ash behaviour and its effects on heat and mass transfer has also been developed and tested. The results of this research have led to the following conclusions:

1. The good agreement between the experimental values and model predictions over a variety of operating conditions indicates that the model can reliably predict packed bed char combustion for the range of experimental operating conditions studied. As expected, to obtain this agreement the CO_2 reduction reaction pre-exponential had to be fitted; however, no modifications had to be made to the published heat and mass transfer correlations.
2. The incorporation of ash build-up into the model appears to have been done correctly. Predictions of the ash fraction agree well with experiment and the effect of ash layer buildup on gas analyses and temperature agrees very well with data.
3. Ash proved to have a significant influence on the heat and mass transfer processes in the bed. To accurately simulate packed bed combustion the modifications made to account for the effect of ash in the heat transfer correlation and the effective solid thermal conductivity have to be included.
4. The ash properties (d_{PA}, ρ_A, ε_A) were found to be highly dependent on the operating conditions (i.e., temperature). Model predictions of the thickness of the ash layer are very sensitive to the ash properties which in turn affects the bed concentration and temperature

profiles; therefore, accurate determination of the ash properties is necessary for the model inputs.

5. Model predictions of the temperature and concentration profiles were found to be very sensitive to the fluid-to-particle transfer correlations. The low heat and mass transfer rates of Bhattacharyya and Pei (1975) produce predictions which provide good agreement with experiment.
6. Concentration and temperature profiles in the oxidation and reduction zones are not affected by the oxidation kinetics, indicating diffusional control for this reaction.
7. Bed concentration and temperature profiles are affected by the reduction reaction kinetics, indicating a large degree of kinetic control for reduction. As char reactivity is known to vary, the CO_2 reduction rate parameters inputted to the model will be different for each char used. With kinetic control the reactants have time to diffuse into the pores before reacting; thus, the pore diffusion model should be used in the calculation of the reduction reaction kinetics.
8. Bed concentration profiles were found to vary only with bed thickness. Increasing the airflow rate has no effect on the species concentrations, as it causes a proportional increase in the char conversion rates.

7.0 RECOMMENDATIONS

1. Experiments should be performed using char with known CO_2 reduction reaction parameters and compared with model predictions, as this is the only "fitting" that was done in this study.
2. Research should be done to study the variation of particle pore properties (a_l, ε_p, τ) with time and examine the degree of internal burning that particles undergo. The variation of fuel particle density (ρ_C) should also be investigated and included in the model.
3. Research should be done to support the modifications made to the correlations for heat and mass transfer in beds with two different particles.
4. The effect of operating conditions (i.e., temperature) on the ash properties should be studied in more detail and included in the model.
5. More research should be done to examine the oxidation kinetics when the ash concentration is high, as chemical kinetics play a role in determining the unburnt carbon residue in the ash.
6. Transient experiments, with ignition from the top and no fuel feeding, should be conducted to study combustion as it would occur on inclined or travelling grates. The model should also be modified to include an option which allows for transient collapse of the bed.

8.0 REFERENCES

"SC-207X Series User Manual", National Instruments, Austin, TX (1995).

American Society for Testing and Materials, "E230-93 Standard Temperature-Electromotive Force (EMF) Tables for Standardized Thermocouples",1995 Annual Book of ASTM Standards, v.14.03 (1995).

American Society for Testing and Materials, "D167-93 Standard Test Method for Apparent and True Specific Gravity and Porosity of Lump Coke", 1995 Annual Book of ASTM Standards, v.05.05 (1995).

American Society for Testing and Materials, "D3174-93 Standard Test Method for Ash in the Analysis of Coal and Coke from Coal", 1995 Annual Book of ASTM Standards, v.05.05 (1995).

Amundson, N.R. and L.E. Arri, "Char Gasification in a Countercurrent Reactor", A.I.Ch.E. Journal **24**, 87-101 (1978).

Arai, N., M. Hasatani and Y. Nakai, "In-furnace Reduction of NO_x during the Parallel-flow Moving Bed Combustion of Surplus Activated Sludge Char by an Active Use of Self-evolved Ammonia", Fuel **68**, 591-595 (1989).

Barriga, A. and R.H. Essenhigh, "A Mathematical Model of a Combustion Pot: Comparison of Theory and Experiment", ASME Paper No. 80-WA/HT-32, 1-7 (1980).

Becker, H.A., "Physical Probes", in "Instrumentation for Flows with Combustion", A.M. Taylor, Ed., Academic Press, England (1993), pp.53-112.

Ben Aïm, R and P. le Goff, "Effet de Paroi dans les Empilements Désordonnés de Sphères et Application à la Porosité de Mélanges Binaires", Powder Technology **1**, 281-290 (1967/68).

Benson, S.A., M.L. Jones and J.N. Harb, "Ash Formation and Deposition", in "Fundamentals of Coal Combustion: for Clean and Efficient Use", L.D. Smoot, Ed., Elsevier Science Publishers, Netherlands (1993), pp. 299-373.

Bhattacharya, A., L. Salam, M.P. Dudukovlc and B. Joseph, "Experimental and Modeling Studies in Fixed-Bed Char Gasification", Industrial and Engineering Chemistry Process Design and Development **25**, 988-996 (1986).

Bhattacharyya, D. and D.C. Pei, "Heat Transfer in Fixed Bed Gas-Solid Systems", Chemical Engineering Science **30**, 293-300 (1975).

Bilger, R.W., "Probe Measurement in Turbulent Flows", in "Combustion Measurements: Modern Techniques and Instrumentation", R. Goulard, Ed., Academic Press, New York, NY (1976), pp. 333-340.

Bird, R.B., W.E. Stewart and E.N. Lightfoot, "Transport Phenomena", John Wiley & Sons, New York, NY (1960).

Braithwaite, A., "Chromatographic Methods", 5th ed., Blackie Academic & Professional, New York, NY (1996).

Burton, K.A. and H.D. Ladouceur, "An Improved Noncatalytic Coating for Thermocouples", Combustion Science and Technology **81**, 141-145 (1992).

Chu, J.C., J. Kalil and A. Wetteroth, "Mass Transfer in a Fluidized Bed", Chemical Engineering Progress **49**, 141-149 (1953).

Cooper, J., "A Numerical Model for Char Combustion in Packed Bed Reactors", M. A. Sc. Chemical Engineering Thesis, University of Ottawa (1996).

Denbigh, K.G. and J.C Turner, "Chemical Reactor Theory",Cambridge University Press, Cambridge, England (1984).

Dietz, W.A., "Response Factors for Gas Chromatographic Analyses", Journal of Gas Chromatography **5**, 68-71 (1967).

Dunningham, A.C., "Fuel-Bed Temperatures", Journal of the Institute of Fuel **23**, 242-246 (1950).

Eapen, T., R. Blackadar and R.H. Essenhigh, "Kinetics of Gasification in a Combustion Pot: A Comparison of Theory and Experiment", 16th Symposium (International) on Combustion, The Combustion Institute, Pittsburgh, PA (1977), pp.515-522.

Ely, F.G. and D.H. Barnhart, "Coal Ash - Its Effect on Boiler Availability", in "Chemistry of Coal Utilization, Supplementary Volume", H.H. Lowry, Ed., John Wiley & Sons, New York, NY (1963), pp. 820-891.

Ergun, S., "Fluid Flow Through Packed Columns", Chemical Engineering Progress **48**, 89-94 (1952).

Ergun, S., "Determination of Geometric Surface Area of Crushed Porous Solids", Analytical Chemistry **24**, 388-393 (1952).

Ergun, S., "Determination of Particle Density of Crushed Porous Solids", Analytical Chemistry **23**, 151-156 (1951).

Essenhigh, R.H., "Fundamentals of Coal Combustion", in "Chemistry of Coal Utilization, Second Supplementary Volume", M.A. Elliott, Ed., John Wiley & Sons, New York, NY (1981), pp. 1153-1312.

Field, M.A., "Rate of Combustion of Size-Graded Fractions of Char from a Low-rank Coal between 1200°K and 2000°K", Combustion and Flame **13**, 237-252 (1969).

Finkers, H.J. and A.C. Hoffmann, "Structural Ratio for Predicting the Voidage of Binary Particle Mixtures", A.I.Ch.E. Journal **44**, 495-498 (1998).

Ford, N., M.J. Cooke and M.D. Petit, "The Use of a Laboratory Fixed-grate Furnace to Simulate Industrial Stoker-fired Plant", Journal of the Institute of Energy **65**, 137-143 (1992).

Friedman, R., "Measurement of the Temperature Profile in a Laminar Flame", 4th Symposium (International) on Combustion, The Combustion Institute, Pittsburgh, PA (1952), pp. 259-263.

Fristrom, R.M. and A.A. Westenburg, "Flame Structure", McGraw-Hill, New York, NY (1965).

Geankoplis, C.J., "Transport Processes and Unit Operations", 3rd ed., Prentice-Hall Inc., Englewood Hill, NJ (1993).

Geldart, D., "Estimation of Basic Particle Properties for Use in Fluid-Particle Process Calculations", Powder Technology **60**, 1-13 (1990).

Goetz, G.J., N.Y. Nsakala, K.L. Patel and T.C. Loa, "Combustion and Gasification Kinetics of Chars from Four Commercially Significant Coals of Varying Rank", 2nd Annual EPRI Conference on Coal Gasification (1982), pp. 15-1-15-27.

Goldman, J., D. Xieu, A. Oko, R Milne and R. Essenhigh, "A Comparison of Prediction and Experiment in the Gasification of Anthracite in Air and Oxygen-Enriched/Steam Mixtures", 20th Symposium (International) on Combustion, The Combustion Institute, Pittsburgh, PA (1985), pp. 1365-1372.

Gransden, J., personal communication (1997).

Hallett, W.L.H., Combustion Notes, University of Ottawa (1996).

Heitor, M.V. and A.L.N. Moreira, "Thermocouples and Sample Probes for Combustion Studies", Progress in Energy and Combustion Science **19**, 259-278 (1993).

Hinkley, J.T. and A.G. Waters, "Theoretical Explanation for the Dependence of Green Bed Permeability of Ferrous Sinter Mixes on Moisture Content", 18th Australasian Chemical Engineering Conference, University of Auckland, New Zealand (1990), pp. 930-937.

Hobbs, M.L., P.T. Radulovic and L.D. Smoot, "Combustion and Gasification of Coals in Fixed-Beds", Progress in Energy and Combustion Science **19**, 505-586 (1993).

Hobbs, M.L., P.T. Radulovic and L.D. Smoot, "Modeling of Fixed-Bed Coal Gasifiers", A.I.Ch.E Journal **38**, 681-702 (1992).

Holman, J.P., "Heat Transfer", 7th ed., McGraw-Hill, New York, NY (1990).

Ichida, M., Y. Isozaki and K. Tamura, "Estimation of Void Fraction and Shape Factor in a Moving Bed of Sinter and Coke", Journal of the Iron and Steel Industry of Japan **77**, 23-30 (1991).

Kaskan, W.E., "The Dependence of Flame Temperature on Mass Burning Velocity", 6th Symposium (International) On Combustion, The Combustion Institute, Pittsburgh, PA (1957), pp. 134-143.

Kent, J. H., "A Noncatalytic Coating for Platinum-Rhodium Thermocouples", Combustion and Flame **14**, 279-281 (1970).

Kreisinger, H., F.K. Ovitz and C.E. Augustine, "Combustion in the Fuel Bed of Hand-Fired Furnaces", U.S. Bureau of Mines Technical Paper No.137 (1916).

La Nauze, R.D., "Fundamentals of Coal Combustion in Fluidized Beds", Chemical Engineering Research and Development **63**, 3-33 (1985).

Leah, A.S. and N. Carpenter, "The Estimation of Atomic Oxygen in Open Flames and the Measurement of Temperature", 4th Symposium (International) on Combustion, The Combustion Institute, Pittsburgh, PA (1952), pp. 274-285.

Lin, C.I., C.W. Chen and Y.L. Lu, "Determination of the Shape Factor of a Sinter", Powder Technology **63**, 285-287 (1990).

Madson, J.M. and E.A. Theby, "SiO_2 Coated Thermocouples", Combustion Science and Technology **36**, 205-209 (1984).

Margiatto, C.A. and J.H. Siegell, "Determination of Porous Particle Density", Powder Technology **34**, 105-106 (1983).

Marskell, W.G. and J.M. Miller, "Mode of Combustion of Coal on a Chain Grate Stoker: The Effect of Rate of Combustion on the Composition of the Fuel Bed", Fuel in Science and Practice **25**, 4-12 (1946a).

Marskell, W.G. and J.M. Miller, "Mode of Combustion of Coal on a Chain Grate Stoker: Effect of Primary Air Temperature and Air Rate on Combustion", Fuel in Science and Practice **25**, 50-58 (1946b).

McCabe, W.L., J.C. Smith and P. Harriott, "Unit Operations in Chemical Engineering", 5th ed., McGraw-Hill, New York, NY (1993).

Mehta, D. and M.C. Hawley, "Wall Effect in Packed Columns", Industrial and Engineering Chemistry Process Design and Development **8**, 280-282 (1969).

Merrick, D., "Mathematical Models of the Thermal Decomposition of Coal, 4. Heat Transfer and Temperature Profiles in a Coke-oven Charge", Fuel **62**, 553-561 (1983b).

Merrick, D., "Mathematical Models of the Thermal Decomposition of Coal, 2. Specific Heats and Heats of Reaction", Fuel **62**, 540-546 (1983a).

Messner, A.E., D.M. Rosie and P.A. Argabright, "Correlation of Thermal Conductivity Cell Response with Molecular Weight and Structure", Analytical Chemistry **31**, 230-233 (1959).

Miller, J.M., "Chromatography: Concepts and Contrasts", John Wiley & Sons, New York, NY (1988).

Mills, K.C. and J.M. Rhine, "The Measurement and Estimation of the Physical Properties of Slags Formed During Coal Gasification: Properties Relevant to Fluid Flow", Fuel **68**, 193-200 (1989).

Moles, F.D. and M.W. Thring, "Minimum Burning Rates in Coke Fuel Beds", Conference on Science in The Use of Coal, The Institute of Fuel (1958), pp. 26-29.

Nichols, P., "Underfeed Combustion, Effect of Preheat, and Distribution of Ash in Fuel Beds", Fuel in Science and Practice **14**, 205-211 (1935).

Patankar, S.V., "Numerical Heat Transfer and Fluid Flow", McGraw-Hill, New York, NY (1980).

Rankin, W.J., P.W. Roller and R.J. Batterham, "Analysis of the Permeability of Granulated Iron Sinter Feeds Using the Ergun Equation", Transactions of the American Institute of Mining, Metallurgical and Petroleum Engineers **278**, 53-59 (1985).

Reid, W.T., "Fundamentals of Coal Combustion", in "Chemistry of Coal Utilization, Second Supplementary Volume", M.A. Elliott, Ed., John Wiley & Sons, New York, NY (1981), pp. 1389-1445.

Rogers, J.E., A.F. Sarofim and J.B. Howard, "Effect of Underfire Air Rate on a Burning Simulated Refuse Bed", Proceedings of 1972 National Incinerator Conference, American Society of Mechanical Engineers, New York, NY (1972) pp.135-144.

Rosie, D.M. and E.F. Barry, "Quantitation of Thermal Conductivity Detectors", Journal of Chromatographic Science **11**, 237-250 (1973).

Schwartz, C.E. and J.M. Smith, "Flow Distribution in Packed Beds", Industrial and Engineering Chemistry **45**, 1209-1218 (1953).

Siegel, R. and J.R. Howell, "Thermal Radiation Heat Transfer", McGraw-Hill, New York, NY (1972).

Singer, J.G., "Combustion - Fossil Power Systems", Combustion Engineering (1981).

Smith, I.W., "The Combustion Rates of Coal Chars: A Review", 19th Symposium International on Combustion, The Combustion Institute, Pittsburgh, PA (1982), pp. 1045-1056.

Smith, I.W., "The Intrinsic Reactivity of Carbons to Oxygen", Fuel **57**, 409-414 (1978).

Smithells, C.J., "Smithells' Metals Reference Book", 7th ed., Butterworths, London (1992).

Smoot L.D. and P.J. Smith, "Coal Combustion and Gasification", Plenum Press, New York, NY (1985).

Solomon, P.R. and J.M. Beer, "Fundamentals of Coal Conversion and Relation to Coal Properties", Energy **12**, 837-860 (1987).

Standish, N. and G. McGregor, "The Average Shape of a Mixture of Particles in a Packed Bed", Chemical Engineering Science **33**, 618-619 (1978).

Thibaut, C.G., "Solid Products of Carbonization", in "Chemistry of Coal Utilization, Supplementary Volume", H.H. Lowry, Ed., John Wiley & Sons, New York, NY (1963), pp. 494-538.

Valix, M.G., D.L. Trimm, I.W. Smith and D.J. Harris, "Mass Transfer Effects in Coal Combustion", Chemical Engineering Science **47**, 1607-1617 (1992).

Wadell, H., "Volume, Shape and Roundness of Rock Particles", Journal of Geology **40**, 443-450 (1932).

Wagstaff, J.B. and E.A. Nirmaier, "Air Flow in Beds of Granular Solids", Industrial and Engineering Chemistry **47**, 1129-1135 (1955).

Westman, A.E., "The Packing of Particles: Empirical Equations for Intermediate Diameter Ratios", Journal of the American Ceramic Society **19**, 127-129 (1936).

Yagi, S. and D. Kunii, "Studies on Effective Thermal Conductivity in Packed Beds", A.I.Ch.E. Journal **3**, 373-381 (1957).

Yerazunis, S., S.W. Cornell and B. Winter, "Dense Random Packing of Binary Mixtures of Spheres", Nature **207**, 835-837 (1965).

Yoon, H., J. Wei and M. Denn, "A Model for Moving-Bed Coal Gasification Reactors", A.I.Ch.E. **24**, 885-903 (1978).

Yoshida, F., D. Ramaswami and O.A. Hougen, "Temperature and Partial Pressures at the Surfaces of Catalyst Particles", A.I.Ch.E. Journal **8**, 5-11 (1962).

Yu, A., N. Standish and A. McLean, "Porosity Calculation of Binary Mixtures of Nonspherical Particles", Journal of the American Ceramic Society **76**, 2813-2816 (1993).

APPENDIX A: Discretization of Particle Number Balance

The method of Patankar (1980) expresses the discretized differential equations in the following general form:

$$a_P\phi_P = a_N\phi_N + a_S\phi_S + b \tag{A-2}$$

where ϕ is the dependent variable being solved. The subscript P applies to the node being solved and the subscripts N and S apply to the nodes to the north and south of P.

In the particle number balance (see equation 3-56), the dependent variable ϕ is the fuel particle mass m_{PC}, and the coefficients are given by:

$$a_P = (1-\varepsilon)\rho_C X_C \Delta x - \left(\rho_C v_C\right)_s \Delta t \tag{A-3}$$

$$a_N = \left[\!\left[0, \left(-\rho_C v_C\right)_N \Delta t\right]\!\right] \tag{A-4}$$

$$a_S = 0 \tag{A-5}$$

$$b = \frac{1}{m_{PC}^{o}}\left(1-\varepsilon^{o}\right)\rho_C X_C^{o} \Delta x \tag{A-6}$$

where the superscript ° refers to the value of the variable at the beginning of the time step involved. Note that variables which are not indexed with N or S occur at the node P.

APPENDIX B: Char Combustion Model Program Code

```
*     PROGRAM CHAR
*
*     CALCULATES TEMPERATURE AND CONCENTRATION PROFILES FOR BURNING
*     FIXED BEDS
**********************************************************************
*
*     Development history:
*
*     Written by Judy Cooper 1994-95 (MASc Thesis CHG 1996)
*
*  1. General Revision June 1997 by WH:
*     Eucken equation (gas thermal conductivity) corrected 8 June 97
*     Effect: gas temperatures reduced by up to 100 C, solid
*     temperatures little affected. Convergence criterion loosened -
*     CRIT divided by number of nodes before testing - reduced no. of
*     iterations per time step for nearly steady state from 20 to 2.
*     Specific heat replaced by van Wylen polynomials - slight rise in
*     highest temps. Modified for non-spherical particles. Separate
*     mass transfer coefficients for individual species introduced -
*     raises peak temperatures by 20-30 degrees. Separate effective
*     diffusivities for components introduced - makes virtually no
*     difference. Steel bar grate model written. Radiation boundary
*     conditions at bed exit changed to allow for refractory surfaces
*     surrounding bed. CO rxn source term in TDMATG rewritten with an
*     artificial SP term to improve stability - this eliminated temp.
*     overshoots in the first few time steps.
*
*  2. Aug. 1997 Reverse reaction for CO oxidation implemented to
*     account for dissociation at high temp. (>2000 K). As of 19 Aug:
*     With Howard and Fine kinetics good results - peak temps. drop by
*     50 - 100 K in response to dissociation. Convergence rapid, energy
*     error about 1%.
*     With Westbrook and Dryer kinetics, large number of iterations
*     required (about 50), large energy error (about 15%) even at
*     steady state. More dissociation, larger reduction in peak temps.
*     than with Howard. However, much higher temps downstream of
*     oxidation zone, owing (presumably) to consumption of oxygen
*     released upstream by dissociation. Magnitude of effect doesn't
*     seem reasonable, and energy error is suspicious - must be
*     convergence problem. Recommend that WD model not be used.
*     Set ICOB = 0 if you want to turn off the reverse rxn.
*
*  3. March 1998 - Implemented ash buildup in the bed
*     The char particles burn until their diameters are equal to the
*     diameter of an ash particle (calculated from the mass fraction
*     of ash). The carbon consumption (G) is then set to zero in the
*     particular bed slice. Ash buildup is controlled by the IBUILD
*     variable.
*     Effect: Overtime the ash will buildup in the bottom of the bed
*     and shifting the reaction zones to higher in the bed.
*
*  4. April 1998 - Implemented new particle equation (used to calculate
*     the particle diameter).
*     The old particle number balance equation drove the diameter values
```

```
*     in the two bottom nodes of the bed to a fixed ratio of 4/3(dN/dP).
*     This was fixed by solving the particle number balance for 1/mP,
*     which allows for mP to decrease continually until G=0.
*     Effect: The effect was limited to the particle diameter which now
*     decreases overtime until is reaches the ash particle diameter.
*     This change did not affect the temperature or concentration
*     profiles.
*
*  5. May 1998 - Introduced a separate solid conductivity for the ash
*     layer (kS = 1.09).
*     Effect: The temperatures increased in the grate and ash layer
*     whereas they decreased in the reduction zone.  Changes to the
*     concentrations were only observed in the reduction zone
*     (CO decreased by ~2%).
*
*  6. June-Aug 1998 - Introduced:
*     Ignition zone - a hot zone on top of the grate which is of a given
*     height (ALAYER) and temperature (TIGNIT).
*     Grate properties - Cp=f(TS), kS=f(TS), rho
*     Ash properties - Cp=f(T)
*     Effects: None
*
*  7. Sept 1998 - The radiation boundary at the top of the bed was
*     modified such that the height of the refractory lining above the
*     bed is a function of bed depth.
*     Effect: Slight decrease in both gas and solid temperatures.
*
*  8. Oct 1998 - Introduced two different particle sizes
*     The bed is now comprised of two different particles(ash and char).
*     These particles have different densities, void fractions,
*     sphericities and diameters.  To include the effect of the two
*     particles the following changes were made:
*     - all of the balances now include transients
*     - the char mass flux (vc) is calculated
*     - the overall bed void fraction is calculated using the Westman
*     equation (this is solved using a Newton-Raphson method)
*     - for heat transfer calculations the total specific surface area
*     (SSB) is used whereas for mass transfer calculations the char
*      specific surface area (SSC) is used
*     -the solid density is a function of the fraction of char and ash
*     Note - the change detailed in #3 March 1998 is no longer used
*     Effect: Shifted the reaction zones to lower in the bed.  Increased
*     the temperatures in the grate but lowered the peak and reduction
*     zone temperatures. The concentration profiles were similar (number
*     wise) but occurred lower in the bed due to a much thinner
*     oxidation zone. The differences increased overtime.
*
*  9. Jan 1999 - Modified the effective solid thermal conductivity
*     (kSeff)
*     The kSeff model used does not account for the effect of two
*     different particles.  This effect was included by assuming that
*     the heat transfer operations of the two particles act in parallel.
*     Effect: This had virtually no effect on the temperatures.
*     Initially(time=1hr) the concentrations in the reduction zone were
*     effected (CO decreased by ~1%), but after 3 hours no differences
*     were observed.
*     The kSeff increased in the ash layer and decreased in the rest of
```

```
*     the bed.
* 10. Feb. 1999 - Modified ash emissivity to be a function of temp.
*     Effect: None
*
* 11. March 1999
*     a) The radiation model was revised to include radiation from the
*     bed through the spaces in the grate bars.
*     Effect: None
*     b) The mass transfer coefficient was corrected to account for that
*     in the ash layer the O2 in some of the channels may not contact
*     any char particles - reducing mass transfer.  The mass transfer
*     coefficient (AKAY) was mulitiplied by a factor (FVOID) which is a
*     function of void volume in contact with the particle.
*     Effect: This caused the reaction zones to shift to higher in the
*     bed, due to a decrease in the oxygen consumption rate in the ash
*     layer. This effect increases with timeThe amount of carbon in "ash
*     layer" increased.
*     c) The effective solid conductivity (kSeff) was revised for a bed
*     with two particle sizes (change #9 Jan. 1999 is no longer used).
*     The model of Yagi and Kuni was modified to include a sixth mode
*     of heat transfer - conduction through the ash phase.
*     Effect: This has the same effect as (b).
*     d) Modified the calculation of the char oxidation kinetics.
*     The kinetics can either be calculated using the effectiveness
*     (IFIELD=0) or using the Field equation (IFIELD=1).
*     Effect: Using IFIELD = 0 shifts the reaction zones to lower in the
*     bed, increases peak and oxidation zone temperatures, decreases O2
*     penetration and increases the CO in the reduction zone.  All of
*     these changes were less marked then those seen due to the changes
*     in(b) and (c).
*     e) Model predictions, for a composite graph, are printed if
*     IGRAPH=1
*     *NOTE: The equation(s) which correlate sampling position with time
*     have to be entered in GRAPHING.  The equation(s) are different for
*     each test.
*
* 13. April 1999 - Modified the calculation of the char reduction
*     kinetics.
*     The kinetics can either be calculated using the effectiveness
*     (IEFFECT=1) or using the reduction reaction parameters, A1 and
*     ER1 (IEFFECT=0).
*************************************************************************

      PARAMETER (N=50)
      DIMENSION TG(N),TGI(N),TGO(N),TS(N),TSI(N),TSO(N)
      DIMENSION FE(N),XB(N),DXN(N)
      DIMENSION AKG(N),AKAG(N),AKAS(N),AKY(N,3),DEFF(N,3),H(N)
      DIMENSION CPG(N),AMWG(N),RE(N)
      DIMENSION VOIDO(N),XCO(N),RHOSO(N),APHI(N),APHIO(N)
      DIMENSION VC(N),VS(N)
      DIMENSION RCO(N),RCOB(N)
      DIMENSION VOID(N),SLAB(N),SSB(N),SSBO(N),RHOS(N),G(N)
      DIMENSION DIAMC(N),SSC(N),SSCO(N),XC(N)
      DIMENSION VG(N),RHOG(N),RHOGO(N)
      DIMENSION Y8O2(N),Y8CO2(N),Y8CO(N),Y8N2(N),Y8O2O(N),Y8CO2O(N)
      DIMENSION Y8COO(N),Y8N2O(N)
      DIMENSION YRO2(N),YRCO2(N),YRCO(N),YRN2(N)
```

```
      DIMENSION G1(N),G2(N),X(N),S(N)
      DIMENSION TESTTG(N),TESTTS(N),TESTCO(N)
      DIMENSION CPGREG(N)
      DIMENSION DIFF(N,3)
      COMMON/BED/VOID,E,SLAB,SSB,SSBO,RHOS,G
      COMMON/CHAR/CARB,DIAMC,RHOC,VOIDC,SPHERC,SSC,SSCO,XC
      COMMON/ASH/ASH,DIAMA,RHOA,VOIDA,SPHERA,IBUILD
      COMMON/GAS/VG,RHOG,RHOGO
      COMMON/Y/Y8O2,Y8CO2,Y8CO,Y8N2,Y8O2O,Y8CO2O,Y8COO,Y8N2O
      COMMON/YR/YRO2,YRCO2,YRCO,YRN2
      COMMON/INFO/WTN2,WTO2,WTCO2,WTCO,R,P,BETA,GAMMA,THI
      COMMON/STOIC/SCO2,SCO,S3,S2,DH1,DH2,DH3,DH4
      COMMON/GE/A,A1,ER,ER1,ALPHA1,ALPHA2,ALPHA3
      COMMON/PORE/IFIELD,IEFFECT,SSP,TAU,VOIDP
      COMMON/REACT/G1,G2,X,S,IREACT
      COMMON/RAD/TSG,TSB,TSW,HRG,HRB,HRW,F12B,F12W,BOLTZ,TCOAL
      COMMON/FLUXES/FO2,FC,FCO2,FTG,FTS
      COMMON/GRATE/GRATE,GRTSOL,GRTBAR,IGMOD,GRTRHO,GRTPD,GRTSPACE
      COMMON/TIME/IFLAG,ITIME,ITERNS,TURNS,IB,IG,ICOB,TIMES,DT
      COMMON/TEST/TESTTG,TESTTS,TESTCO,CRIT
      COMMON/EXTRA/CPGREG

*     READ IN SYSTEM PARAMETERS

      OPEN (1,FILE='RUN09.DAT',STATUS='OLD')
      OPEN (2,FILE='CONSTANT.DAT',STATUS='OLD')
      OPEN (3,FILE='CHARG.OUT')

*     PROGRAMME CONTROL:
*         IFLAG:    = 2 - KEEP ITERATING
*                   = 3 - NEXT TIME STEP
*                   = 4 - HALT X, END OF ALLOTTED TIME
*         IREACT:   = 0 - TURNS OFF ALL REACTIONS
*                   = 1 - TURNS OFF CO2 REDUCTION
*                   = 2 - ALL REACTIONS ON
*         IRXN:     = 1980 - WESTBROOK AND DRYER CO KINETICS
*                   = 1970 - HOWARD AND FINE CO KINETICS
*         ICOB:     = 0 - TURNS OFF REVERSE CO (EQUIL'M) RXN
*                   = 1 - TURNS ON REVERSE CO (EQUIL'M) RXN
*         IHTTR: CONTROLS SELECTION OF GAS/SOLID HT. TR. CORRELATION
*                   = 1970 - BATMAN AND PEI 1974
*                   = 1960 - YOSHIDA ET AL. 1962
*                   = 1950 - CHU
*         IGMOD: SELECTS GRATE MODEL
*                   = 1 - PACKED BED OR POROUS MEDIUM, PARTICLE DIA.
*                   = 2 - STEEL BARS, SPECIFIED WIDTH (GRTBAR), DEPTH
*                      (GRATE) AND SOLIDITY (GRTSOL)
*         IBUILD: SELECTS THE ASH MOVEMENT
*                   = 0 - ASH FALLS THROUGH THE GRATE
*                   = 1 - ASH BUILDS UP IN THE BED
*     TIME STEP INCREASED BY FACTOR OF TWO (ITCUT) TIMES BEFORE END
*     VARIABLES:
*        CURRENT VALUES: TG,TS,Y802...
*        PREVIOUS ITERATION: TGI,TSI,Y8O2I...
*        PREVIOUS TIME STEP: TGO,TSO,Y8O2O...
```

```
      IFLAG = 2
      IFLAG3 = 0
      ITIME=  0
      ITERNS= 1
      ITSTEP = 0
      ICNT = 1
      ICNTN = 25
      IN = 0
      TCGONE = 0
*     FULL PRINTOUT EVERY ICNTN TIME STEPS
      CRIT = 2.0
      CALL READER(1,2,TG,TS,U,US,TIGNIT,ALAYER,HT,IHTTR,IRXN,ITCUT,
     &            TLIMIT,IEND,IGRID,IGRAPH)
      CALL DIVIDE(HT,FE,XB,DXN,IGRID)
      CALL SETUP(TG,TGO,TS,TSO,U,US,VS,VC,TIGNIT,ALAYER,HT,APHIO,VOIDO,
     &           XCO,RHOSO)
      TIMES = 0.0
      IF (IGRAPH.EQ.1) THEN
         OPEN(4,FILE='GRAPH.OUT')
         WRITE(4,100)
100      FORMAT('TIME',6X,'X'6X,'O2',5X,'CO2',5X,'CO',5X,'TG',5X,'TS')
         WRITE(4,101)
101      FORMAT('MIN',6X,'CM')
      ENDIF
      WRITE(3,131)
131   FORMAT('PROFILES FOR OVERFEED FUEL BED')
      WRITE(3,132)
132   FORMAT(/,'OPERATING CONDITIONS:')
      WRITE(3,133)HT,VG(1),TG(1)
133   FORMAT(F4.1,' CM DEEP BED WITH',F7.5,' KG/M2 S AIR AT ',F5.0,' K')
      WRITE(3,134)100.*(1.-ASH),100.*ASH
134   FORMAT('FUEL: ',F4.1,'% FIXED CARBON, ',F4.1,'% ASH')
      WRITE(3,135)DIAMC(IG+IB)*100.0,VOIDC,SPHERC
135   FORMAT('CHAR PARTICLES: ',F4.2,' CM DIAMETER,',F4.2,
     & ' VOID FRACTION, ',F3.2,' SPHERICITY')
      WRITE(3,136)DIAMA*100.0,VOIDA,SPHERA
136   FORMAT('ASH PARTICLES: ',F4.2,' CM DIAMETER,',F4.2,
     &' VOID FRACTION, ',F3.2,' SPHERICITY')
      IF (IGMOD.EQ.1) THEN
         WRITE(3,141)GRATE,GRTPD
141      FORMAT(/,'GRATE MODEL 1: PACKED BED ',F4.0,' MM THICK, PARTIC
     &      LE SIZE ',F5.2,' MM, CONDUCTIVITY ',F7.4,' W/MK')
      ENDIF
      IF (IGMOD.EQ.2) THEN
         WRITE(3,142)GRATE,GRTBAR,GRTSOL*100.
142      FORMAT(/,'GRATE MODEL 2: STEEL BARS ',F4.0,' MM DEEP X ',
     &   F4.0,' MM WIDE, SOLIDITY 'F5.1,'%')
      ENDIF
      IF (IBUILD.EQ.0) THEN
         WRITE(3,152)
152      FORMAT('ASH FALLS THROUGH THE GRATE')
      ENDIF
      IF (IBUILD.EQ.1) THEN
         WRITE(3,153)
153      FORMAT('ASH BUILDS UP IN THE BED')
      ENDIF
      IF (IRXN.EQ.1980.AND.ICOB.NE.0)THEN
```

```
          WRITE(*,*)'WD WITH EQUILIBRIUM'
          WRITE(3,144)
144       FORMAT('WESTBROOK AND DRYER KINETICS FOR CO OXIDATION WITH
     &       REVERSE RXN. FOR EQUILIBRIUM')
         ENDIF
         IF (IRXN.EQ.1980.AND.ICOB.EQ.0)THEN
          WRITE(*,*)'WD, ONE STEP (NO REVERSE)'
          WRITE(3,149)
149       FORMAT('WESTBROOK AND DRYER KINETICS FOR CO OXIDATION',
     &       ' WITHOUT REVERSE RXN.')
         ENDIF
         IF (IRXN.EQ.1970.AND.ICOB.EQ.0)THEN
          WRITE(*,*)'HF ONE STEP (NO REVERSE)'
          WRITE(3,145)
145       FORMAT('HOWARD AND FINE KINETICS FOR CO OXIDATION ',
     &       'WITHOUT REVERSE REACTION')
         ENDIF
         IF (IRXN.EQ.1970.AND.ICOB.NE.0)THEN
          WRITE(*,*)'HF WITH EQUILIBRIUM'
          WRITE(3,150)
150       FORMAT('HOWARD AND FINE KINETICS FOR CO OXIDATION ',
     &       'WITH REVERSE REACTION (EQUILIBRIUM)')
         ENDIF
         WRITE(3,160)A1,ER1
160      FORMAT('CO2 REDUCTION RATE COEFFICIENTS: A = ',F7.1,', E = ',F7.1)
         IF (IFIELD.EQ.0) THEN
          WRITE(3,161)
161       FORMAT('C OXIDATION CALCULATED FROM THE EFFECTIVENESS')
         ELSE
          WRITE(3,162)
162       FORMAT('C OXIDATION CALCULATED USING THE FIELD EQUATION')
         ENDIF
         IF (IHTTR.EQ.1970)THEN
          WRITE(3,146)
146       FORMAT('BHATTACHARYA AND PEI HEAT TR. COEFFICIENT')
         ENDIF
         IF (IHTTR.EQ.1960)THEN
          WRITE(3,147)
147       FORMAT('YOSHIDA ET AL. HEAT TR. COEFFICIENT')
         ENDIF
         IF (IHTTR.EQ.1950)THEN
          WRITE(3,148)
148       FORMAT('CHU HEAT TR. COEFFICIENT')
         ENDIF
         WRITE(3,143)F12W,TS(IG+IB)
143      FORMAT('VIEW FACTOR F12 = ',F5.3,' FROM BED TO THE SURROUNDINGS
     &AT ',F5.0,' K')
         WRITE(3,200)F12B,TS(1)
200      FORMAT('VIEW FACTOR F12 = ',F5.3,' FROM BED TO THE ASHPAN AT ',
     &       F5.0,' K')
         WRITE(3,140)
140      FORMAT(/,'ALL CONCENTRATIONS ARE VOLUMETRIC')

*************************************************************************
*     RECURSION OF MAIN TIME LOOP                                       *
*************************************************************************
66       CONTINUE
```

```
      IF ((TIMES.GE.TLIMIT).AND.(IFLAG3.EQ.5)) THEN
         IFLAG = 4
         WRITE(*,138) VG(1),TG(1)
138      FORMAT(6X,F7.5,'KG/M2 S AIR AT ',F5.0,'K')
         AVGCGONE = TCGONE/IN
         WRITE(*,199) AVGCGONE*3600.0
199      FORMAT(6X,'AVERAGE BURNING RATE: ',F7.2,' KG/M2 HR ')
         CALL PRINT(3,TG,TS,VS,VC,AMWG,RE,AKAS,CGONE,XB,AKY)
         CALL ENERGY(TG,TS,VS,CPG,ERROR)
         WRITE(3,44) ERROR
         GO TO 111
      ENDIF
      IF (ITERNS.EQ.IEND) THEN
         WRITE(3,*) 'THE DAMN THING DNCV'
         GO TO 111
      ENDIF

      CALL STOICH(TS)
      CALL GEE(TG,TSO,AMWG,CGONE,DIFF)
      CALL DEE(VC,APHI,APHIO,VOIDO,XCO)
      CALL WESTMAN(VOIDO)
      CALL BEDCOND
      IF ((ITERNS.EQ.1).OR.(ITIME.EQ.0).OR.(ITIME.EQ.1))THEN
         CALL GPROP(IHTTR,TG,TS,RE,CPG,AKG,AKAG,AKY,DEFF,H,DIFF)
      ENDIF
      CALL GFLUX(VOIDO)
      CALL SFLUX(3,VS,VOIDO,RHOSO,ISTOP)
      CALL CFLUX(VS,VC)
      IF (ISTOP.GT.0) THEN
         GO TO 111
      ENDIF
      IF ((ITERNS.EQ.1).OR.(ITIME.EQ.0).OR.(ITIME.EQ.1))THEN
         CALL COND(TG,TS,AKG,AKAS)
      ENDIF
      CALL PCONC(AKY)
      CALL TDMACN(TGO,VOIDO,DEFF,IRXN,RCO,RCOB,DXN,FE)
      CALL TDMATG(TG,TGI,TGO,TS,VOIDO,CPG,AKAG,H,RCO,RCOB,DXN,FE)
      CALL TDMATS(TG,TS,TSI,TSO,VOIDO,RHOSO,VS,AKAS,H,DXN,FE)
      CALL STOCK(TG,TGI,TGO,TS,TSO,TSI,APHI,APHIO,VOIDO,RHOSO,XCO,
     &           CGONE,DTEMP)

*     NEED ANOTHER ITERATION
      IF (IFLAG.EQ.2) THEN
         ITERNS = ITERNS+1
         GO TO 66
      ENDIF

*     PROCEED TO THE NEXT TIMESTEP, CHECK ERROR
      IF (IFLAG.EQ.3) THEN
         IN = IN+1
         TCGONE = TCGONE+CGONE
         IF (ICNT.EQ.ICNTN) THEN
            CALL PRINT(3,TG,TS,VS,VC,AMWG,RE,AKAS,CGONE,XB,AKY)
            IF (IGRAPH.EQ.1) THEN
               CALL GRAPHING(4,XB,AMWG,TG,TS)
            ENDIF
            CALL ENERGY(TG,TS,VS,CPG,ERROR)
```

```
            WRITE(3,44) ERROR
            WRITE(*,44) ERROR
            ICNT = 0
         ENDIF
         ITEST = INT(ICNT/5)*5-ICNT
         ICNT = ICNT+1
         IF (ITEST.EQ.0) THEN
            WRITE (*,170) TIMES,TG(20),TS(20),DTEMP/(IB+IG)/2.,ITERNS
         ENDIF
170      FORMAT(1X,'TIME ',F6.0,' S; TG20 ',F5.0,'  TS20 ',F5.0,
     &      '  DTEMP/IT ',F5.1,'  ITERNS',I3)
         ITIME = ITIME+1
         IF ((ABS(DTEMP).LE.2.0*2.*(IB+IG)).AND.(ITSTEP.LT.ITCUT)) THEN
            DT = DT*2.0
            ITSTEP = ITSTEP+1
         ENDIF
         TIMES = TIMES+DT
         ITERNS = 1
         IFLAG3 = 5
         GO TO 66
      ENDIF
*************************************************************************
*     END OF MAIN TIME LOOP                                             *
*************************************************************************
43    FORMAT(/,'TIME ELAPSED IS :',F10.1)
44    FORMAT(/,'PERCENT ENERGY ERROR IS:',F10.6)
111   STOP
      END

*************************************************************************

      SUBROUTINE READER(IRUN,ICONST,TG,TS,U,US,TIGNIT,ALAYER,HT,
     &                  IHTTR,IRXN,ITCUT,TLIMIT,IEND,IGRID,IGRAPH)

*     READS IN ALL SYSTEM BOUNDARIES

      CHARACTER*72 TITLE
      PARAMETER (N=50)
      DIMENSION TG(N),TS(N)
      DIMENSION VOID(N),SLAB(N),SSB(N),SSBO(N),RHOS(N),G(N)
      DIMENSION DIAMC(N),SSC(N),SSCO(N),XC(N)
      DIMENSION Y8O2(N),Y8CO2(N),Y8CO(N),Y8N2(N),Y8O2O(N),Y8CO2O(N)
      DIMENSION Y8COO(N),Y8N2O(N)
      DIMENSION G1(N),G2(N),X(N),S(N)
      COMMON/BED/VOID,E,SLAB,SSB,SSBO,RHOS,G
      COMMON/CHAR/CARB,DIAMC,RHOC,VOIDC,SPHERC,SSC,SSCO,XC
      COMMON/ASH/ASH,DIAMA,RHOA,VOIDA,SPHERA,IBUILD
      COMMON/Y/Y8O2,Y8CO2,Y8CO,Y8N2,Y8O2O,Y8CO2O,Y8COO,Y8N2O
      COMMON/INFO/WTN2,WTO2,WTCO2,WTCO,R,P,BETA,GAMMA,THI
      COMMON/STOIC/SCO2,SCO,S3,S2,DH1,DH2,DH3,DH4
      COMMON/GE/A,A1,ER,ER1,ALPHA1,ALPHA2,ALPHA3
      COMMON/PORE/IFIELD,IEFFECT,SSP,TAU,VOIDP
      COMMON/REACT/G1,G2,X,S,IREACT
      COMMON/RAD/TSG,TSB,TSW,HRG,HRB,HRW,F12B,F12W,BOLTZ,TCOAL
      COMMON/GRATE/GRATE,GRTSOL,GRTBAR,IGMOD,GRTRHO,GRTPD,GRTSPACE
      COMMON/TIME/IFLAG,ITIME,ITERNS,TURNS,IB,IG,ICOB,TIMES,DT
```

```
      REWIND IRUN
      REWIND ICONST
      READ(IRUN,99) TITLE
      READ(IRUN,*) IB,IG,TLIMIT,DT,ITCUT,IEND
      IT= IG+IB
      READ(IRUN,99) TITLE
      READ(IRUN,*) DIAMC(IT),CARB,RHOC,VOIDC,SPHERC,E,TCOAL
      READ(IRUN,99) TITLE
      READ(IRUN,*) DIAMA,ASH,RHOA,VOIDA,SPHERA
      READ(IRUN,99) TITLE
      READ(IRUN,*) HT,U,P
      READ(IRUN,99) TITLE
      READ(IRUN,*) A1,ER1,A,ER
      READ(IRUN,99) TITLE
      READ(IRUN,*) IREACT,IHTTR,IRXN,ICOB,IBUILD
      READ(IRUN,99) TITLE
      READ(IRUN,*) TS(1),TG(1),TG(IT),TS(IT),TIGNIT,ALAYER
      READ(IRUN,99) TITLE
      READ(IRUN,*) IGRAPH,IGRID
      READ(IRUN,99) TITLE
      READ(IRUN,*) IFIELD,IEFFECT,SSP,TAU,VOIDP
      READ(ICONST,99) TITLE
      READ(ICONST,*) R,BOLTZ,WTN2,WTO2,WTCO2,WTCO
      READ(ICONST,99) TITLE
      READ(ICONST,*) BETA,GAMMA,THI,ALPHA1,ALPHA2
      READ(ICONST,99) TITLE
      READ(ICONST,*) SCO,SCO2,S3,S2,DH1,DH2,DH3,DH4
      READ(ICONST,99) TITLE
      READ(ICONST,*) US,G(1),G(IT)
      READ(ICONST,99) TITLE
      READ(ICONST,*)Y8O2(1),Y8CO(1),Y8CO2(1),Y8O2(IT),Y8CO(IT),Y8CO2(IT)
      READ(ICONST,99) TITLE
      READ(ICONST,*) IGMOD,GRATE,GRTPD,GRTSPACE,GRTBAR,GRTRHO
99    FORMAT(A72)
      RETURN
      END

*************************************************************************

      SUBROUTINE DIVIDE(HT,FE,XB,DXN,IGRID)

*     GENERATES THE GRID

      PARAMETER (N=50)
      DIMENSION FE(N),XB(N),DXN(N)
      DIMENSION VOID(N),SLAB(N),SSB(N),SSBO(N),RHOS(N),G(N)
      COMMON/BED/VOID,E,SLAB,SSB,SSBO,RHOS,G
      COMMON/GRATE/GRATE,GRTSOL,GRTBAR,IGMOD,GRTRHO,GRTPD,GRTSPACE
      COMMON/TIME/IFLAG,ITIME,ITERNS,TURNS,IB,IG,ICOB,TIMES,DT

*************************************************************************
*     COORDINATE SYSTEM: ORIGIN IS AT TOP OF GRATE. NODES 1 TO IG ARE
*     GRATE NODES, IG+1 TO IB+IG ARE THE BED ITSELF. THE COORDINATE
*     XB LOCATES THE NORTH (TOP) INTERFACE OF THE CELL. SLAB IS THE
*     CELL THICKNESS AND DXN THE DISTANCE FROM NODE I TO NODE I+1. THE
*     TOP OF THE BED IS AT THE NORTH FACE OF CELL (IG+IB-1). NODES ARE
*     CENTRED IN THE CELLS. AT PRINTOUT, COORDS ARE TRANSFORMED SO THAT
```

```
*     THE X COORDINATE BECOMES THE NODE LOCATION.
*************************************************************************

      IF (IGRID.EQ.0) THEN
         XB(IG) = 0.0
         SLAB(IG) = GRATE/(IG-1.0)*0.001
         DO 20 I=IG+1,IG+IB
            SLAB(I) = HT/(IB-1.0)*0.01
            XB(I) = SLAB(I)+XB(I-1)
20       CONTINUE
         DO 21 I=IG-1,1,-1
            SLAB(I) = GRATE/(IG-1.0)*0.001
            XB(I) = XB(I+1)-SLAB(I)
21       CONTINUE
      ELSE
         DEL1 = LOG(HT+1.0)/(IB-1)
         DEL2 = LOG(GRATE+1.0)/(IG-1)
         DO 10 I=IG+1,IB+IG
            XB(I) = (EXP((I-IG)*DEL1)-1.0)*.01
10       CONTINUE
         DO 11 I=1,IG
            XB(IG-I+1) = -(EXP((I-1)*DEL2)-1.0)*.001
11       CONTINUE
         DO 12 I=1,IB+IG
            IF (I.EQ.1) THEN
               SLAB(I) = ABS(XB(I+1)-XB(I))
            ELSE
               SLAB(I) = ABS(XB(I)-XB(I-1))
            ENDIF
12       CONTINUE
      ENDIF
      DO 13 I=1,IB+IG-1
         DXN(I) = ABS(SLAB(I)+SLAB(I+1))/2.0
         FE(I) = 0.5*SLAB(I)/DXN(I)
13    CONTINUE
      RETURN
      END

*************************************************************************

      SUBROUTINE SETUP(TG,TGO,TS,TSO,U,US,VS,VC,TIGNIT,ALAYER,HT,APHIO,
     &                 VOIDO,XCO,RHOSO)

*     CALCULATES THE INITIAL PROFILES AND BOUNDARIES

      PARAMETER (N=50)
      PARAMETER (PI=3.141592654)
      DIMENSION TG(N),TGO(N),TS(N),TSO(N),VS(N),VC(N)
      DIMENSION APHIO(N),VOIDO(N),XCO(N),RHOSO(N)
      DIMENSION VOID(N),SLAB(N),SSB(N),SSBO(N),RHOS(N),G(N)
      DIMENSION DIAMC(N),SSC(N),SSCO(N),XC(N)
      DIMENSION VG(N),RHOG(N),RHOGO(N)
      DIMENSION Y8O2(N),Y8CO2(N),Y8CO(N),Y8N2(N),Y8O2O(N),Y8CO2O(N)
      DIMENSION Y8COO(N),Y8N2O(N)
      DIMENSION YRO2(N),YRCO2(N),YRCO(N),YRN2(N)
      DIMENSION G1(N),G2(N),X(N),S(N)
      DIMENSION SSA(N)
```

```
      COMMON/BED/VOID,E,SLAB,SSB,SSBO,RHOS,G
      COMMON/CHAR/CARB,DIAMC,RHOC,VOIDC,SPHERC,SSC,SSCO,XC
      COMMON/ASH/ASH,DIAMA,RHOA,VOIDA,SPHERA,IBUILD
      COMMON/GAS/VG,RHOG,RHOGO
      COMMON/Y/Y8O2,Y8CO2,Y8CO,Y8N2,Y8O2O,Y8CO2O,Y8COO,Y8N2O
      COMMON/YR/YRO2,YRCO2,YRCO,YRN2
      COMMON/REACT/G1,G2,X,S,IREACT
      COMMON/RAD/TSG,TSB,TSW,HRG,HRB,HRW,F12B,F12W,BOLTZ,TCOAL
      COMMON/GRATE/GRATE,GRTSOL,GRTBAR,IGMOD,GRTRHO, GRTPD,GRTSPACE
      COMMON/TIME/IFLAG,ITIME,ITERNS,TURNS,IB,IG,ICOB,TIMES,DT

      IT = IB+IG
      DO 10 I=2,IT-1
         TS(I) = TS(IT)
         TG(I) = TG(1)
         Y8O2(I) = Y8O2(1)
         Y8CO2(I)= Y8CO2(1)
         Y8CO(I) = Y8CO(1)
10    CONTINUE

*     SETS UP TEMPERATURES IN THE IGNITION ZONE
      ZONE = 0.0
      DO 11 I=IG,IT
         IF (ZONE.LT.ALAYER) THEN
            ZONE = ZONE+SLAB(I)
            IIGNIT = I
         ENDIF
11    CONTINUE
      DO 12 I=IG,IIGNIT
         TS(I) = TIGNIT
12    CONTINUE

      DO 13 I=1,IT
         RHOG(I) = DENS(TG(I),I)
         RHOGO(I) = RHOG(I)
         G1(I) = G(IT)
         G2(I) = G(IT)
         YRO2(I) = Y8O2(I)
         YRCO2(I) = Y8CO2(I)
         YRCO(I) = Y8CO(I)
         YRN2(I) = 1.0-YRO2(I)-YRCO2(I)-YRCO(I)
         TGO(I) = TG(I)
         TSO(I) = TS(I)
         Y8O2O(I) = Y8O2(I)
         Y8CO2O(I) = Y8CO2(I)
         Y8COO(I) = Y8CO(I)
         VS(I) = US*RHOC*ASH
         VC(I) = US*RHOC*ASH
         VG(I) = U*RHOG(I)
13    CONTINUE

      DO 14 I=IG+1,IT-1
         DIAMC(I) = DIAMC(IT)
         APHIO(I) = 6.0/(PI*RHOC*DIAMC(IT)**3.0)
         VOID(I) = VOIDC
         VOIDO(I) = VOID(I)
         XC(I) = 1.0/(1.0+RHOC/RHOA*ASH
```

```
     &            *(DIAMC(IT)**3.0/DIAMC(I)**3.0-1.0))
          XCO(I) = XC(I)
          RHOS(I) = XC(I)*RHOC+(1.0-XC(I))*RHOA
          RHOSO(I) = RHOS(I)
          SSC(I) = 6.0/(DIAMC(I)*SPHERC)*XC(I)*(1.0-VOID(I))
          SSCO(I) = SSC(I)
          SSA(I) = 6.0/(DIAMA*SPHERA)*(1.0-XC(I))*(1.0-VOID(I))
          SSB(I) = SSC(I)+SSA(I)
          SSBO(I) = SSB(I)
14        CONTINUE

          RHOS(IT) = RHOC
          VOID(IT) = VOIDC
          SSB(IT) = SSB(IT-1)
          SSC(IT) = SSC(IT-1)
          XC(IT) = XC(IT-1)

          IF (IGMOD.EQ.1) THEN
             DO 15 I = 1,IG
                VOID(I) = VOIDA
                DIAMC(I) = GRTPD/1000.0
                SSB(I) = 6.0*(1.0-VOID(I))/DIAMC(I)/SPHERA
15           CONTINUE
          ENDIF

          IF (IGMOD.EQ.2) THEN
             GRTSOL = GRTBAR/(GRTSPACE+GRTBAR)
             DO 16 I = 1,IG
                SSB(I) = 2.0*GRTSOL/(GRTBAR/1000.0)
                SSBO(I) = SSB(I)
                VOID(I) = 1.0-GRTSOL
                VOIDO(I) = VOID(I)
                DIAMC(I) = 6.0*(1.0-VOID(I))/SSB(I)
                RHOS(I) = GRTRHO
                RHOSO(I) = RHOS(I)
16           CONTINUE
             SSB(2) = SSB(2)+GRTSOL/SLAB(2)
             SSBO(2) = SSB(2)
          ENDIF

*         RADIATION
*         GRATE TO ASHPAN
          TSG = (TS(1)+TS(2))/2.0
          HRG = BOLTZ*(TS(1)**2.0+TSG**2.0)*(TS(1)+TSG)*GRTSOL
*         BED TO ASHPAN
          TSB = (TS(IG)+TS(IG+1))/2.0
          RH = GRATE/GRTSPACE
          F12B = SQRT(1.0+RH**2.0)-RH
          F12B = 1.0/(2.0/(1.0+F12B)+1.0/E-1.0)
          HRB = BOLTZ*F12B*(TSB**2.0+TS(1)**2.0)*(TSB+TS(1))
*         BED TO WALLS
          TSW = (TS(IT-1)+TS(IT))/2.0
          RH = 4.5/(8.0-HT/2.54)
          RX = 1.0+(1.0+RH**2.0)/RH**2.0
          F12W = 0.5*(RX-(RX**2.0-4.0)**0.5)
          F12W = 1.0/(2.0/(1.0+F12W)+1.0/E-1.0)
          HRW = BOLTZ*F12W*(TS(IT)**2.0+TSW**2.0)*(TS(IT)+TSW)
```

```
      RETURN
      END

*****************************************************************************

      SUBROUTINE STOICH(TS)

*     CALCULATES THE CO/CO2 RATIO AND MASS C BURNED PER CO+CO2 PRODUCT

      PARAMETER (N=50)
      DIMENSION TS(N)
      DIMENSION G1(N),G2(N),X(N),S(N)
      COMMON/INFO/WTN2,WTO2,WTCO2,WTCO,R,P,BETA,GAMMA,THI
      COMMON/STOIC/SCO2,SCO,S3,S2,DH1,DH2,DH3,DH4
      COMMON/REACT/G1,G2,X,S,IREACT
      COMMON/TIME/IFLAG,ITIME,ITERNS,TURNS,IB,IG,ICOB,TIMES,DT

      S(1) = 0.0
      X(1) = 0.0
      DO 10 I=2,IG+IB-1
         X(I) = 2500.0*EXP(-6240.0/TS(I))*WTCO/WTCO2
         X(I) = 1.0/(1.0+X(I))
         S(I) = (1.0+SCO2)*(1.0+SCO)
         S(I) = S(I)/(X(I)*(1.0+SCO)+(1.0-X(I))*(1.0+SCO2))
         S(I) = S(I)-1.0
10    CONTINUE
      S(IB+IG) = 0.0
      X(IB+IG) = 0.0
      RETURN
      END

*****************************************************************************

      SUBROUTINE GEE(TG,TSO,AMWG,CGONE,DIFF)

*     CALCULATES THE CARBON CONSUMPTION RATES

      PARAMETER (N=50)
      DIMENSION TG(N),TSO(N),AMWG(N),DIFF(N,3)
      DIMENSION VOID(N),SLAB(N),SSB(N),SSBO(N),RHOS(N),G(N)
      DIMENSION DIAMC(N),SSC(N),SSCO(N),XC(N)
      DIMENSION VG(N),RHOG(N),RHOGO(N)
      DIMENSION YRO2(N),YRCO2(N),YRCO(N),YRN2(N)
      DIMENSION G1(N),G2(N),X(N),S(N)
      COMMON/BED/VOID,E,SLAB,SSB,SSBO,RHOS,G
      COMMON/CHAR/CARB,DIAMC,RHOC,VOIDC,SPHERC,SSC,SSCO,XC
      COMMON/ASH/ASH,DIAMA,RHOA,VOIDA,SPHERA,IBUILD
      COMMON/GAS/VG,RHOG,RHOGO
      COMMON/YR/YRO2,YRCO2,YRCO,YRN2
      COMMON/INFO/WTN2,WTO2,WTCO2,WTCO,R,P,BETA,GAMMA,THI
      COMMON/GE/A,A1,ER,ER1,ALPHA1,ALPHA2,ALPHA3
      COMMON/PORE/IFIELD,IEFFECT,SSP,TAU,VOIDP
      COMMON/REACT/G1,G2,X,S,IREACT
      COMMON/TIME/IFLAG,ITIME,ITERNS,TURNS,IB,IG,ICOB,TIMES,DT

      CGONE = 0.0
      G1(1) = 0.0
```

```
      G2(1) = 0.0
      DO 10 I=2,IG
         G(I) = 0.0
         G1(I) = 0.0
         G2(I)= 0.0
10    CONTINUE
      DO 11 I=1,IB+IG-1
         AMWG(I) = RHOG(I)*R*TG(I)/P
11    CONTINUE
      DO 12 I=IG+1,IB+IG-1
*     SET PARTIAL PRESSURES OF GASES IN THE BED SLABS (IN KPA)
         IF (IREACT.GT.0) THEN
            PO2 = P*YRO2(I)*AMWG(I)/WTO2
            PCO = P*YRCO(I)*AMWG(I)/WTCO
            PCO2 = P*YRCO2(I)*AMWG(I)/WTCO2

*     CHAR OXIDATION RXN
            IF (IFIELD.EQ.0) THEN
               AKIP = 678.0*EXP(-179400/(R*TSO(I)))
               AKIM = AKIP*R*TSO(I)/12.0
               IF (TIMES.EQ.0.0) THEN
                  DIFF(I,1) = 0.000247
               ENDIF
               DEFFP = DIFF(I,1)*VOIDP/TAU
               THIELE = DIAMC(I)/2.0*SQRT(AKIM*SSP/DEFFP)
               EFFECT = 3.0/(THIELE**2.0)
     &                  *(THIELE*(TANH(THIELE))**(-1.0)-1.0)
               AKP = DIAMC(I)/6.0*EFFECT*SSP*AKIP
               G1(I) = AKP*PO2
            ELSE
               G1(I) = A*EXP(-ER/TSO(I))*PO2
            ENDIF
            G2(I) = 0.0

*     CHAR REDUCTION RXN
            IF (IREACT.GT.1) THEN
               AK1 = A1*EXP(-ER1/TSO(I))/101.3
               IF (IEFFECT.EQ.0) THEN
                  G2(I) = AK1*PCO2
               ELSE
                  AKIP = AK1
                  AKIM = AKIP*R*TSO(I)/12.0
                  IF (TIMES.EQ.0.0) THEN
                     DIFF(I,2) = 0.000199
                  ENDIF
                  DEFFP = DIFF(I,2)*VOIDP/TAU
                  THIELE = DIAMC(I)/2.0*SQRT(AKIM*SSP/DEFFP)
                  EFFECT = 3.0/(THIELE**2.0)
     &                  *(THIELE*(TANH(THIELE))**(-1.0)-1.0)
                  AKP = DIAMC(I)/6.0*EFFECT*SSP*AKIP
                  G2(I) = AKP*PCO2
               ENDIF
            ENDIF

            IF (DIAMC(I).LT.DIAMC(IG+IB)/1000.0) THEN
               G1(I) = 0.0
               G2(I) = 0.0
```

```
            ENDIF
            G(I) = G1(I)+G2(I)
         ELSE
            G1(I) = 0.0
            G2(I) = 0.0
            G(I) = G1(I)+G2(I)
         ENDIF
12    CONTINUE
      G1(IB+IG) = 0.0
      G2(IB+IG) = 0.0
      RETURN
      END

*************************************************************************

      SUBROUTINE DEE(VC,APHI,APHIO,VOIDO,XCO)

*     CALCULATES THE CHAR PARTICLE DIAMETER

      PARAMETER (N=50)
      PARAMETER (PI=3.141592654)
      DIMENSION VC(N),APHI(N),APHIO(N),VOIDO(N),XCO(N)
      DIMENSION VOID(N),SLAB(N),SSB(N),SSBO(N),RHOS(N),G(N)
      DIMENSION DIAMC(N),SSC(N),SSCO(N),XC(N)
      DIMENSION PD(N),QD(N),AMASSC(N)
      COMMON/BED/VOID,E,SLAB,SSB,SSBO,RHOS,G
      COMMON/CHAR/CARB,DIAMC,RHOC,VOIDC,SPHERC,SSC,SSCO,XC
      COMMON/ASH/ASH,DIAMA,RHOA,VOIDA,SPHERA,IBUILD
      COMMON/TIME/IFLAG,ITIME,ITERNS,TURNS,IB,IG,ICOB,TIMES,DT

      AD = 1.0
      BD = 0.0
      CD = 0.0
      DD = 6.0/(PI*RHOC*DIAMC(IB+IG)**3.0)
      PD(IB+IG) = BD/AD
      QD(IB+IG) = DD/AD
      DO 10 I=IB+IG-1,IG+1,-1
         BD = AMAX1(0.0,-VC(I)*DT)
         CD = 0.0
         AD = RHOC*XC(I)*(1.0-VOID(I))*SLAB(I)-VC(I-1)*DT
         DD = RHOC*XCO(I)*(1.0-VOIDO(I))*SLAB(I)*APHIO(I)
         PD(I) = CD/(AD-BD*PD(I+1))
         QD(I) = (BD*QD(I+1)+DD)/(AD-BD*PD(I+1))
10    CONTINUE
      APHI(IG+1) = QD(IG+1)
      AMASSC(IG+1) = 1.0/APHI(IG+1)
      DIAMC(IG+1) = (6.0*AMASSC(IG+1)/(RHOC*PI))**(1.0/3.0)
      DO 11 I=IG+2,IG+IB-1
         APHI(I) = PD(I)*APHI(I-1)+QD(I)
         AMASSC(I) = 1.0/APHI(I)
         DIAMC(I) = (6.0*AMASSC(I)/(RHOC*PI))**(1.0/3.0)
11    CONTINUE
      RETURN
      END

*************************************************************************
```

```
      SUBROUTINE WESTMAN(VOIDO)

*     CALCULATES THE BED VOID FRACTION USING THE WESTMAN EQUATION

      PARAMETER (N=50)
      DIMENSION VOID(N),SLAB(N),SSB(N),SSBO(N),RHOS(N),G(N)
      DIMENSION DIAMC(N),SSC(N),SSCO(N),XC(N)
      COMMON/BED/VOID,E,SLAB,SSB,SSBO,RHOS,G
      COMMON/CHAR/CARB,DIAMC,RHOC,VOIDC,SPHERC,SSC,SSCO,XC
      COMMON/ASH/ASH,DIAMA,RHOA,VOIDA,SPHERA,IBUILD
      COMMON/TIME/IFLAG,ITIME,ITERNS,TURNS,IB,IG,ICOB,TIMES,DT

      DO 10 I=IG+1,IG+IB-1
         DIAML = DIAMC(I)
         DIAMS = DIAMA
         VOIDL = VOIDC
         VOIDS = VOIDA
         XL = XC(I)

         RATIO = DIAMS/DIAML
         RSTR = (1.0/VOIDL-1.0)*RATIO**3.0/(1.0-VOIDS)
         AK = -0.63
         GWEST = RSTR**AK+(1.0-VOIDL**(-AK))

*     TEST FOR PHYSICALLY REASONABLE SOLUTION
         VL = 1.0/(1.0-VOIDL)
         VS = 1.0/(1.0-VOIDS)
         VMIN = VL*VS/(VL+VS-1.0)
         XMIN = (1.0-VOIDL)/(1.0-VOIDL*VOIDS)
         VTEST1 = VS+(VMIN-VS)*XL/XMIN
         VTEST1 = 0.995*VTEST1
         VTEST2 = VMIN+(VL-VMIN)*(XL-XMIN)/(1.0-XMIN)
         VTEST2 = 0.995*VTEST2

         CALL NEWTON(I,GWEST,VOIDO,V)
         IF ((V.LT.VTEST1).OR.(V.LT.VTEST2)) THEN
            VOIDO = AMAX1(VOIDC,VOIDA)
            CALL NEWTON(I,GWEST,VOIDO,V)
            PRINT*,'NEWTON CALLED AGAIN - V =',V
         ENDIF
         IF ((V.LT.VTEST1).OR.(V.LT.VTEST2)) THEN
            PRINT*,'UNREASONABLE VOID FRACTION'
            STOP
         ENDIF
         VOID(I) = 1.0-1.0/V
10    CONTINUE
      RETURN
      END

*************************************************************************

      SUBROUTINE NEWTON(I,GWEST,VOIDO,V)

*     SOLVES THE WESTMAN EQUATION USING THE NEWTON-RAPHSON METHOD

      PARAMETER (N=50)
      DIMENSION VOIDO(N)
```

```
      DIMENSION DIAMC(N),SSC(N),SSCO(N),XC(N)
      COMMON/CHAR/CARB,DIAMC,RHOC,VOIDC,SPHERC,SSC,SSCO,XC
      COMMON/ASH/ASH,DIAMA,RHOA,VOIDA,SPHERA,IBUILD

      J = 0
      JMAX = 100
      TOL = 1.0E-6
      VOLD = 1.0/(1.0-VOIDO(I))
1     CONTINUE
      IF (J.LE.JMAX) THEN
         VNEW = VOLD-F(VOLD,I,GWEST)/DF(VOLD,I,GWEST)
         J = J+1
         IF (DABS(VNEW-VOLD).LT.TOL) THEN
            V = (VNEW+VOLD)*0.5
            RETURN
         ELSE
            VOLD = VNEW
         ENDIF
         GO TO 1
      ENDIF
      IF (J.GT.JMAX) THEN
         PRINT*,'MAXIMUM NUMBER OF ITERATIONS EXCEEDED IN NEWTON'
         STOP
      ENDIF
      RETURN
      END

*****************************************************************************

      SUBROUTINE BEDCOND

*     CALCULATES THE BED CONDITIONS

      PARAMETER (N=50)
      DIMENSION VOID(N),SLAB(N),SSB(N),SSBO(N),RHOS(N),G(N)
      DIMENSION DIAMC(N),SSC(N),SSCO(N),XC(N)
      DIMENSION SSA(N)
      COMMON/BED/VOID,E,SLAB,SSB,SSBO,RHOS,G
      COMMON/CHAR/CARB,DIAMC,RHOC,VOIDC,SPHERC,SSC,SSCO,XC
      COMMON/ASH/ASH,DIAMA,RHOA,VOIDA,SPHERA,IBUILD
      COMMON/TIME/IFLAG,ITIME,ITERNS,TURNS,IB,IG,ICOB,TIMES,DT

      DO 10 I=IG+1,IG+IB-1
         XC(I) = 1.0/(1.0+RHOC/RHOA*ASH
     &           *(DIAMC(IB+IG)**3.0/DIAMC(I)**3.0-1.0))
         RHOS(I) = XC(I)*RHOC+(1.0-XC(I))*RHOA
         SSC(I) = 6.0/(DIAMC(I)*SPHERC)*XC(I)*(1.0-VOID(I))
         SSA(I) = 6.0/(DIAMA*SPHERA)*(1.0-XC(I))*(1.0-VOID(I))
         SSB(I) = SSC(I)+SSA(I)
10    CONTINUE
      RETURN
      END

*****************************************************************************

      SUBROUTINE GPROP(IHTTR,TG,TS,RE,CPG,AKG,AKAG,AKY,DEFF,H,DIFF)
```

```
*     CALCULATES THE GAS PROPERTIES

      PARAMETER (N=50)
      DIMENSION TG(N),TS(N),RE(N),CPG(N),AKG(N),AKAG(N),AKY(N,3)
      DIMENSION DEFF(N,3),H(N)
      DIMENSION VOID(N),SLAB(N),SSB(N),SSBO(N),RHOS(N),G(N)
      DIMENSION DIAMC(N),SSC(N),SSCO(N),XC(N)
      DIMENSION VG(N),RHOG(N),RHOGO(N)
      DIMENSION Y8O2(N),Y8CO2(N),Y8CO(N),Y8N2(N),Y8O2O(N),Y8CO2O(N)
      DIMENSION Y8COO(N),Y8N2O(N)
      DIMENSION YRO2(N),YRCO2(N),YRCO(N),YRN2(N)
      DIMENSION CPGREG(N)
      DIMENSION EKAI(3),SIGMI(3),WT(3),DIFF(N,3),SCHM(3),AMWG(N)
      COMMON/BED/VOID,E,SLAB,SSB,SSBO,RHOS,G
      COMMON/CHAR/CARB,DIAMC,RHOC,VOIDC,SPHERC,SSC,SSCO,XC
      COMMON/ASH/ASH,DIAMA,RHOA,VOIDA,SPHERA,IBUILD
      COMMON/GAS/VG,RHOG,RHOGO
      COMMON/Y/Y8O2,Y8CO2,Y8CO,Y8N2,Y8O2O,Y8CO2O,Y8COO,Y8N2O
      COMMON/YR/YRO2,YRCO2,YRCO,YRN2
      COMMON/INFO/WTN2,WTO2,WTCO2,WTCO,R,P,BETA,GAMMA,THI
      COMMON/STOIC/SCO2,SCO,S3,S2,DH1,DH2,DH3,DH4
      COMMON/GRATE/GRATE,GRTSOL,GRTBAR,IGMOD,GRTRHO,GRTPD,GRTSPACE
      COMMON/TIME/IFLAG,ITIME,ITERNS,TURNS,IB,IG,ICOB,TIMES,DT
      COMMON/EXTRA/CPGREG

      AV = 1.16145
      BV = 0.14874
      CV = 0.52487
      DV = 0.77320
      EV = 2.16178
      FV = 2.43787

      AD = 1.06036
      BD = 0.15610
      CD = 0.19300
      DD = 0.47635
      ED = 1.03587
      FD = 1.52996
      GD = 1.76474
      HD = 3.89411

      SIGN2 = 3.798
      EKAN2 = 71.4
      SIGMI(1) = 3.467
      EKAI(1) = 106.7
      WT(1) = WTO2
      SIGMI(2) = 3.941
      EKAI(2) = 195.2
      WT(2) = WTCO2
      SIGMI(3) = 3.690
      EKAI(3) = 91.7
      WT(3) = WTCO

      DO 10 I=1,IB+IG

      IF (I.LE.IG) THEN
         DIAM = DIAMC(I)
```

```
      ELSE
         DIAM = 1.0/(XC(I)/DIAMC(I)+(1.0-XC(I))/DIAMA)
      ENDIF

*     CALCULATION OF THERMAL CONDUCTIVITY
         TASTA = TG(I)/EKAN2
         OMEGN2 = AV/TASTA**BV+CV/EXP(DV*TASTA)+EV/EXP(FV*TASTA)
         AMU = 2.6693E-06*SQRT(WTN2*TG(I))/((SIGN2**2.0)*OMEGN2)
         CPG(I) = CPGBAR(TG(I),I)
         AMWG(I) = RHOG(I)*TG(I)*R/P
         AKG(I) = (CPGREG(I)+(5.0/4.0)*(R/AMWG(I)*1000.0))*AMU

*     CALCULATION OF COMPONENT DIFFUSIVITIES (M2/S)
         PATM = P/101.3
         DO 11 J=1,3
            SNI = (SIGN2+SIGMI(J))/2.0
            EKNI = (EKAN2*EKAI(J))**(1.0/2.0)
            TASTA = TG(I)/EKNI
            OMEGAD = AD/TASTA**BD+CD/EXP(DD*TASTA)+ED/EXP(FD*TASTA)
     &                +GD/EXP(HD*TASTA)
            DIFF(I,J) = 1.858E-3*TG(I)**(3.0/2.0)*((WTN2+WT(J))
     &                  /(WTN2*WT(J)))**(1.0/2.0)
     &                  /(PATM*SNI**2.0*OMEGAD)*1.0E-4
            SCHM(J) = AMU/RHOG(I)/DIFF(I,J)
11       CONTINUE

         ALEFF = 1.0
         BM = (Y8O2(I)-YRO2(I))/(SCO+YRO2(I))
         IF (ABS(BM).LE.1.0E-3) THEN
            CORRKY = 1.0
         ELSE
            CORRKY = (LOG(1.0+BM))/BM
         ENDIF
         BT = ((1.0+BM)**ALEFF)-1.0
         IF ((BT.LE.1.0E-3).OR.(ABS(BM).LT.1.0E-3)) THEN
            CORRH = 1.0
         ELSE
            CORRH = (LOG(1.0+BT))/BT
         ENDIF
         RE(I) = VG(I)/(AMU*SSB(I))
         AR = (DIAM**3.0)*9.8*RHOG(I)*(RHOS(I)-RHOG(I))/(AMU**2.0)
         PR = AMU*CPGREG(I)/AKG(I)

*     BHATTACHARYA AND PEI HEAT TR OPTION
         IF (IHTTR.EQ.1970) THEN
            AJH = 0.018*(AR/(RE(I)*RE(I)*36.0))**(0.25)
         ENDIF

*     YOSHIDA AND WEN OPTION
         IF (IHTTR.EQ.1960) THEN
            IF (RE(I).LT.50.0) THEN
               AJH = 0.91*(RE(I)**(-0.51))
            ELSE
               AJH = 0.61*(RE(I)**(-0.41))
            ENDIF
         ENDIF
```

```
*      CHU OPTION
          IF (IHTTR.EQ.1950) THEN
             AJH = 1.77*(RE(I)*6.0)**(-0.44)
             AJD = 5.7*(RE(I)*6.0)**(-0.78)
          ELSE
             AJD = AJH
          ENDIF

          FVOID = 1.0-VOIDA/VOID(I)*(1.0-VOID(I))/(1.0-VOIDA)*(1.0-XC(I))
          DO 12 J=1,3
             IF ((I.EQ.1).OR.(I.EQ.IB+IG)) THEN
                AKY(I,J) = 0.0
             ELSE
                AKY(I,J) = (AJD*VG(I)/(SCHM(J)**(0.66)))*CORRKY
                AKY(I,J) = AKY(I,J)*FVOID
              ENDIF
              DDEFF = 1.0+(9.7*VOID(I)*RHOG(I)*DIFF(I,J)/(VG(I)*DIAM))
              DDEFF = 0.73*DIFF(I,J)+0.5*VG(I)*DIAM/VOID(I)/RHOG(I)/DDEFF
              DEFF(I,J) = DDEFF*VOID(I)
12        CONTINUE

          AKAG(I) = 1.0+(9.7*VOID(I)*AKG(I)/(VG(I)*DIAM*CPGREG(I)))
          AKAG(I) = 0.73*VOID(I)*AKG(I)
     &              +0.5*VG(I)*DIAM*CPGREG(I)/AKAG(I)
          IF ((I.EQ.1).OR.(I.EQ.IB+IG)) THEN
             H(I) = 0.0
          ELSE
             H(I) = AJH*CORRH*CPGREG(I)*VG(I)/(PR**(0.66))
          ENDIF
10     CONTINUE

*      CALCULATE HEAT TRANSFER COEFFICIENT TO GRATE BARS
*      PROPERTIES, ETC. BASED ON NODE 3
       IF (IGMOD.EQ.2) THEN
          TFILM = (TG(3)+TS(3))/2.0
          AMU = 2.6693E-06*SQRT(WTN2*TFILM)/((SIGN2**2.0)*OMEGN2)
          REGRT = VG(3)*GRTBAR/1000.0/AMU
          AKGGRT = (CPGREG(3)+(5.0/4.0)*(R/AMWG(3)*1000.0))*AMU
          PR = AMU*CPGREG(3)/AKGGRT
          XNU = (0.43+0.5*REGRT**0.5)*PR**0.38
          HGRT = AKGGRT*XNU/(GRTBAR/1000.0)
          DO 13 I=1,IG
             RE(I) = REGRT
             AKAG(I) = (1.0-GRTSOL)*AKG(I)
             H(I) = HGRT
             DO 14 J=1,3
                DEFF(I,J) = (1.0-GRTSOL)*DIFF(I,J)
14           CONTINUE
13        CONTINUE
       ENDIF
       RETURN
       END

*****************************************************************************

       SUBROUTINE GFLUX(VOIDO)
```

```
*     CALCULATES THE GAS MASS VELOCITIES THROUGH THE BED SLABS

      PARAMETER (N=50)
      DIMENSION VOIDO(N)
      DIMENSION VOID(N),SLAB(N),SSB(N),SSBO(N),RHOS(N),G(N)
      DIMENSION DIAMC(N),SSC(N),SSCO(N),XC(N)
      DIMENSION VG(N),RHOG(N),RHOGO(N)
      COMMON/BED/VOID,E,SLAB,SSB,SSBO,RHOS,G
      COMMON/CHAR/CARB,DIAMC,RHOC,VOIDC,SPHERC,SSC,SSCO,XC
      COMMON/GAS/VG,RHOG,RHOGO
      COMMON/TIME/IFLAG,ITIME,ITERNS,TURNS,IB,IG,ICOB,TIMES,DT

*     THE VARIABLE VG IS ACTUALLY THE MASS FLUX RHOG*VG

      DO 10 I = 2,IB+IG-1
         VG(I) = G(I)*SLAB(I)*SSCO(I)
     &           -(VOID(I)*RHOG(I)-VOIDO(I)*RHOGO(I))*SLAB(I)/DT
         VG(I) = VG(I)+VG(I-1)
10    CONTINUE
      VG(IB+IG) = VG(IB+IG-1)
      RETURN
      END

*****************************************************************************

      SUBROUTINE SFLUX(IO,VS,VOIDO,RHOSO,ISTOP)

*     CALCULATES THE SOLID (CHAR+ASH) MASS VELOCITIES THROUGH THE BED
*     SLABS

      PARAMETER (N=50)
      DIMENSION VS(N),VOIDO(N),RHOSO(N)
      DIMENSION VOID(N),SLAB(N),SSB(N),SSBO(N),RHOS(N),G(N)
      DIMENSION DIAMC(N),SSC(N),SSCO(N),XC(N)
      DIMENSION VG(N),RHOG(N),RHOGO(N)
      COMMON/BED/VOID,E,SLAB,SSB,SSBO,RHOS,G
      COMMON/CHAR/CARB,DIAMC,RHOC,VOIDC,SPHERC,SSC,SSCO,XC
      COMMON/ASH/ASH,DIAMA,RHOA,VOIDA,SPHERA,IBUILD
      COMMON/GAS/VG,RHOG,RHOGO
      COMMON/GRATE/GRATE,GRTSOL,GRTBAR,IGMOD,GRTRHO,GRTPD,GRTSPACE
      COMMON/TIME/IFLAG,ITIME,ITERNS,TURNS,IB,IG,ICOB,TIMES,DT

*     THE VARIABLE VS IS ACTUALLY THE MASS FLUX RHOS*VS

      ISTOP = 0
      ICOUNT = 0

*     IF THE ASH FALLS THROUGH THE GRATE
      IF (IBUILD.EQ.0) THEN
*     RESET A GUESS FUEL INLET MASS VELOCITY UNTIL CONVERGENCE
333      DO 10 I=2,IB+IG-1
            VS(I) = -G(I)*SLAB(I)*SSCO(I)
     &              -((1-VOID(I))*RHOS(I)
     &              -(1-VOIDO(I))*RHOSO(I))*SLAB(I)/DT
            VS(I) = VS(I)+VS(I-1)
10       CONTINUE
         IF (ASH.GT.0.0)THEN
```

```
            VS(IB+IG) = VS(1)/ASH
         ELSE
            VS(IB+IG) = VS(IG+IB-1)
         ENDIF
*     CONVERGENCE CRITERION FOR FEED FLOW RATE IS BASED ON INLET
*     AIR FLOW RATE/6 (ROUGHLY STOICH. AIR FOR C TO CO) AS A REFERENCE
*     SOLID FLUX. THIS IS DONE BECAUSE DURING BED STARTUP ACTUAL SOLIDS
*     FLUX MAY BECOME 0. TIGHTENING CONVERGENCE CRITERION FROM 1E-3 TO
*     1E-4 INCREASED ITERATIONS WITHOUT IMPROVING ACCURACY.
         VCHK = ABS(VS(IB+IG)-VS(IB+IG-1))
         VCRIT = VG(1)/6.0
         IF ((VCHK/VCRIT).GT.1.0E-03) THEN
            VS(1) = VS(IB+IG-1)*ASH
            ICOUNT = ICOUNT+1
            IF (ICOUNT.GT.100) THEN
               WRITE(IO,*) 'RESULTS INVALID - VS DNCNV'
               WRITE(IO,*) VCHK
               ISTOP = 1
               GO TO 33
            ENDIF
            GO TO 333
         ENDIF
      ENDIF

*     IF THE ASH BUILDS UP IN THE BED
      IF (IBUILD.EQ.1) THEN
         DO 11 I=1,IG
            VS(I) = 0.0
11       CONTINUE
         DO 12 I=IG+1,IG+IB-1
            VS(I) = -G(I)*SLAB(I)*SSCO(I)
     &              -((1-VOID(I))*RHOS(I)
     &              -(1-VOIDO(I))*RHOSO(I))*SLAB(I)/DT
            VS(I) = VS(I)+VS(I-1)
12       CONTINUE
         VS(IG+IB) = VS(IG+IB-1)
      ENDIF
33    RETURN
      END
*****************************************************************************

      SUBROUTINE CFLUX (VS,VC)

*     CALCULATES THE CHAR VELOCITIES THROUGH THE BED SLABS

      PARAMETER (N=50)
      DIMENSION VC(N),VS(N)
      DIMENSION VOID(N),SLAB(N),SSB(N),SSBO(N),RHOS(N),G(N)
      DIMENSION DIAMC(N),SSC(N),SSCO(N),XC(N)
      COMMON/BED/VOID,E,SLAB,SSB,SSBO,RHOS,G
      COMMON/CHAR/CARB,DIAMC,RHOC,VOIDC,SPHERC,SSC,SSCO,XC
      COMMON/ASH/ASH,DIAMA,RHOA,VOIDA,SPHERA,IBUILD
      COMMON/TIME/IFLAG,ITIME,ITERNS,TURNS,IB,IG,ICOB,TIMES,DT

*     THE VARIABLE VC IS ACTUALLY THE MASS FLUX RHOC*VC

*     DO 10 I=1,IG
```

```
*       VC(I) = 0.0
*10     CONTINUE
*       DO 11 I=IG+1,IG+IB-1
*          VC(I) = -G(I)*SLAB(I)*SSCO(I)*(1+ASH)
*     &            -(XC(I)*(1-VOID(I))
*     &            -XCO(I)*(1-VOIDO(I)))*RHOC*SLAB(I)/DT
*          VC(I) = VC(I)+VC(I-1)
*11     CONTINUE
*       VC(IG+IB) = VC(IG+IB-1)

        DO 12 I=1,IG+IB
           VC(I) = RHOC/RHOS(I)*XC(I)*VS(I)
12      CONTINUE
        RETURN
        END

*****************************************************************************

        SUBROUTINE COND(TG,TS,AKG,AKAS)

*       CALCULATES THE EFFECTIVE CONDUCTIVITY OF THE SOLID PHASE

        PARAMETER (N=50)
        DIMENSION TG(N),TS(N),AKG(N),AKAS(N)
        DIMENSION VOID(N),SLAB(N),SSB(N),SSBO(N),RHOS(N),G(N)
        DIMENSION DIAMC(N),SSC(N),SSCO(N),XC(N)
        DIMENSION TC(N),GRATEK(N)
        COMMON/BED/VOID,E,SLAB,SSB,SSBO,RHOS,G
        COMMON/CHAR/CARB,DIAMC,RHOC,VOIDC,SPHERC,SSC,SSCO,XC
        COMMON/ASH/ASH,DIAMA,RHOA,VOIDA,SPHERA,IBUILD
        COMMON/INFO/WTN2,WTO2,WTCO2,WTCO,R,P,BETA,GAMMA,THI
        COMMON/GRATE/GRATE,GRTSOL,GRTBAR,IGMOD,GRTRHO,GRTPD,GRTSPACE
        COMMON/TIME/IFLAG,ITIME,ITERNS,TURNS,IB,IG,ICOB,TIMES,DT

        DO 10 I=1,IG
           TC(I) = TS(I)-273.0
           IF (IGMOD.EQ.2) THEN
              GRATEK(I) = 0.0137*TC(I)+15.086
              AKAS(I) = GRTSOL*GRATEK(I)
           ENDIF
10      CONTINUE

        DO 11 I=IG+1,IB+IG
           TC(I) = TS(I)-273.0
           TM = (TS(I)+TG(I))/2.0
*       EFFECTIVE ASH CONDUCTIVITY
           EA = E
           AKSA = 1.09
           HRSA = 0.2268*(EA/(2.0-EA))*((TM/100.0)**3.0)
           HRVA = 0.2268/(1.0+(0.5*VOIDA/(1.0-VOIDA))*((1.0-EA)/EA))
     &            *((TM/100.0 )**3.0)
           AKASA = BETA*(1.0-VOIDA)
     &             /(GAMMA/AKSA+1.0/(AKG(I)/THI+HRSA*DIAMA))
     &            +VOIDA*BETA*DIAMA*HRVA

           VCHAR = XC(I)*(1.0-VOID(I))
           CHECK = (1.0-VOIDC)/(1.0-VOIDC*VOIDA)
```

```
            IF (XC(I).LE.CHECK) THEN
               CHIA = 1.0
            ELSE
               CHIA = (1.0-VOIDC)/(1.0-VOIDA)*(1.0-XC(I))/(VOIDC*XC(I))
            ENDIF

*        EFFECTIVE BED CONDUCTIVITY
            AKS = ((RHOC/4511.0)**3.5)*TS(I)**0.5
            HRS = 0.2268*(E/(2.0-E))*((TM/100.0)**3.0)
            HRV = 0.2268/(1.0+(0.5*VOID(I)/(1.0-VOID(I)))*((1.0-E)/E))
     &           *((TM/100.0)**3.0)
            AKAS(I) = VCHAR*BETA
     &                /(GAMMA/AKS+1.0/(AKG(I)/THI+HRS*DIAMC(I)))
     &                +(1.0-VCHAR)*(1-CHIA)*BETA*DIAMC(I)*HRV
     &                +(1.0-VCHAR)*CHIA*AKASA
11       CONTINUE
         RETURN
         END

*************************************************************************

         SUBROUTINE PCONC(AKY)

*        CALCULATES THE GAS CONCENRATIONS AT THE PARTICLE SURFACE

         PARAMETER (N=50)
         DIMENSION AKY(N,3)
         DIMENSION VOID(N),SLAB(N),SSB(N),SSBO(N),RHOS(N),G(N)
         DIMENSION Y8O2(N),Y8CO2(N),Y8CO(N),Y8N2(N),Y8O2O(N),Y8CO2O(N)
         DIMENSION Y8COO(N),Y8N2O(N)
         DIMENSION YRO2(N),YRCO2(N),YRCO(N),YRN2(N)
         DIMENSION G1(N),G2(N),X(N),S(N)
         DIMENSION YRCO2I(N),YRCOI(N),YRO2I(N)
         COMMON/BED/VOID,E,SLAB,SSB,SSBO,RHOS,G
         COMMON/Y/Y8O2,Y8CO2,Y8CO,Y8N2,Y8O2O,Y8CO2O,Y8COO,Y8N2O
         COMMON/YR/YRO2,YRCO2,YRCO,YRN2
         COMMON/STOIC/SCO2,SCO,S3,S2,DH1,DH2,DH3,DH4
         COMMON/REACT/G1,G2,X,S,IREACT
         COMMON/TIME/IFLAG,ITIME,ITERNS,TURNS,IB,IG,ICOB,TIMES,DT

         DO 10 I=2,IG+IB-1
            YRCO2I(I) = YRCO2(I)
            YRO2I(I) = YRO2(I)
            YRCOI(I) = YRCO(I)
            FACTOR = G(I)+(S(I)*G1(I))/YRO2I(I)
            YRO2(I) = Y8O2(I)/(1.0+(1.0/AKY(I,1))*FACTOR)
            YRCO2(I) = X(I)*(1.0+S(I))*G1(I)/AKY(I,2)+Y8CO2(I)
            YRCO2(I) = YRCO2(I)/(1.0+(1.0/AKY(I,2))*(G(I)
     &                 +S2*G2(I)/YRCO2I(I)))
            ADD = (1.0-X(I))*(1.0+S(I))*G1(I)+AKY(I,3)*Y8CO(I)
            YRCO(I) = ((1.0+S2)*G2(I)+ADD)/(G(I)+AKY(I,3))
            IF (YRCO(I).LE.1.0E-38) THEN
               YRCO(I) = 1.0E-38
            ENDIF
            IF (YRO2(I).LE.1.0E-38) THEN
               YRO2(I) = 1.0E-38
            ENDIF
```

```
          IF (YRCO2(I).LE.1.0E-38) THEN
             YRCO2(I) = 1.0E-38
          ENDIF
10     CONTINUE
       RETURN
       END

*****************************************************************************

       SUBROUTINE TDMACN(TGO,VOIDO,DEFF,IRXN,RCO,RCOB,DXN,FE)

*      CALCULATES THE SPECIES CONCENTRATION PROFILES

       PARAMETER (N=50)
       DIMENSION TGO(N),VOIDO(N),DEFF(N,3),RCO(N),RCOB(N),DXN(N),FE(N)
       DIMENSION DIAMC(N),SSC(N),SSCO(N),XC(N)
       DIMENSION VOID(N),SLAB(N),SSB(N),SSBO(N),RHOS(N),G(N)
       DIMENSION VG(N),RHOG(N),RHOGO(N)
       DIMENSION Y8O2(N),Y8CO2(N),Y8CO(N),Y8N2(N),Y8O2O(N),Y8CO2O(N)
       DIMENSION Y8COO(N),Y8N2O(N)
       DIMENSION G1(N),G2(N),X(N),S(N)
       DIMENSION TESTTG(N),TESTTS(N),TESTCO(N)
       DIMENSION Y8CO2I(N),Y8COI(N),Y8O2I(N)
       DIMENSION AC(N),CC(N,3),QC(N),PC(N),CONC(N)
       DIMENSION FN(N),DN(N,3),FS(N),DS(N,3),PEN(N,3),PES(N,3)
       DIMENSION SPO2(N),SCOO2(N),SPCO(N),SCCO(N),SPCO2(N),SCCO2(N)
       COMMON/BED/VOID,E,SLAB,SSB,SSBO,RHOS,G
       COMMON/CHAR/CARB,DIAMC,RHOC,VOIDC,SPHERC,SSC,SSCO,XC
       COMMON/GAS/VG,RHOG,RHOGO
       COMMON/Y/Y8O2,Y8CO2,Y8CO,Y8N2,Y8O2O,Y8CO2O,Y8COO,Y8N2O
       COMMON/INFO/WTN2,WTO2,WTCO2,WTCO,R,P,BETA,GAMMA,THI
       COMMON/STOIC/SCO2,SCO,S3,S2,DH1,DH2,DH3,DH4
       COMMON/REACT/G1,G2,X,S,IREACT
       COMMON/RAD/TSG,TSB,TSW,HRG,HRB,HRW,F12B,F12W,BOLTZ,TCOAL
       COMMON/FLUXES/FO2,FC,FCO2,FTG,FTS
       COMMON/TIME/IFLAG,ITIME,ITERNS,TURNS,IB,IG,ICOB,TIMES,DT
       COMMON/TEST/TESTTG,TESTTS,TESTCO,CRIT

*      NUMBERING OF GASES (J): 1 = O2, 2 = CO2, 3 = CO

       DO 10 I=2,IB+IG-1
          Y8O2I(I) = Y8O2(I)
          Y8CO2I(I) = Y8CO2(I)
          Y8COI(I) = Y8CO(I)
          IF (Y8CO2I(I).LE.1.0E-38) THEN
             Y8CO2I(I) = 1.0E-38
          ENDIF
          IF (Y8O2I(I).LE.1.0E-38) THEN
             Y8O2I(I) = 1.0E-38
          ENDIF
          FN(I) = VG(I)*DT
          FS(I) = VG(I-1)*DT
          DO 11 J=1,3
             DN(I,J) = FE(I)*DEFF(I,J)+(1.0-FE(I))*DEFF(I+1,J)
             DN(I,J) = RHOG(I)*DN(I,J)*DT/DXN(I)
             DS(I,J) = FE(I-1)*DEFF(I-1,J)+(1.0-FE(I-1))*DEFF(I,J)
             DS(I,J) = RHOG(I-1)*DS(I,J)*DT/DXN(I-1)
```

```
            PEN(I,J) = FN(I)/DN(I,J)
            PES(I,J) = FS(I)/DS(I,J)
11        CONTINUE

*      WESTBROOK AND DRYER CO KINETICS OPTION
          IF (IRXN.EQ.1980) THEN
             IF ((IREACT.LT.2))THEN
                RCO(I) = 0.0
             ELSE
                RCO(I) =(Y8O2I(I)**0.25)*(1.8562E+10)*EXP(-20130./TGO(I))
                RCO(I) = RCO(I)*(RHOG(I)**1.75)*Y8COI(I)*VOID(I)
     &                    *SLAB(I)*DT
*      REVERSE REACTION FOR EQUILIBRIUM
                RCOB(I) = 9.74E12*RHOG(I)*Y8CO2I(I)*EXP(-46490.0/TGO(I))
*               RCOB(I) = 3.69E13*RHOG(I)*Y8CO2I(I)*EXP(-51566.0/TGO(I))
                RCOB(I) = RCOB(I)*VOID(I)*SLAB(I)*DT
               IF (ICOB.EQ.0)THEN
                  RCOB(I) = 0.0
               ENDIF
             ENDIF
          ENDIF

*      HOWARD AND FINE CO KINETICS OPTION
          IF (IRXN.EQ.1970) THEN
             IF ((IREACT.LT.2))THEN
                RCO(I) = 0.0
             ELSE
                RCO(I) = (Y8O2I(I)**0.5)*(4.5319E+8)*EXP(-15098./TGO(I))
                RCO(I) = RCO(I)*(RHOG(I)**2.0)*Y8COI(I)*VOID(I)
     &                    *SLAB(I)*DT
             ENDIF
             RCOB(I) = 4.8E11*RHOG(I)*Y8CO2I(I)*EXP(-46500./TGO(I))
             RCOB(I) = RCOB(I)*VOID(I)*SLAB(I)*DT
             IF (ICOB.EQ.0)THEN
                RCOB(I) = 0.0
             ENDIF
          ENDIF

          ECO2 = (Y8CO2I(I)+0.30)/2.0
          ECO = (Y8COI(I)+0.3472)/2.0
          EO2 = (Y8O2I(I)+0.2322)/2.0
          SPCO2(I) = -S2*G2(I)*SSCO(I)*SLAB(I)*DT/Y8CO2I(I)
          SPCO2(I) = SPCO2(I)-RCO(I)*(1.0+S3)/(ECO2-Y8CO2I(I))
          SPCO2(I) = SPCO2(I)-RCOB(I)*(1.0+S3)/Y8CO2I(I)
          SCCO2(I) = X(I)*(1.0+S(I))*G1(I)*SSCO(I)*SLAB(I)*DT
          SCCO2(I) = SCCO2(I)+(1.0+S3)*RCO(I)*ECO2/(ECO2-Y8CO2I(I))
          SPO2(I) = (-S(I)*G1(I)*SSCO(I)*SLAB(I)*DT-S3*RCO(I))/Y8O2I(I)
          SPO2(I) = SPO2(I)-S3*RCOB(I)/(EO2-Y8O2I(I))
*         SCOO2(I) = S3*RCOB(I)
          SCOO2(I) = S3*RCOB(I)*EO2/(EO2-Y8O2I(I))
          SPCO(I) = -RCO(I)/Y8COI(I)
          SPCO(I) = SPCO(I)-RCOB(I)/(ECO-Y8COI(I))
          SCCO(I) = (1.0-X(I))*(1.0+S(I))*G1(I)
          SCCO(I) = (SCCO(I)+(1.0+S2)*G2(I))*SSCO(I)*SLAB(I)*DT
*         SCCO(I) = SCCO(I)+RCOB(I)
          SCCO(I) = SCCO(I)+RCOB(I)*ECO/(ECO-Y8COI(I))
10     CONTINUE
```

```
      IF (IREACT.GT.0) THEN
         DO 12 J=1,3
            DO 13 I=2,IB+IG-1
               AC(1) = 1.0
               PC(1) = 0.0
               BC = DN(I,J)*AMAX1(0.0,(1.0-0.1*ABS(PEN(I,J)))**5.0)
               BC = BC+AMAX1(0.0,-FN(I))
               IF (I.EQ.IB+IG-1) THEN
                  BC = 0.0
               ENDIF
               CC(I,J) = DS(I,J)*AMAX1(0.0,(1.0-0.1*ABS(PES(I,J)))**5.0)
               CC(I,J) = CC(I,J)+AMAX1(0.0,FS(I))
               AC(I) = VOID(I)*SLAB(I)*RHOG(I)+BC+CC(I,J)+FN(I)-FS(I)
               IF (J.EQ.1) THEN
                  AC(I) = AC(I)-SPO2(I)
                  DDC = Y8O2(1)
                  DC = VOIDO(I)*SLAB(I)*RHOGO(I)*Y8O2O(I)+SCOO2(I)
               ENDIF
               IF (J.EQ.2) THEN
                  AC(I) = AC(I)-SPCO2(I)
                  DDC = Y8CO2(1)
                  DC = VOIDO(I)*SLAB(I)*RHOGO(I)*Y8CO2O(I)+SCCO2(I)
               ENDIF
               IF (J.EQ.3) THEN
                  AC(I) = AC(I)-SPCO(I)
                  DDC = Y8CO(1)
                  DC = VOIDO(I)*SLAB(I)*RHOGO(I)*Y8COO(I)+SCCO(I)
               ENDIF
               QC(1) = DDC/AC(1)
               PC(I) = BC/( AC(I)-CC(I,J)*PC(I-1))
               QC(I) =(CC(I,J)*QC(I-1)+DC)/(AC(I)-CC(I,J)*PC(I-1))
13          CONTINUE
            PC(IB+IG) = 0.0
            QC(IB+IG) = QC(IG+IB-1)/(1.0-PC(IG+IB-1))
            CONC(IB+IG) = QC(IB+IG)

            DO 14 I=IB+IG-1,2,-1
               CONC(I) = CONC(I+1)*PC(I)+QC(I)
               IF (J.EQ.1) THEN
                  Y8O2(IB+IG) = CONC(IB+IG)
                  Y8O2(I) = CONC(I)
               ENDIF
               IF (J.EQ.2) THEN
                  Y8CO2(IB+IG) = CONC(IB+IG)
                  Y8CO2(I) = CONC(I)
               ENDIF
               IF (J.EQ.3) THEN
                  Y8CO(IB+IG) = CONC(IB+IG)
                  Y8CO(I) = CONC(I)
                  TESTCO(I) = ABS(Y8CO(I)-Y8COI(I))
               ENDIF
14          CONTINUE
12       CONTINUE

         FLUXB = CC(2,1)
         FLUXA = CC(2,1)-AMAX1(FS(2),0.0)+AMAX1(-FS(2),0.0)
         FO2 = (FLUXB*Y8O2(1)-FLUXA*Y8O2(2))/DT
```

```
            FLUXB = CC(2,2)
            FLUXA = CC(2,2)-AMAX1(FS(2),0.0)+AMAX1(-FS(2),0.0)
            FCO2 = (FLUXB*Y8CO2(1)-FLUXA*Y8CO2(2))/DT
            FLUXB = CC(2,3)
            FLUXA = CC(2,3)-AMAX1(FS(2),0.0)+AMAX1(-FS(2),0.0)
            FC = (FLUXB*Y8CO(1)-FLUXA*Y8CO(2))/DT
         ENDIF
         RETURN
         END

*************************************************************************

         SUBROUTINE TDMATG(TG,TGI,TGO,TS,VOIDO,CPG,AKAG,H,RCO,RCOB,DXN,FE)

*        CALCULATES THE GAS TEMPERATURE PROFILES

         PARAMETER (N=50)
         DIMENSION TG(N),TGI(N),TGO(N),TS(N),VOIDO(N),CPG(N),AKAG(N),H(N)
         DIMENSION RCO(N),RCOB(N),DXN(N),FE(N)
         DIMENSION VOID(N),SLAB(N),SSB(N),SSBO(N),RHOS(N),G(N)
         DIMENSION VG(N),RHOG(N),RHOGO(N)
         DIMENSION G1(N),G2(N),X(N),S(N)
         DIMENSION TESTTG(N),TESTTS(N),TESTCO(N)
         DIMENSION FS(N),CGT(N),PGT(N),QGT(N)
         COMMON/BED/VOID,E,SLAB,SSB,SSBO,RHOS,G
         COMMON/GAS/VG,RHOG,RHOGO
         COMMON/INFO/WTN2,WTO2,WTCO2,WTCO,R,P,BETA,GAMMA,THI
         COMMON/STOIC/SCO2,SCO,S3,S2,DH1,DH2,DH3,DH4
         COMMON/REACT/G1,G2,X,S,IREACT
         COMMON/RAD/TSG,TSB,TSW,HRG,HRB,HRW,F12B,F12W,BOLTZ,TCOAL
         COMMON/FLUXES/FO2,FC,FCO2,FTG,FTS
         COMMON/TIME/IFLAG,ITIME,ITERNS,TURNS,IB,IG,ICOB,TIMES,DT
         COMMON/TEST/TESTTG,TESTTS,TESTCO,CRIT

         AGT = 1.0
         BGT = 0.0
         DGT = TG(1)
         PGT(1) = BGT/AGT
         QGT(1) = DGT/AGT
         DO 10 I=2,IB+IG-1
            TGI(I) = TG(I)
            FN = VG(I)*CPG(I)*DT
            FS(I) = VG(I-1)*CPG(I-1)*DT
            DN = (FE(I)*AKAG(I)+(1.0-FE(I))*AKAG(I+1))*DT/DXN(I)
            DS = (FE(I-1)*AKAG(I-1)+(1.0-FE(I-1))*AKAG(I))*DT/DXN(I-1)
            PEN = FN/DN
            PES = FS(I)/DS
            BGT = DN*AMAX1(0.0,(1.0-0.1*ABS(PEN))**5.0)
            BGT = (BGT+AMAX1(0.0,-FN))
            IF (I.EQ.IG+IB-1) THEN
               BGT = 0.0
            ENDIF
            CGT(I) = DS*AMAX1(0.0,(1.0-0.1*ABS(PES))**5.0)
            CGT(I) = (CGT(I)+AMAX1(0.0,FS(I)))
            SPT = -RCO(I)*DH4/(2600.0-TGI(I))
            SPT = SPT-RCOB(I)*DH4/TGI(I)
            SCT = RCO(I)*DH4*2600.0/(2600.0-TGI(I))
```

```
            AGT = VOID(I)*SLAB(I)*RHOG(I)*CPG(I)+BGT+CGT(I)
            AGT = AGT+(FN-FS(I))+H(I)*SSBO(I)*SLAB(I)*DT
            AGT = AGT-SPT
            DGT = VOIDO(I)*SLAB(I)*RHOGO(I)*CPGBAR(TGO(I),I)*TGO(I)
            DGT = DGT+H(I)*SSBO(I)*TS(I)*SLAB(I)*DT
            DGT = DGT+SCT
            PGT(I) = BGT/(AGT-CGT(I)*PGT(I-1))
            QGT(I) = CGT(I)*QGT(I-1)+DGT
            QGT(I) = QGT(I)/(AGT-CGT(I)*PGT(I-1))
10      CONTINUE
        CGT(IB+IG) = 0.0
        PGT(IG+IB) = 0.0
        QGT(IG+IB) = QGT(IG+IB-1)/(1.0-PGT(IB+IG-1))
        TG(IB+IG) = QGT(IB+IG)

        DO 11 I=IB+IG-1,2,-1
           TG(I) = PGT(I)*TG(I+1)+QGT(I)
           TESTTG(I) = ABS(TG(I)-TGI(I))
           IF (TG(I).GT.3000.0) THEN
              TG(I) = 3000.0
              WRITE(*,*)'TG OVERFLOW AT NODE ',I
           ENDIF
11      CONTINUE
        FLUXB = CGT(2)/DT
        FLUXA = CGT(2)/DT-AMAX1(FS(2),0.0)/DT+AMAX1(-FS(2),0.0)/DT
        FTG = FLUXB*TG(1)-FLUXA*TG(2)
        RETURN
        END

*****************************************************************************

        SUBROUTINE TDMATS(TG,TS,TSI,TSO,VOIDO,RHOSO,VS,AKAS,H,DXN,FE)

*       CALCULATES THE SOLID TEMPERATURE PROFILE

        PARAMETER (N=50)
        DIMENSION TG(N),TS(N),TSI(N),TSO(N),VOIDO(N),RHOSO(N),VS(N)
        DIMENSION AKAS(N),H(N),DXN(N),FE(N)
        DIMENSION VOID(N),SLAB(N),SSB(N),SSBO(N),RHOS(N),G(N)
        DIMENSION DIAMC(N),SSC(N),SSCO(N),XC(N)
        DIMENSION VG(N),RHOG(N),RHOGO(N)
        DIMENSION G1(N),G2(N),X(N),S(N)
        DIMENSION TESTTG(N),TESTTS(N),TESTCO(N)
        DIMENSION PST(N),QST(N)
        COMMON/BED/VOID,E,SLAB,SSB,SSBO,RHOS,G
        COMMON/CHAR/CARB,DIAMC,RHOC,VOIDC,SPHERC,SSC,SSCO,XC
        COMMON/ASH/ASH,DIAMA,RHOA,VOIDA,SPHERA,IBUILD
        COMMON/GAS/VG,RHOG,RHOGO
        COMMON/INFO/WTN2,WTO2,WTCO2,WTCO,R,P,BETA,GAMMA,THI
        COMMON/STOIC/SCO2,SCO,S3,S2,DH1,DH2,DH3,DH4
        COMMON/REACT/G1,G2,X,S,IREACT
        COMMON/RAD/TSG,TSB,TSW,HRG,HRB,HRW,F12B,F12W,BOLTZ,TCOAL
        COMMON/FLUXES/FO2,FC,FCO2,FTG,FTS
        COMMON/GRATE/GRATE,GRTSOL,GRTBAR,IGMOD,GRTRHO,GRTPD,GRTSPACE
        COMMON/TIME/IFLAG,ITIME,ITERNS,TURNS,IB,IG,ICOB,TIMES,DT
        COMMON/TEST/TESTTG,TESTTS,TESTCO,CRIT
```

```
IT = IB+IG
AST = 1.0
BST = 0.0
CST = 0.0
DST = TS(1)
EST = 0.0
PST(1) = BST/AST
QST(1) = DST/AST
TSG = (2.0*AKAS(2)/SLAB(2))*TS(2)+HRG*TS(1)
TSG = TSG/(2.0*AKAS(2)/SLAB(2)+HRG)
HRG = BOLTZ*(TS(1)**2.0+TSG**2.0)*(TS(1)+TSG)*GRTSOL
TSB = AKAS(IG+1)*TS(IG+1)+SLAB(IG+1)/2.0*HRB*TS(1)
TSB = TSB/(AKAS(IG+1)+SLAB(IG+1)/2.0*HRB)
HRB = BOLTZ*F12B*(TSB**2.0+TS(1)**2.0)*(TSB+TS(1))
TSW = (2.0*AKAS(IT-1)/SLAB(IT-1))*TS(IT-1)+HRW*TS(IT)
TSW = TSW/(2.0*AKAS(IT-1)/SLAB(IT-1)+HRW)
HRW = BOLTZ*F12W*(TS(IT)**2.0+TSW**2.0)*(TS(IT)+TSW)
DO 10 I=2,IT-1
   TSI(I) = TS(I)
   FN = VS(I)*CPS(TS(I+1),I)*DT
   FS = VS(I-1)*CPS(TS(I),I)*DT
   IF (I.EQ.2) THEN
      FS = VS(I-1)*CPS(TSG,I)*DT
   ENDIF
   IF (I.EQ.IT-1) THEN
      T = TCOAL
      FN = VS(I)*CPS(T,I)*DT
   ENDIF
   DN = ((1.0-FE(I))/AKAS(I)+FE(I)/AKAS(I+1))**(-1.0)
   DN = DN*DT/DXN(I)
   DS = ((1.0-FE(I-1))/AKAS(I-1)+FE(I-1)/AKAS(I))**(-1.0)
   DS = DS*DT/DXN(I-1)
   PEN = FN/DN
   PES = FS/DS
   BST = DN*AMAX1(0.0,(1.0-0.1*ABS(PEN))**5.0)
   BST = (BST+AMAX1(0.0,-FN))
   IF (I.EQ.IT-1) THEN
      BST = (AKAS(I)*DT)/(SLAB(I)/2.0)
      BST = BST*(1.0/(1.0+2.0*AKAS(I)/(SLAB(I)*HRW)))
   ENDIF
   CST = DS*AMAX1(0.0,(1.0-0.1*ABS(PES) )**5.0)
   CST = (CST+AMAX1(0.0,FS))
   IF (I.EQ.2) THEN
      CST= (AKAS(I)*DT)/(SLAB(2)/2.0)
      CST = CST*(1.0/(1.0+2.0*AKAS(I)/(SLAB(2)*HRG)))
   ENDIF
   DENOM= X(I)*12.0/44.0+(1.0-X(I))*12.0/28.0
   SC = (DH1*X(I)*12.0/44.0)/DENOM
   SC = SC+(DH2*(1.0-X(I))*12.0/28.0)/DENOM
   SC = (G1(I)*SC)*SSCO(I)*SLAB(I)*DT
   DST = (1.0-VOIDO(I))*SLAB(I)*RHOSO(I)*CPS(TSO(I),I)*TSO(I)
   DST = DST+H(I)*SSBO(I)*(TG(I)-TSI(I))*SLAB(I)*DT+SC
   IF (I.EQ.IG+1) THEN
      DST = DST-(1.0-GRTSOL)*HRB*(TSB-TS(1))*DT
   ENDIF
   AST = (1.0-VOID(I))*RHOS(I)*SLAB(I)*CPS(TS(I),I)
   SP = G2(I)*DH3*SSCO(I)*SLAB(I)*DT
```

```
            IF ((I.NE.IT-1).AND.(I.NE.2)) THEN
               AST = AST+BST+CST+FN-FS-SP/TSI(I)
            ENDIF
            IF (I.EQ.IT-1) THEN
               AST = AST+BST+CST-FS-SP/TSI(I)
               DST = DST-FN*TCOAL
            ENDIF
            IF (I.EQ.2) THEN
               AST = AST+BST+CST+FN-SP/TSI(I)
               DST = DST+FS*TSG
            ENDIF
            PST(I) = BST/(AST-CST*PST(I-1))
            QST(I) = CST*QST(I-1)+DST
            QST(I) = QST(I)/(AST-CST*PST(I-1))
10       CONTINUE
         DO 11 I=IT-1,2,-1
            TS(I) = PST(I)*TS(I+1)+QST(I)
            TESTTS(I) = ABS(TS(I)-TSI(I))
11       CONTINUE
         RETURN
         END

*************************************************************************

         SUBROUTINE STOCK(TG,TGI,TGO,TS,TSO,TSI,APHI,APHIO,VOIDO,RHOSO,
        &                 XCO,CGONE,DTEMP)

         PARAMETER (N=50)
         DIMENSION TG(N),TGI(N),TGO(N),TS(N),TSO(N),TSI(N),APHI(N)
         DIMENSION APHIO(N),VOIDO(N),RHOSO(N),XCO(N)
         DIMENSION VOID(N),SLAB(N),SSB(N),SSBO(N),RHOS(N),G(N)
         DIMENSION DIAMC(N),SSC(N),SSCO(N),XC(N)
         DIMENSION VG(N),RHOG(N),RHOGO(N)
         DIMENSION Y8O2(N),Y8CO2(N),Y8CO(N),Y8N2(N),Y8O2O(N),Y8CO2O(N)
         DIMENSION Y8COO(N),Y8N2O(N)
         DIMENSION TESTTG(N),TESTTS(N),TESTCO(N)
         COMMON/BED/VOID,E,SLAB,SSB,SSBO,RHOS,G
         COMMON/CHAR/CARB,DIAMC,RHOC,VOIDC,SPHERC,SSC,SSCO,XC
         COMMON/GAS/VG,RHOG,RHOGO
         COMMON/Y/Y8O2,Y8CO2,Y8CO,Y8N2,Y8O2O,Y8CO2O,Y8COO,Y8N2O
         COMMON/GE/A,A1,ER,ER1,ALPHA1,ALPHA2,ALPHA3
         COMMON/TIME/IFLAG,ITIME,ITERNS,TURNS,IB,IG,ICOB,TIMES,DT
         COMMON/TEST/TESTTG,TESTTS,TESTCO,CRIT

         IFLAG = 3
         DO 10 I=2,IG+IB-1
            CRIT = AMAX1(TESTTS(I),TESTTG(I))/(IG+IB)
            IF (CRIT.GT.0.02) THEN
               IFLAG = 2
            ENDIF
            CRITCO = TESTCO(I)/(IG+IB)
*           IF (CRITCO.GT.1.0E-5) THEN
            IF (CRITCO.GT.0.5E-05) THEN
               IFLAG = 2
            ENDIF
10       CONTINUE
```

```
      IF ((IFLAG.EQ.3).OR.(IFLAG.EQ.4)) THEN
         TURNS = ITERNS
         DTEMP = 0.0
         CGONE = 0.0
         DO 11 I=1,IG+IB
            DTEMP = DTEMP+ABS(TG(I)-TGO(I))+ABS(TS(I)-TSO(I))
            TGO(I) = TG(I)
            Y8O2O(I) = Y8O2(I)
            Y8CO2O(I) = Y8CO2(I)
            Y8COO(I) = Y8CO(I)
            RHOGO(I) = RHOG(I)
            CGONE = CGONE+G(I)*SLAB(I)*SSC(I)
11       CONTINUE

         DO 12 I=2,IG+IB-1
            TSO(I)=TS(I)
12       CONTINUE
         DO 13 I=IG+1,IG+IB-1
            SSBO(I) = SSB(I)
            SSCO(I) = SSC(I)
            APHIO(I) = APHI(I)
            VOIDO(I) = VOID(I)
            RHOSO(I) = RHOS(I)
            XCO(I) = XC(I)
13       CONTINUE
      ELSE
         DO 14 I=2,IG+IB-1
            TG(I) = ALPHA1*TG(I)+(1.0-ALPHA1)*TGI(I)
            TS(I) = ALPHA2*TS(I)+(1.0-ALPHA2)*TSI(I)
14       CONTINUE
         IFLAG = 2
      ENDIF

*     UPDATE DENSITY
      DO 15 I=2,IG+IB
         RHOG(I) = DENS(TG(I),I)
15    CONTINUE
      RETURN
      END

*****************************************************************************

      SUBROUTINE PRINT(IO,TG,TS,VS,VC,AMWG,RE,AKAS,CGONE,XB,AKY)

      PARAMETER (N=50)
      DIMENSION TG(N),TS(N),VS(N),VC(N),AMWG(N),RE(N),AKAS(N),XB(N)
      DIMENSION AKY(N,3)
      DIMENSION VOID(N),SLAB(N),SSB(N),SSBO(N),RHOS(N),G(N)
      DIMENSION DIAMC(N),SSC(N),SSCO(N),XC(N)
      DIMENSION VG(N),RHOG(N),RHOGO(N)
      DIMENSION Y8O2(N),Y8CO2(N),Y8CO(N),Y8N2(N),Y8O2O(N),Y8CO2O(N)
      DIMENSION Y8COO(N),Y8N2O(N)
      DIMENSION Y8O2PR(N),Y8COPR(N),Y8C2PR(N)
      DIMENSION XN(N)
      COMMON/BED/VOID,E,SLAB,SSB,SSBO,RHOS,G
      COMMON/CHAR/CARB,DIAMC,RHOC,VOIDC,SPHERC,SSC,SSCO,XC
      COMMON/GAS/VG,RHOG,RHOGO
```

```
      COMMON/Y/Y8O2,Y8CO2,Y8CO,Y8N2,Y8O2O,Y8CO2O,Y8COO,Y8N2O
      COMMON/INFO/WTN2,WTO2,WTCO2,WTCO,R,P,BETA,GAMMA,THI
      COMMON/TIME/IFLAG,ITIME,ITERNS,TURNS,IB,IG,ICOB,TIMES,DT

      TIMEH = AINT(TIMES/3600.0)
      TIMEM = (TIMES/3600.0-TIMEH)*60.0
      WRITE(IO,132) TIMES,TIMEH,TIMEM
132   FORMAT(/,'      TIME = ',F6.0,' SEC.;  ',F3.0,' HOURS ',F4.1,
     &   ' MIN.')
      WRITE(IO,130)
      WRITE(IO,134)
      DO 10 J=1,IB+IG
         XN(J) = (XB(J)-0.5*SLAB(J))*100.0
         Y8O2PR(J) = Y8O2(J)*AMWG(J)/WTO2*100.0
         Y8C2PR(J) = Y8CO2(J)*AMWG(J)/WTCO2*100.0
         Y8COPR(J) = Y8CO(J)*AMWG(J)/WTCO*100.0
         WRITE(IO,135) J,XN(J),Y8O2PR(J),Y8C2PR(J),Y8COPR(J),VG(J),
     &          VS(J),VC(J),XC(J),G(J),TG(J),TS(J),DIAMC(J)*100.0,
     &          VOID(J),RE(J),AKAS(J),CPS(TS(J),J),SSB(J),SSC(J),AKY(J,1)
10    CONTINUE

      WRITE(*,136) CGONE,CGONE*3600.0,CGONE*2.2*0.0929*3600.0
      WRITE(IO,136) CGONE,CGONE*3600.0,CGONE*2.2*0.0929*3600.0
136   FORMAT(6X,'BURNING RATE: ',F7.5,' KG/M2 S; ',F7.2,' KG/M2 HR; ',
     &       F7.2,' LB/FT2 HR')
130   FORMAT(/,2X,'I',6X,'X',5X,'O2',6X,'CO2',5X,'CO',5X,
     &       'RHO*VG',4X,'RHO*VS',4X,'RHO*VC',6X,'XC',6X,'G',
     &       9X,'TG',8X,'TS',6X,'DIAM',4X,'VOID',5X,'RE',5X,'AKAS',5X,
     &       'CPS',6X,'AB',6X,'AC',6X,'AKY')
134   FORMAT(8X,'CM',7X,'PERCENT VOLUME',7X,'KG/M2S',4X,'KG/M2S',4X,
     &      'KG/M2S',12X,'KG/M2S'6X,'K',9X,'K',8X,'CM ',20X,
     &      'W/M K',3X,'J/KG K')
135   FORMAT(1X,I2,3X,F5.2,3X,F5.2,3X,F5.2,3X,F5.2,3X,F6.5,3X,
     &      F7.5,3X,F7.5,3X,F6.4,3X,F6.5,3X,F7.2,3X,F7.2,3X,F6.4,
     &      3X,F5.4,3X,F4.1,3X,F6.3,3X,F6.1,3X,F6.1,3X,F6.1,3X,F7.3)
      RETURN
      END

*****************************************************************************

      SUBROUTINE GRAPHING(IO,XB,AMWG,TG,TS)

      PARAMETER (N=50)
      DIMENSION XB(N),AMWG(N),TG(N),TS(N)
      DIMENSION VOID(N),SLAB(N),SSB(N),SSBO(N),RHOS(N),G(N)
      DIMENSION Y8O2(N),Y8CO2(N),Y8CO(N),Y8N2(N),Y8O2O(N),Y8CO2O(N)
      DIMENSION Y8COO(N),Y8N2O(N)
      COMMON/BED/VOID,E,SLAB,SSB,SSBO,RHOS,G
      COMMON/Y/Y8O2,Y8CO2,Y8CO,Y8N2,Y8O2O,Y8CO2O,Y8COO,Y8N2O
      COMMON/INFO/WTN2,WTO2,WTCO2,WTCO,R,P,BETA,GAMMA,THI
      COMMON/TIME/IFLAG,ITIME,ITERNS,TURNS,IB,IG,ICOB,TIMES,DT

*     NOTE: THESE EQUATIONS ARE DIFFERENT FOR EACH EXPERIMENT

      XS = 6.0045-0.0527*TIMES/60.0
      IF (XS.LT.2.9) THEN
         XS = 3.6358-0.0116*TIMES/60.0
```

```
      ENDIF

      DO 10 I=IG+1,IG+IB
         DELTA = SLAB(I)/2.0*100.0
         X = XB(I)*100.0-DELTA
         IF ((X.GT.(XS-DELTA)).AND.(X.LT.(XS+DELTA))) THEN
            O2PLOT = Y8O2(I)*AMWG(I)/WTO2*100.0
            CO2PLOT = Y8CO2(I)*AMWG(I)/WTCO2*100.0
            COPLOT = Y8CO(I)*AMWG(I)/WTCO*100.0
            TGPLOT = TG(I)
            TSPLOT = TS(I)
            WRITE(IO,100) TIMES/60.0,XS,O2PLOT,CO2PLOT,COPLOT,TGPLOT,
     &                    TSPLOT
         ENDIF
10    CONTINUE
100   FORMAT(1X,F5.1,3X,F6.3,3X,F5.2,3X,F5.2,3X,F5.2,3X,F6.1,3X,F6.1)
      RETURN
      END

*************************************************************************

      SUBROUTINE ENERGY(TG,TS,VS,CPG,ERROR)

      PARAMETER (N=50)
      DIMENSION TG(N),TS(N),VS(N),CPG(N)
      DIMENSION VG(N),RHOG(N),RHOGO(N)
      DIMENSION Y8O2(N),Y8CO2(N),Y8CO(N),Y8N2(N)
      DIMENSION Y8O2O(N),Y8CO2O(N),Y8COO(N),Y8N2O(N)
      COMMON/GAS/VG,RHOG,RHOGO
      COMMON/Y/Y8O2,Y8CO2,Y8CO,Y8N2,Y8O2O,Y8CO2O,Y8COO,Y8N2O
      COMMON/RAD/TSG,TSB,TSW,HRG,HRB,HRW,F12B,F12W,BOLTZ,TCOAL
      COMMON/GRATE/GRATE,GRTSOL,GRTBAR,IGMOD,GRTRHO,GRTPD,GRTSPACE
      COMMON/FLUXES/FO2,FC,FCO2,FTG,FTS
      COMMON/TIME/IFLAG,ITIME,ITERNS,TURNS,IB,IG,ICOB,TIMES,DT

      IT = IB+IG
      T = TCOAL
      ENIN = FTG+BOLTZ*(TS(1)**4.0-TSG**4.0)*GRTSOL
     &       +BOLTZ*F12B*(TS(1)**4.0-TSB**4.0)
      IF (VS(1).LT.0.0) THEN
         ENIN = ENIN+VS(1)*TSG*CPS(TSG,I)
      ENDIF
      ENOUT = VG(IT)*CPG(IT)*TG(IT)+BOLTZ*F12W*(TSW**4.0-TS(IT)**4.0)
      ENOUT = ENOUT+VS(IT)*TCOAL*CPS(T,I)
      ENB = ENOUT-ENIN
      ENR = (VG(IT)*Y8CO(IT)-FC)*9.3E06*12.0/28.0
      ENR = ENR+(VG(IT)*Y8CO2(IT)-FCO2)*32.8E06*12.0/44.0
      ERROR = 100.0*(ENB-ENR)/AMIN1(ENB,ENR)
      RETURN
      END

*************************************************************************

      REAL FUNCTION F(V,I,GWEST)

*     WESTMAN EQUATION
```

```
      PARAMETER (N=50)
      DIMENSION DIAMC(N),SSC(N),SSCO(N),XC(N)
      COMMON/CHAR/CARB,DIAMC,RHOC,VOIDC,SPHERC,SSC,SSCO,XC
      COMMON/ASH/ASH,DIAMA,RHOA,VOIDA,SPHERA,IBUILD

      VOIDL = VOIDC
      VOIDS = VOIDA
      XL = XC(I)
      XS = 1.0-XC(I)
      VL = 1.0/(1.0-VOIDL)
      VS = 1.0/(1.0-VOIDS)
      F = ((V-VL*XL)/VS)**2.0
     &    +2.0*GWEST*((V-VL*XL)/VS)*((V-XL-VS*XS)/(VL-1.0))
     &    +((V-XL-VS*XS)/(VL-1.0))**2.0-1.0
      RETURN
      END

*************************************************************************

      REAL FUNCTION DF(V,I,GWEST)

*     DERIVATIVE OF THE WESTMAN EQUATION

      PARAMETER (N=50)
      DIMENSION DIAMC(N),SSC(N),SSCO(N),XC(N)
      COMMON/CHAR/CARB,DIAMC,RHOC,VOIDC,SPHERC,SSC,SSCO,XC
      COMMON/ASH/ASH,DIAMA,RHOA,VOIDA,SPHERA,IBUILD

      VOIDL = VOIDA
      VOIDS = VOIDC
      XL = 1.0-XC(I)
      XS = XC(I)
      VL = 1.0/(1.0-VOIDL)
      VS = 1.0/(1.0-VOIDS)
      DF = 2.0*((V-VL*XL)/VS)*(1.0/VS)
     &    +2.0*GWEST*((V-VL*XL)/VS)*(1.0/(VL-1.0))
     &    +2.0*GWEST*(1.0/VS)*((V-XL-VS*XS)/(VL-1.0))
     &    +2.0*((V-XL-VS*XS)/(VL-1.0))*(1.0/(VL-1.0))
      RETURN
      END

*************************************************************************

      REAL FUNCTION DENS(T,I)

*     CALCULATES THE GAS DENSITY

      PARAMETER (N=50)
      DIMENSION Y8O2(N),Y8CO2(N),Y8CO(N),Y8N2(N),Y8O2O(N),Y8CO2O(N)
      DIMENSION Y8COO(N),Y8N2O(N)
      COMMON/Y/Y8O2,Y8CO2,Y8CO,Y8N2,Y8O2O,Y8CO2O,Y8COO,Y8N2O
      COMMON/INFO/WTN2,WTO2,WTCO2,WTCO,R,P,BETA,GAMMA,THI

      Y8N2(I) = 1.0-Y8CO(I)-Y8O2(I)-Y8CO2(I)
      STORE = (Y8O2(I)/WTO2)+(Y8CO(I)/WTCO)+(Y8CO2(I)/WTCO2)
      STORE = 1.0/(STORE+(Y8N2(I)/WTN2))
      DENS = P*STORE/(R*T)
```

```
      RETURN
      END

*****************************************************************************

      REAL FUNCTION CPS(T,I)

*     CALCULATES THE SOLID HEAT CAPACITIES

      PARAMETER (N=50)
      DIMENSION DIAMC(N),SSC(N),SSCO(N),XC(N)
      COMMON/CHAR/CARB,DIAMC,RHOC,VOIDC,SPHERC,SSC,SSCO,XC
      COMMON/ASH/ASH,DIAMA,RHOA,VOIDA,SPHERA,IBUILD
      COMMON/GRATE/GRATE,GRTSOL,GRTBAR,IGMOD,GRTRHO,GRTPD,GRTSPACE
      COMMON/INFO/WTN2,WTO2,WTCO2,WTCO,R,P,BETA,GAMMA,THI
      COMMON/TIME/IFLAG,ITIME,ITERNS,TURNS,IB,IG,ICOB,TIMES,DT

      TC = T-273.0
      IF ((IGMOD.EQ.1).AND.(I.LE.IG)) THEN
         CPS = 754.0+0.293*TC
      ELSE IF ((IGMOD.EQ.2).AND.(I.LE.IG)) THEN
         CPS = 0.2087*TC+492.74
      ELSE
         A = 1.0/12.0
         X1 = 380.0/T
         X1 = 1.0/(EXP(X1)-1.0)
         X2 = 1800.0/T
         X2 =  1.0/(EXP(X2)-1.0)
         CPC = (1000.0/T)*(R*A)*(380.0*X1+3600.0*X2)
         CPA = 754.0+0.293*TC
         CPS = (RHOC*XC(I)*CPC+RHOA*(1.0-XC(I))*CPA)
     &         /(RHOC*XC(I)+RHOA*(1.0-XC(I)))
      ENDIF
      RETURN
      END

*****************************************************************************

      REAL FUNCTION CPGBAR(T,I)

*     CALCULATES THE SPECIFIC HEATS

      PARAMETER (N=50)
      DIMENSION Y8O2(N),Y8CO2(N),Y8CO(N),Y8N2(N),Y8O2O(N),Y8CO2O(N)
      DIMENSION Y8COO(N),Y8N2O(N)
      DIMENSION G1(N),G2(N),X(N),S(N)
      DIMENSION CPGREG(N)
      COMMON/Y/Y8O2,Y8CO2,Y8CO,Y8N2,Y8O2O,Y8CO2O,Y8COO,Y8N2O
      COMMON/INFO/WTN2,WTO2,WTCO2,WTCO,R,P,BETA,GAMMA,THI
      COMMON/STOIC/SCO2,SCO,S3,S2,DH1,DH2,DH3,DH4
      COMMON/REACT/G1,G2,X,S,IREACT
      COMMON/EXTRA/CPGREG

*     THIS FUNCTION COMPUTES MEAN SPECIFIC HEAT CPGBAR AND REAL
*     SPECIFIC HEAT CPGREG IN J/KG K, BASED ON SP. HT. POLYNOMIALS
*     FROM SMITH AND VAN NESS
```

```
      Y8N2(I) = 1.0-Y8O2(I)-Y8CO(I)-Y8CO2(I)

*     AO2 = 3.639
*     BO2 = 5.06e-04
*     DO2 = -2.27e04
*     ACO = 3.376
*     BCO = 5.57e-04
*     DCO = -3.1e03
*     ACO2 = 5.457
*     BCO2 = 1.045E-03
*     DCO2 = -1.157E05
*     AN2 = 3.2800
*     BN2 = 5.93E-04
*     DN2 = -4.0E03

*     CPO2B = AO2+BO2*T/2.0-DO2*(T**(-2))
*     CPO2B = (R/WTO2*1000.)*CPO2B
*     CPCOB = ACO+BCO*T/2.0-DCO*( T**(-2))
*     CPCOB = (R/WTCO*1000.)*CPCOB
*     CPCO2B = ACO2+BCO2*T/2.0-DCO2*(T**(-2))
*     CPCO2B = (R/WTCO2*1000.)*CPCO2B
*     CPN2B = AN2+BN2*T/2.0-DN2*(T**(-2))
*     CPN2B = (R/WTN2*1000.)*CPN2B

*     CPO2 = AO2+BO2*T+DO2*(T**(-2))
*     CPO2 = (R/WTO2*1000.)*CPO2
*     CPCO = ACO+BCO*T+DCO*(T**(-2))
*     CPCO = (R/WTCO*1000.)*CPCO
*     CPCO2 = ACO2+BCO2*T+DCO2*(T**(-2))
*     CPCO2 = (R/WTCO2*1000.)*CPCO2
*     CPN2 = AN2+BN2*T+DN2*(T**(-2))
*     CPN2 = (R/WTN2*1000.0)*CPN2

*     VAN WYLEN AND SONNTAG SPECIFIC HEAT EXPRESSIONS. THESE ARE
*     SLIGHTLY MORE ACCURATE, BUT BEHAVE VERY STRANGELY BELOW 200 K,
*     SO THAT ONE MUST CALCULATE (h - h298) AND THEN ADD h AT 298 K
*     FROM PERFECT GAS TABLES TO GET CORRECT VALUES OF CP BAR.

      THET = T/100.0
      CPO2 = 37.432+0.020102*THET**1.5-178.57/(THET**1.5)
      CPO2 = (CPO2+236.88/THET/THET)/WTO2*1000.0
      CPCO = 69.145-0.70463*THET**0.75-200.77/(THET**0.5)
      CPCO = (CPCO+176.76/(THET**0.75))/WTCO*1000.0
      CPCO2 = -3.7357+30.529*THET**0.5-4.1034*THET
      CPCO2 = (CPCO2+0.024198*THET*THET)/WTCO2*1000.0
      CPN2 = 39.060-512.79/(THET**1.5)+1072.7/THET/THET
      CPN2 = (CPN2-820.40/(THET**3))/WTN2*1000.

      HO2 = 37.432*THET+0.020102/2.5*THET**2.5+178.57*2./(THET**0.5)
      HO2 = (HO2-236.88/THET)
      HCO = 69.145*THET-0.70463/1.75*THET**1.75-200.77*2.*(THET**0.5)
      HCO = (HCO+176.76*4.*(THET**0.25))
      HCO2 = -3.7357*THET+30.529/1.5*THET**1.5-4.1034/2.*THET**2
      HCO2 = (HCO2+0.024198/3.*THET**3)
      HN2 = 39.060*THET+512.79*2./(THET**0.5)-1072.7/THET
      HN2 = (HN2+820.40/2./(THET**2))
```

```
THT3 = 2.98
HO23 = 37.432*THT3+0.020102/2.5*THT3**2.5+178.57*2./(THT3**0.5)
HO23 = (HO23-236.88/THT3)
HCO3 = 69.145*THT3-0.70463/1.75*THT3**1.75-200.77*2.*(THT3**0.5)
HCO3 = (HCO3+176.76*4.*(THT3**0.25))
HCO23 = -3.7357*THT3+30.529/1.5*THT3**1.5-4.1034/2.*THT3**2
HCO23 = (HCO23+0.024198/3.*THT3**3)
HN23 = 39.060*THT3+512.79*2./(THT3**0.5)-1072.7/THT3
HN23 = (HN23+820.40/2./(THT3**2))

CPO2B = ((HO2-HO23)*100.+8682.)/T/WTO2*1000.0
CPCOB = ((HCO-HCO3)*100.+8669.)/T/WTCO*1000.0
CPCO2B = ((HCO2-HCO23)*100.+9364.)/T/WTCO2*1000.0
CPN2B = ((HN2-HN23)*100.+8669.)/T/WTN2*1000.0

CPEFF = (1.0+S(I))*CPCO-S(I)*CPO2
CPGBAR = Y8O2(I)*CPO2B+Y8CO2(I)*CPCO2B
CPGBAR = CPGBAR+Y8N2(I)*CPN2B+Y8CO(I)*CPCOB
CPGREG(I) = Y8O2(I)*CPO2+Y8CO2(I)*CPCO2
CPGREG(I) = CPGREG(I)+Y8N2(I)*CPN2+Y8CO(I)*CPCO
RETURN
END
```

APPENDIX C: Char Combustion Model Data Files

Constant.dat

```
R       BOLTZ    WTN2   WTO2   WTCO2   WTCO
8.314   5.67E-08  28.0   32.0   44.0    28.0
BETA   GAMMA    THI    ALPHA1   ALPHA2
1.0     1.0    0.05    0.25    0.5
SCO       SCO2       S3      S2       DH1        DH2        DH3         DH4
1.3333  2.66667  0.571  3.667  32.79E06   9.21E06 -14.37E06   10.11E06
US(1)     G(1) G(N)
-0.0011   0.0    0.0
Y8O2(1)   Y8CO(1)   Y8CO2(1) Y8O2(N)   Y8CO(N)   Y8CO2(N)
0.232     0.001     0.003      0.232      0.001     0.003
IGMOD   GRATE(MM)   GRTPD(MM)   GRTSPACE(MM)   GRTBAR(MM)   GRTRHO
  2     19.05         13.7         3.3             3.05       7920.0
```

Run.dat

```
IB   IG   TLIMIT   DT    ITCUT   IEND
40   10   12.4E3   5.0     2    1000
DIAMC(M)   CARB    RHOC    VOIDC   SPHERC    E    TCOAL
0.0102      .936    880.0   0.5      0.5     0.8   300.0
DIAMA(M)    ASH    RHOA    VOIDA   SPHERA
0.00095    0.064 2097.0   0.7      0.18
HT(CM)    U(1)       P(KPA)
5.0       0.113      101.92
A1           ER1        A       ER
5.0        21373.0   860.0 18000.0
IREACT IHTTR   IRXN   ICOB   IBUILD
  2    1970    1970    1       1
TS(1)   TG(1) TG(N)   TS(N) TIGNIT   ALAYER(M)
330.0   294.0  650.0   330.0  1500.0   0.02
IGRAPH IGRID
   1     0
IFIELD IEFFECT   AI           TAU    VOIDP
  1        1      8.8E4         2      0.5
```